Investigations on the Thermal-hydraulic Behavior of Accident Tolerant Fuel Cladding Materials

January 2020

Changing the World's Energy Future

Edited by G.Su[1], M.Bucci[1], and P.Sabharwall[2]

[1]*Massachusetts Institute of Technology,* [2]*Idaho National Laboratory*

With contributions from

M. Bucci, A. Jena, H. Kim, B. Phillips, G. Su

Massachusetts Institute of Technology

M. Anderson, M. Corradini, B. Elward, E. Guiterrez, H. Jo, H. Yeom, K. Sridharan

University of Wisconsin, Madison

J. Rojas, R. Umretiya

Virginia Commonwealth University

N. Brown, J. Gorton

University of Tennessee, Knoxville

M. Chen, M. He, S. Lee, Y. Lee*, A. Prinja

*University of New Mexico, *Seoul National University*

R. Christensen, K. Terrill

University of Idaho

P. Sabharwall, K. Condie, C. Folsom, C. Jensen, D. Wachs

Idaho National Laboratory

C. Deck

General Atomics

R. Rebak

General Electric

R. Harne, J. Strumpell, J. Jones

Framatome

R. Martin

BWTX

G. Wang, W. Byers, Z. Karoutas

Westinghouse Electric Company

Investigations on the Thermal-hydraulic Behavior of Accident Tolerant Fuel Cladding Materials

Edited by G.Su[1], M.Bucci[1], and P.Sabharwall[2]
[1]Massachusetts Institute of Technology,
[2]Idaho National Laboratory

With contributions from
M. Bucci, A. Jena, H. Kim, B. Phillips, G. Su
Massachusetts Institute of Technology

M. Anderson, M. Corradini, B. Elward, E. Guiterrez, H. Jo, H. Yeom, K. Sridharan
University of Wisconsin, Madison

J. Rojas, R. Umretiya
Virginia Commonwealth University

N. Brown, J. Gorton
University of Tennessee, Knoxville

M. Chen, M. He, S. Lee, Y. Lee*, A. Prinja
*University of New Mexico, *Seoul National University*

R. Christensen, K. Terrill
University of Idaho

P. Sabharwall, K. Condie, C. Folsom, C. Jensen, D. Wachs
Idaho National Laboratory

C. Deck
General Atomics

R. Rebak
General Electric

R. Harne, J. Strumpell, J. Jones
Framatome

R. Martin
BWTX

G. Wang, W. Byers, Z. Karoutas
Westinghouse Electric Company

January 2020
Idaho National Laboratory
Idaho Falls, Idaho 83415
http://www.inl.gov

Page intentionally left blank

EXECUTIVE SUMMARY

In 2018, the Department of Energy launched, through the Nuclear Energy University Program (NEUP) four projects aiming at investigating the thermal-hydraulics behavior of ATF cladding materials. These projects have mainly focused on three ATF cladding materials, i.e., Cr-coated Zircaloy, FeCrAl, and SiC. Five technical and scientific questions are being addressed:

(a) How do surface properties of ATF cladding materials, e.g., wettability, change at ambient pressure, and under LWR operating condition?

(b) How do ATF cladding materials perform in atmospheric pool boiling tests?

(c) What is the performance of ATF cladding materials in steady-state and transient flow boiling CHF, particularly under LWR pressure, temperature, and mass flux?

(d) How accurately computer codes model flow boiling CHF on ATF materials, particularly in transient conditions?

(e) How do ATF materials perform in quenching heat transfer, and what is the impact of surface properties on the LFP temperature?

In the year of 2018-2019, significant results have been achieved in surface characterization (structure, morphology, roughness, and contact angle, i.e., wettability), testing (including both pool and flow boiling CHF tests, and droplet quenching tests), and modeling. Lesson learned and near term activities (i.e., to be carried out within the last year of the four NEUP projects) are briefly summarized in four topics, i.e., surface characterization, boiling, modeling and simulation, and quenching.

Surface characterization

Many groups have measured the contact angle (CA) of ATF materials in the air at atmospheric pressure. However, there seems to be some disagreement on the measured CA from the same material with similar surface roughness. These differences may arise from the sample cleaning protocol, or the surface itself. The CA variation from ambient pressure and temperature to LWR operating conditions has been partially clarified by MIT' tests. Systematic CA measurements on ATF materials (from the four projects) with different surface roughnesses could be conducted in LWR conditions using the MIT facility.

Boiling

An analysis of the impact of surface characteristics on CHF has been conducted. However, more experiments should be run before definite conclusions could be drawn.

In pool boiling conditions at atmospheric pressure, the CHF values measured by UWM-1 suggest that Zirlo, FeCrAl, and Cr-coated Zirlo have very similar CHF and that the CHF limit can be captured by a modified version of the Kandlikar correlation.

However, UNM performed flow boiling CHF tests at atmospheric pressure and observed that FeCrAl has a higher CHF limit compared to Zircaloy or Cr-

coated Zircaloy at the same operating conditions. UNM also observed that surface degradation (e.g., increase of surface roughness and wettability) does not affect the CHF limit. UNM has also conducted a test with a transient power pulse on FeCrAl tubes and observed that the transient CHF value is higher than the steady-state value.

UWM-2 has carried out studies on steady-state flow boiling on Cr-coated and bare Zirlo claddings, and have observed that the Cr-coated cladding has a higher boiling heat transfer coefficient and a slightly higher CHF compared uncoated claddings

WEC conducted several flow boiling CHF tests at PWR operating conditions, showing no difference in the CHF values of bare, Cr-coated and cruded Zirlo claddings.

More tests will be carried out in the third year of the project by WEC and UWM-2, with a specific focus on high pressures, ideally covering both PWR (15.5 MPa, 344 °C) and BWR (7.6 MPa, 291 °C) conditions.

Modeling and simulation

UTK has generated a computational framework to simulate flow boiling until post-CHF. UTK also quantified the uncertainty and sensitivity of the CHF value and the post-CHF temperature excursion. According to the UTK analysis, there is a need to improve the modeling of post-CHF heat transfer during power transients. However, the development and validation of these models require more experimental data, particularly for high-pressure conditions.

Quenching

MIT has developed a facility to study droplet quenching, producing demonstrative results on Cr-coated surface. A systematic study will be carried out to quantify the LFP temperature of potential ATF materials. For each material, different surface finish from nano-smooth to PWR cladding-roughness should be tested. The impact of droplet Weber number and subcooling should also be investigated.

On August 13th, 2019, MIT hosted a workshop aiming at sharing the progress of the four projects, summarizing the main findings of the research activities, identifying the challenges and the path forward, and coordinating the efforts from different research teams. Nine technical presentations were given by different organizations involved in the projects. The agenda and the presentation slides are attached in the appendix.

> **Note:** This is a status report and there is additional work to be performed in 2020 prior to completing the projects.

Page intentionally left blank

CONTENTS

FIGURES

TABLES

Page intentionally left blank

Investigations on the Thermal-hydraulic Behavior of Accident Tolerant Fuel Cladding Materials

1. BACKGROUND

Since the 2011 Fukushima accident, significant research has been devoted to developing accident-tolerant fuel (ATF) cladding materials. These investigations have mostly focused on the ability to resist runaway steam oxidation and retain mechanical strength and structural integrity under thermal shocks. However, much remains unknown about the materials' thermal-hydraulic behavior, particularly under light-water reactor (LWR) operating conditions. Two phenomena that determine safety margins in both normal and off-normal operating conditions—i.e., the critical heat flux (CHF) and Leidenfrost point (LFP) temperature—have not been investigated thoroughly for ATF materials.

Surface properties, such as wettability and roughness, are known to influence pool and flow boiling CHF, as well as the LFP temperature. However, little is known about the surface wettability of ATF materials, particularly at LWR pressure and temperature. Little has been done on flow-boiling CHF and quenching heat transfer, especially for droplet quenching.

Nonetheless, it is known that CHF in transient conditions, e.g., an exponentially escalating power transient, can be significantly different from that expected in steady-state operation. Very few studies have investigated transient CHF, either on ATF materials or under LWR pressure and temperature. The thorough understanding of transient CHF under prototypical reactor conditions will benefit not only the deployment of ATF but also the upcoming national efforts to study transient ATF behavior in the Transient Reactor Test Facility (TREAT) at Idaho National Laboratory.

In summary, as a part of ATF development efforts, there is an urgent need to understand how and how much these materials may affect two-phase heat transfer phenomena in nuclear reactor conditions.

2. OVERVIEW OF THE NEUP RESEARCH

In 2018, the Department of Energy launched, through the Nuclear Energy University Program (NEUP), four projects aimed at investigating thermal-hydraulic behavior of ATF cladding materials. These projects involve many organizations, as shown in Figure 1, and are structured as follow:

- Project 17-12549: "Critical Heat Flux Studies for Innovative Accident Tolerant Fuel Cladding Surfaces," led by the University of Wisconsin at Madison (UWM)-1 in collaboration with Westinghouse Electric Company, LLC (WEC) and General Atomics (GA).

- Project 17-12647: "Determination of Critical Heat Flux and Leidenfrost Temperature on Candidate Accident Tolerant Fuel Materials," led by the Massachusetts Institute of Technology (MIT) in collaboration with UWM-2, WEC, and GA.

- Project 17-12688: "An Experimental and Analytical Investigation into Critical Heat Flux Implications for Accident Tolerant Fuel Concepts," led by the University of New Mexico (UNM) in collaboration with the University of Tennessee at Knoxville (UTK), Oregon State University (OSU), Framatome, General Electric (GE), and Idaho National Laboratory (INL).

- Project 17-13019: "Evaluation of Accident Tolerant Fuels Surface Characteristics in Critical Heat Flux Performance," led by Virginia Commonwealth University (VCU) in collaboration with UWM-2, BWX, Framatome, and GE.

Figure 1. An overview of the organizations involved in the four projects sponsored by DOE.

The list of PIs (in bold) and collaborators at the different organizations include (in alphabetical order):

- BWXT: J. Miller
- GA: C. Deck
- GE: R. Rebak
- Framatome: J. Strumpell (UNM lead project), R. Harne, J. Jones (VCU lead project)
- INL: C. Jensen
- MIT: **M. Bucci**, G. Su, B. Phillips
- OSU: W. Marcum
- UTK: N. Brown (previously at PennState)
- UNM: **A. Prinja** (previously **Y. Lee**)
- UWM-1: **M. Corradini**, K. Sridharan, S. Yeom, H. Jo (now at Postech, South Korea)
- UWM-2: M. Anderson, B. Elward
- VCU: **V. Rojas**
- WEC: Z. Karoutas (MIT lead project only), Q. Wang (MIT lead project only), P. Xu, W. Byers.

These projects have mainly focused on three ATF cladding materials—i.e., Cr-coated Zircaloy, FeCrAl, and SiC. Five technical and scientific questions are being addressed:

(a) How do surface properties of ATF-cladding materials, e.g., wettability, change at ambient pressure and under LWR operating condition?

(b) How do ATF-cladding materials perform in atmospheric pool boiling tests?

(c) What is the performance of ATF-cladding materials in steady-state and transient flow-boiling CHF, particularly under LWR pressure, temperature, and mass flux?

(d)   How accurately do computer codes model flow-boiling CHF on ATF materials, particularly in transient conditions?

(e)   How do ATF materials perform in quenching heat transfer, and what is the impact of surface properties on the LFP temperature?

In the year 2018–2019, significant results have been achieved in surface characterization (structure, morphology, roughness, and contact angle (i.e., wettability)), testing (including both pool- and flow-boiling CHF and droplet-quenching tests), and modeling.

In this report, we discuss the contributions and accomplishments of all the organizations involved in these projects in the effort to answer these five technical and scientific questions.

3. RESEARCH PROGRESS

3.1 Surface Characterization

Surface wettability—i.e., the surface contact angle with water—is known to affect boiling heat transfer (e.g., increasing CHF) and quenching heat transfer (e.g., increasing the LFP temperature). The apparent surface wettability depends on surface roughness and intrinsic surface wettability—i.e., the contact angle that one would measure on an ideally smooth surface.

It is essential to characterize the intrinsic wettability of these materials as well as the roughness and the apparent wettability of actual ATF cladding samples to understand how they will affect boiling and quenching heat transfer. Ideally, one would quantify wettability (i.e., static, advancing, and receding contact angles) up to LWR operating conditions—i.e., in fully degassed water at high pressure and temperature.

3.1.1   Contact-angle Measurement

The sessile-drop method is the most-common approach to measure contact angles (CAs). This measurement typically requires an optical goniometer and a high-definition (HD) camera. The HD camera is used to take a magnified, backlit image of a sessile water drop on the test sample. Then, a post-processing algorithm is used to calculate the tangent of the droplet outline at the point of contact with the sample surface. The CA value is then back-calculated from the tangent.

VCU, UWM-1, UNM, and MIT have done CA measurements using goniometers on various ATF materials and surface finishes. Most of these tests were conducted with water droplets in the air under atmospheric pressure. However, MIT developed and operated a new apparatus that is capable of measuring CA in degassed water up to critical pressure and temperature (i.e., 22.06 MPa and 374°C, respectively).

VCU measured the CA in the air at atmospheric pressure on various tubular ATF materials including Zr-2, APMT, and C26M-grade FeCrAl from GE, Zr-4 from Framatome, and Cr-coated Zr-4. A comparison between Zr-2 and FeCrAl is shown in Table 1 (Ra represents the arithmetical-mean deviation of the assessed profile, Rz the average distance between the highest peak and lowest valley in each sampling length, Rsk the skewness of the height measurement, Rku the kurtosis of the height measurement, roughness factor the ratio of the measured area over the projection area, Rsm the root-mean-squared of the assessed height profile). All the samples have a very similar roughness factor, but while the measured CAs on APMT and C26M grade FeCrAl are very close, Zr-2 has a lower CA. This seems to indicate that the intrinsic wettability of FeCrAl is lower than the intrinsic wettability of Zr-2.

Table 1. Comparison of roughness and CA between Zr-2 and APMT and C26M grade FeCrAl (VCU).

Material	Roughness						Contact angle (degree)
	SJ-410 Profilometer				AFM		
	Ra (μm)	Rz (μm)	Rsk	Rku	Roughness factor (r)	Rsm (μm)	
Zircaloy-2	0.36 ±0.04	4.46 ±1.08	0.01 ±0.32	4.46 ±1.79	1.02	0.18	72.33 ±4.28
APMT	0.68 ±0.07	5.94 ±0.84	-0.47 ±0.12	3.17 ±0.29	1.07	0.49	91.97 ±2.78
C26M	0.69 ±0.07	8.59 ±1.34	-1.05 ±0.31	6.23 ±1.76	1.02	0.38	90.43 ±2.28

VCU also examined the separate effect of surface finish on CA using Cr-coated Zr-4 samples provided by Framatome and found that the CA sharply decreased after Zr-4 is coated with ~4 μm Cr by physical vapor deposition (PVD), and that surface finish of the substrate has a secondary effect on CA for both Zr-4 and Cr-coated Zr-4, as shown in Figure 2. These results also indicate that Chromium coated surfaces have a higher wettability than Zirconium alloys. The measured Ra of different samples are summarized in Table 2.
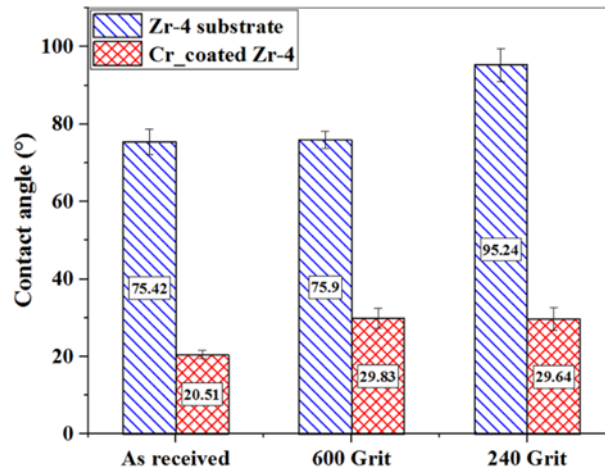
Figure 2. Comparison of static CA for Zr-4 and Cr-coated Zr-4 with a different surface finish of the substrate (VCU).

Table 2. Summary of the measured Ra from different samples.

Sample	Ra (μm)
As received Zr-4 substrate	0.399
600 Grit Zr-4 substrate	0.496
240 Grit Zr-4 substrate	0.776
As received Cr-coated Zr-4	0.442
600 Grit Cr-coated Zr-4	0.498
240 Grit Cr-coated Zr-4	0.910

UWM-1 measured the CA on flat polished Zirlo, on spray-coated Cr on Zirlo, and spray-coated FeCrAl on Zirlo samples provided by WEC. The final sample surfaces were all polished by 600 grit SiC abrasive paper to the same roughness and morphology, as shown in Figure 3. The measured CAs on Zirlo and FeCrAl-coated Zirlo are similar to VCU's measurements. However, there is a large discrepancy between the Cr-coated Zirlo from UWM and the Cr-coated Zr-4 from VCU, the latter of which shows a

much lower CA. Note that the UWM-1 coatings are spray-coated, whereas the VCU coatings are PVD-coated. Thus, the different contact angle may result from different surface morphology.
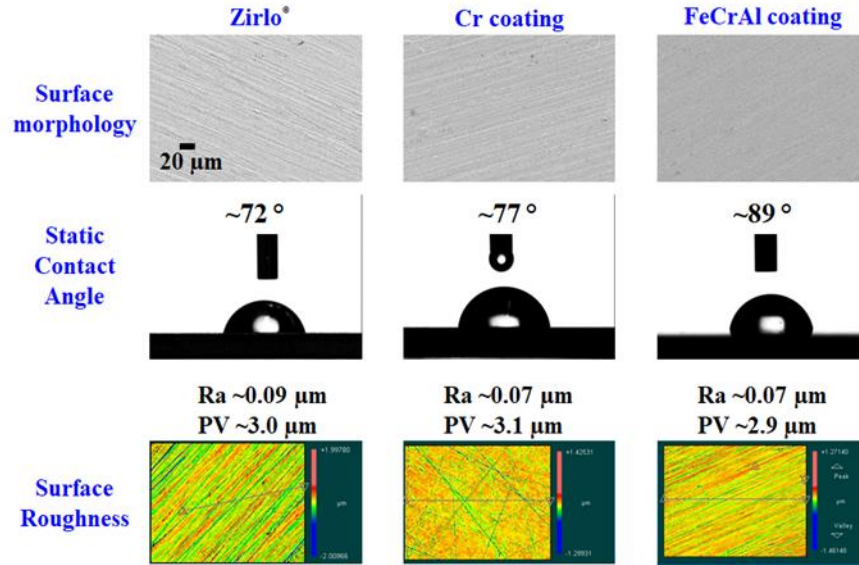
Figure 3. CA, roughness, and surface morphology measurements on various materials polished by 600 grit SiC abrasive paper (UWM-1).

UNM measured the CA on as-received tubular samples made of FeCrAl, Inconel600, and Zr-4 before and after the CHF tests. The results are summarized in Table 3. The CAs of all the samples increased after the CHF tests. In particular, the CA of fresh FeCrAl measured at UNM is lower than the values reported by UWM and VCU.

Table 3. Surface roughness and wettability: as-received/post-CHF experiment (UNM).

	FeCrAl	Inconel600	Zircaloy-4
Roughness, R_a	0.43 μm/4.53 μm	0.24 μm/3.13 μm	0.80 μm/1.61 μm
Surface Wettability	53°/69°	64°/76°	56°/74°

MIT developed an apparatus to measure static, advancing, and receding CAs from subatmospheric conditions up to the critical point of water in a fully degassed, saturated steam-water environment. The configuration of the autoclave-type facility is shown in Figure 4 (left). The autoclave has two sapphire windows at both ends, providing necessary optical access. The two bearings underneath the autoclave enable rotation around the axis of the droplet for measurement of advancing and receding CAs. A natural circulation loop was constructed to supply saturated steam and pressurize the autoclave.

The actual test section for the CA measurement is accommodated inside the autoclave (see Figure 4 [right]), which is equipped with two thermocouples for the temperature measurement of the sample and the autoclave environment. A cartridge heater is imbedded underneath the sample holder in order to maintain the sample temperature and evaporate the residual water after each measurement. The test section can accommodate rectangular samples from 0.5×0.5 cm^2 to 12.5×12.5 cm^2, and thickness from 1–3 mm.
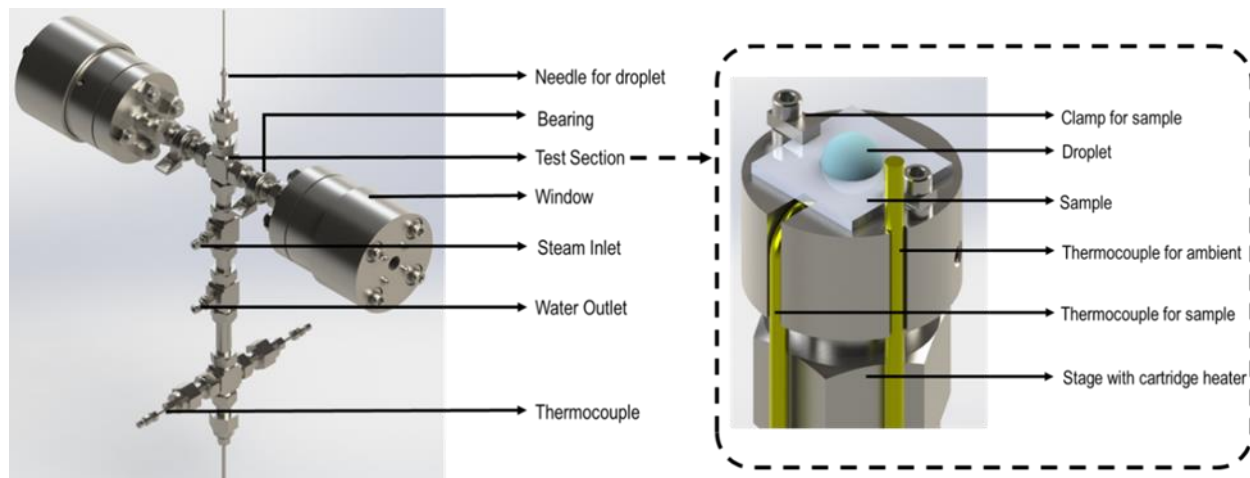
Figure 4. Design of the autoclave (left) and the test section (right) for the CA measurement (MIT).

MIT measured the static CA up to pressurized water reactor (PWR) temperature and pressure on various samples and surface finishes, including as-machined Zr-4 (Ra = 0.18 µm), mirror-polished Zr-4 (Ra ~0.05 µm), oxidized Zr-4 (Ra = 0.2 µm), as-machined monolithic SiC received from GA (Ra = 0.12 µm), and mirror-polished APMT-grade mirror-polished FeCrAl purchased from Kanthal (Ra ~ 0.05 µm). MIT conducted the CA measurements while increasing and decreasing the temperature. As shown in Figure 5, the static CA on all surfaces decreases with increasing temperature and pressure. For some surfaces, the CA at high pressure and temperature becomes zero, which indicates that the surface is super-hydrophilic. The CA decreases faster on rough or oxidized surfaces than on mirror-polished surfaces. On oxidized Zr-4, SiC, and FeCrAl surfaces, a large hysteresis was observed. The potential cause of this hysteresis can be different for different surfaces, and more tests are required in order to draw any conclusion.
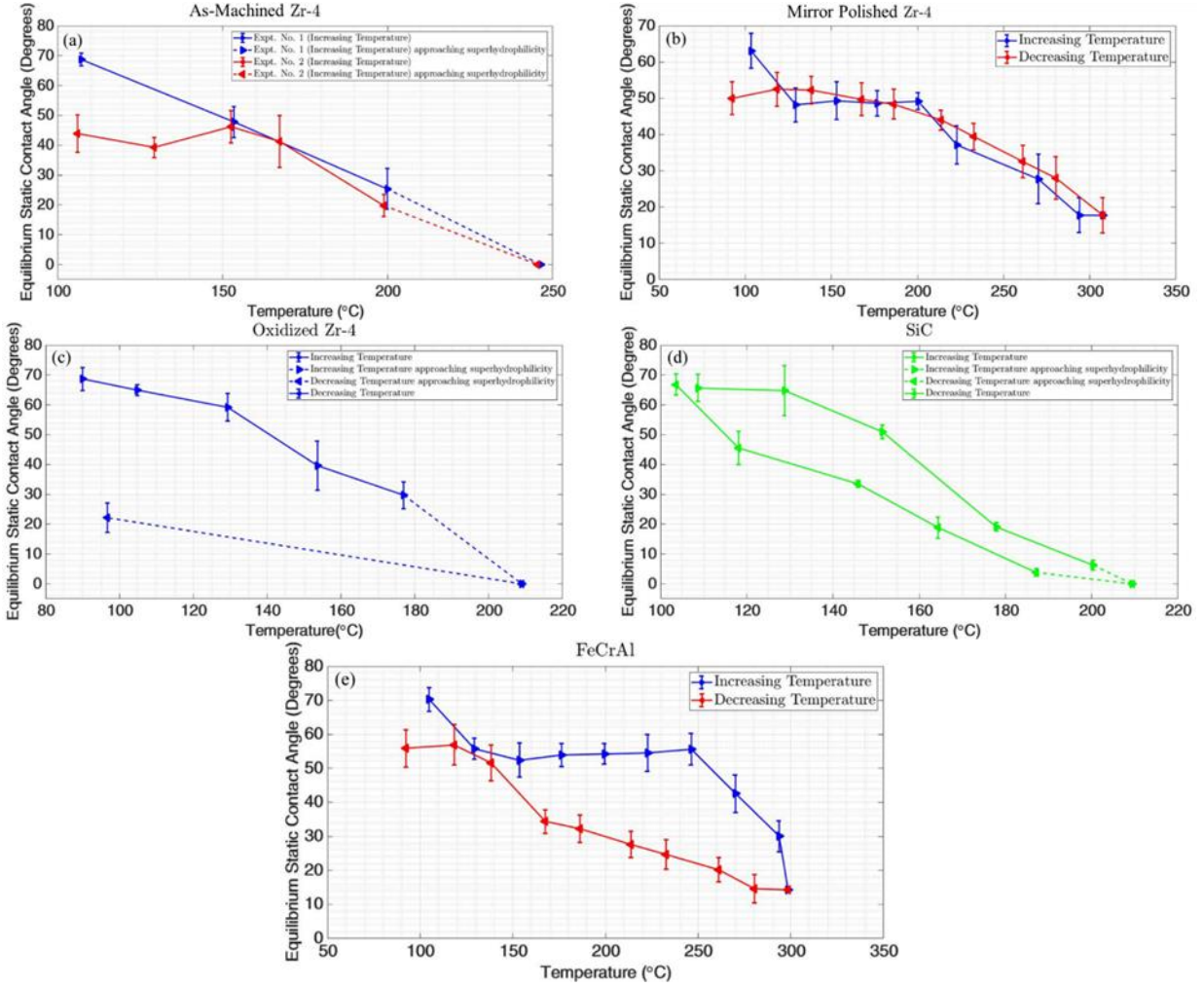
Figure 5. CA measured on: (top left) as-machined Zr-4, (top right) mirror-polished Zr-4, (middle left) oxidized Zr-4, (middle right) as-machined monolithic SiC, and (bottom) mirror-polished FeCrAl (MIT).

3.1.2 Surface Roughness

Many approaches can be used to measure and quantify surface roughness. Different methods reveal different kinds of roughness—e.g., stylus-type profilometer for one-dimensional (1D) microscale, optical profilometer for two-dimensional (2D) micro- or nanoscale, atomic force microscopy (AFM) for 2D nanoscale. For most situations, microscale surface roughness is a good indicator of the boiling and quenching heat-transfer behavior. However, on some surfaces with complicated features, such as hierarchical micro- and nanostructures, nanoscale surface roughness is also required.

VCU quantitatively measured surface roughness using a stylus-type profilometer (2 µm stylus-tip radius and 60 degree stylus-tip angle) following International Organization for Standardization (ISO) standards. Twelve different surface-roughness parameters were collected on a 5 mm sampling length at 0.5 mm/s scan rate. They also used tapping mode AFM to reveal nanoscale features as a supplement and validation to the results obtained by stylus-type profilometry. The results are summarized in Table 1, together with the CA measurements.

UWM-1 used optical profilometry for the surface-roughness measurement. They obtained 2D surface profiles and the associated statistical parameters such as peak-to-valley (PV) distance and root-mean-

square values of roughness, as shown in Figure 3. The close PV and Ra values from different substrate materials prove the repeatability of their polishing process.

UNM measured the surface roughness, Ra, of the samples before and after CHF tests, as summarized in Table 3. UNM observed a significant increase in surface roughness, as high as 13 times, after the CHF tests. However, the CHF value on the same rod barely changed test after test, which seems to suggest that surface roughness has a minor effect on CHF.

3.1.3   Other Surface Characteristics

In addition to CA and surface roughness, VCU used an X-Ray diffractometer (XRD) to measure the crystal structures of the test samples, as shown in Figure 6. The FeCrAl alloys (APMT, C26M) have body-centered cubic (bcc) crystal structure, while Zircaloy-4 and Zircaloy-2 have a hexagonal closed packed (hcp) crystal structure. For the Cr-coated material, the presence of the Cr layer was confirmed by the presence of its characteristic peaks with a cubic crystal structure. VCU also applied scanning electron microscopy (SEM) and X-ray photoelectron spectroscopy (XPS) to examine microscopic surface morphology and elemental composition, separately, as shown in Figure 7. The SEM micrographs of C26M and APMT show an average grain size of 27.98 $\pm$9.81 μm and 41.04 $\pm$13.39 μm, respectively. The smaller grain size of the C26M gives an increase in overall strength, as evidenced in the literature for FeCrAl alloys. The elements detected by EDS exhibit uniform distribution of the elements with no evidence of second-phase precipitates.
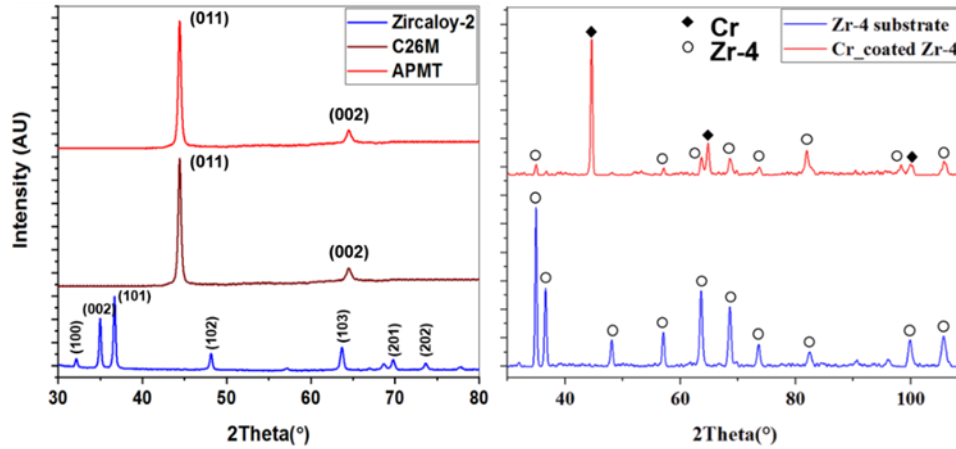
Figure 6. XRD patterns of tested materials (VCU).
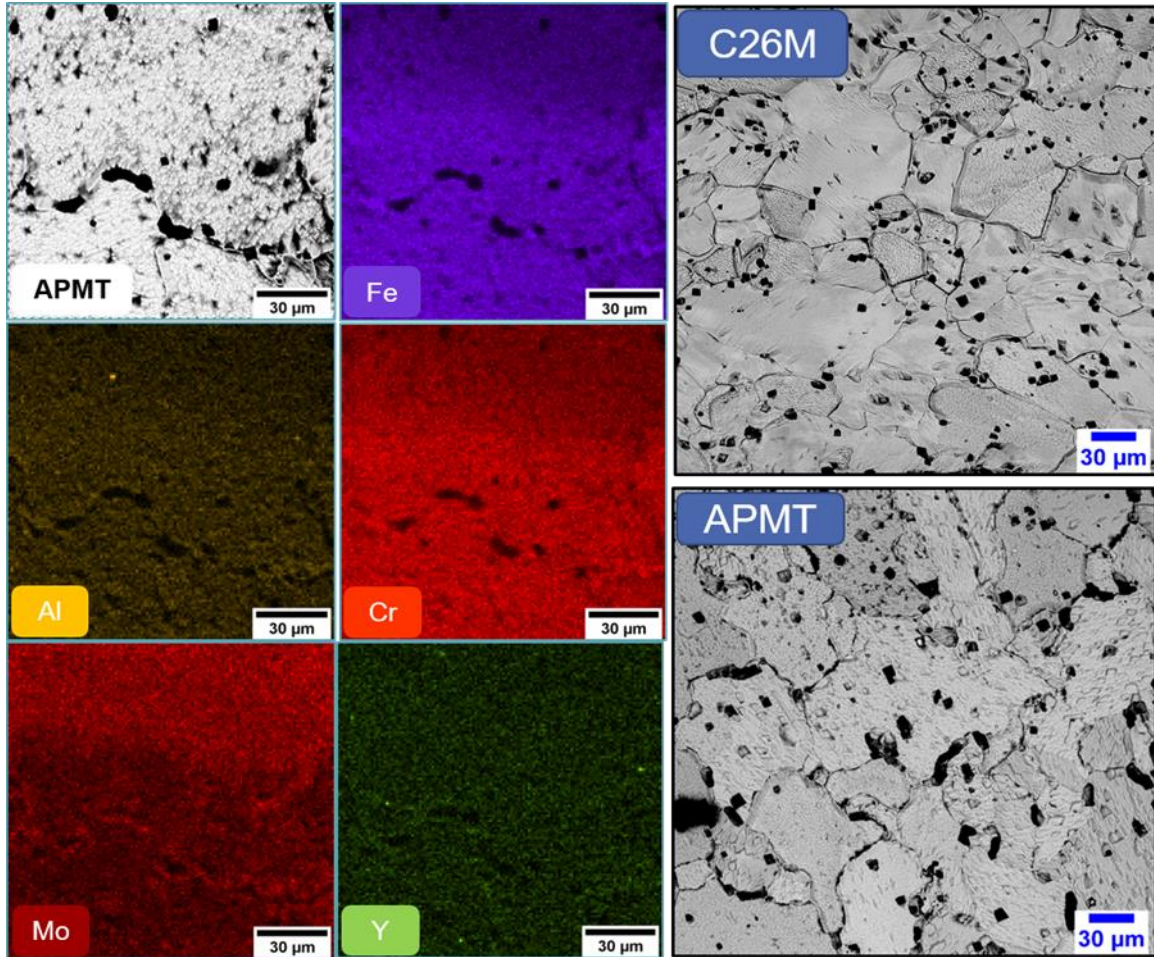
Figure 7. Element map for APMT (left) and SEM micrographs of etched FeCrAl (right) (VCU).

3.2 Pool Boiling

Pool-boiling experiments are commonly carried out to investigate the fundamentals of boiling heat transfer (e.g., bubble dynamics) and to quantify boiling parameters (e.g., the CHF value). They also constitute a valuable screening stage to inform the possible outcomes of flow-boiling tests.

UWM-1 conducted pool-boiling tests on flat samples at atmospheric pressure and saturation temperature (100°C) with deionized water. Material and thickness of the tested samples are listed below:

- 0.4 and 0.8 mm polished Zirlo

- 0.8 mm Zirlo with a Cr coating

- 0.8 mm Zirlo with a Cr coating polished down to 70 and 30 µm, respectively

- 0.8 mm Zirlo with a FeCrAl coating polished down to 40 µm

- 0.457, 0.76, 1.52 mm polished 304 stainless steel

- 0.508, 0.81, 1.27 mm polished brass.

The UWM-1's pool boiling facility for CHF tests of ATF materials is shown in Figure 8. The facility accommodates 2×2 cm^2 flat samples of various thicknesses. The top side of the sample is exposed to water, which is heated up by cartridge heaters inserted inside a copper heater block. Temperature and

subsequent heat-flux measurements were taken using thermocouples located inside the copper heating block at different distances from the boiling surface. The power was slowly increased stepwise through the nucleate-boiling regime until CHF was reached. CHF was then determined as the maximum heat flux before the temperature runaway.
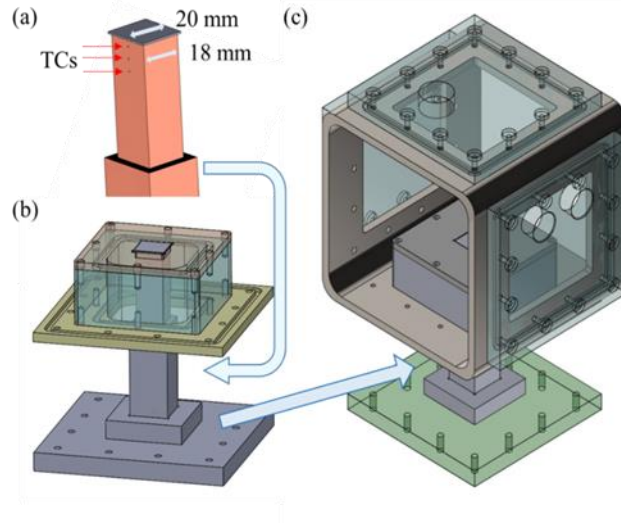
Figure 8. Illustrations of the pool-boiling facility designed and constructed for this study: (a) heater block and sample specimen, (b) assembly of the sample holder and heater block part, and (c) full assembly of the facility (UWM).

UWM-1 observed small differences in wettability on different materials. They attribute such difference to measurement uncertainty and minor inevitable variations resulting from sample surface preparation. However, UWM-1 argued that the effects of these variations on CHF data were not significant. A modified Kandlikar model, taking into account the CA effect with a correction factor for a circular heater (diameter of 10 mm), is compared with the experimental results. Although the sample dimension is slightly different in this study, the predicted values using the model are in good agreement with the experimental results, as shown in Figure 9.
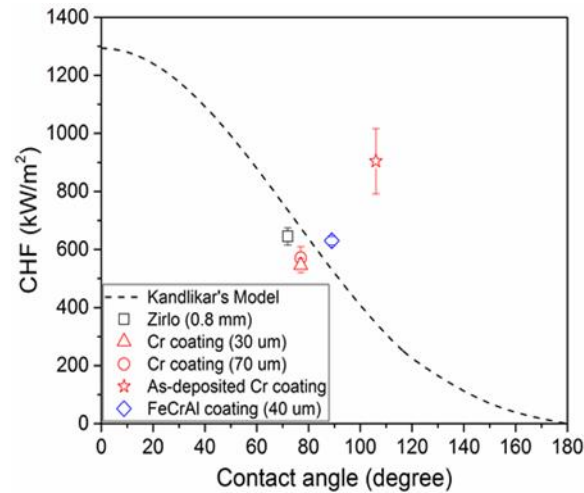
Figure 9. Pool-boiling CHF at atmospheric pressure and saturation temperature as a function of CA and their comparison with modified Kandlikar's model (UWM).

UWM-1's analysis also suggests that the average pool-boiling CHF is a function of thermal activity for samples with the same surface finish. Thermal activity is defined as the effusivity multiplied by the thickness of the sample. The heater in the Cu block and the test sample are assembled as a single unit. However, thermal paste is inserted between the large Cu block and the thin-clad test sample (0.4–0.8 mm) that provides thermal resistance and decouples the thermal response of the sample from the copper block. Thus, while Cu block provides a constant heat-flux boundary condition, the thermal variation due to boiling phenomena does not occur in the Cu block, but only on the test sample. Figure 10 shows that higher thermal activity leads to enhanced CHF by allowing more lateral heat conduction within the test sample.
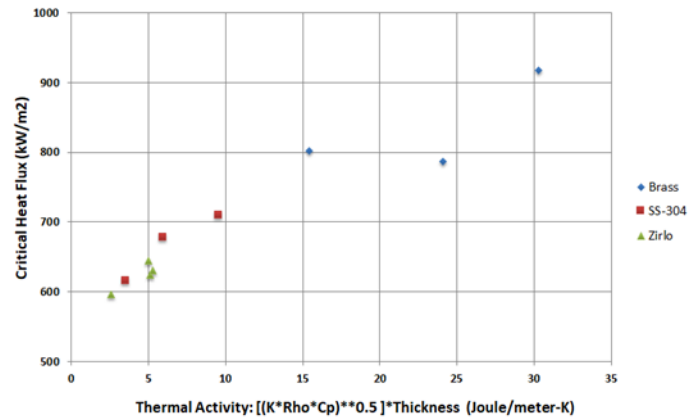
Figure 10. CHF results as a function of the sample thermal activity (UWM).

Table 4 summarizes the CHF data collected from metallic samples (Zirlo [both coated and uncoated], AISI 304 stainless steel, and brass).

Table 4. Summary of CHF results from different metallic test samples (UWM).

	CHF Average [kW/m^2]	CHF Range [kW/m^2]	Static Contact Angle [degrees]	Thickness [mm]
Cr coated Zirlo	571	526–597	77	0.87
FeCrAl coated Zirlo	630	614–639	90	0.84
Bare Zirlo	645	631–656	72	0.8
SS 304	709	695–724	68	0.762
Brass	803	758–979	60	0.81

3.3 Flow Boiling

In LWRs, fuel bundles are cooled in forced-flow conditions. Thus, systematic flow boiling CHF tests are necessary, in particular at LWR pressure and temperature, to better inform the design and deployment of ATF materials. The CHF margins should be examined under both steady-state heating and in transient heating conditions that are representative of accident scenarios (e.g., reactivity insertion accidents [RIAs]). Many groups have conducted steady-state flow-boiling CHF tests on ATF materials at

atmospheric or close-to-atmospheric pressures. WEC has also conducted flow-boiling CHF tests at PWR pressure and temperature. UNM has carried out transient flow boiling CHF tests with pulsed-power input.

UNM constructed an atmospheric pressure flow loop and tested steady-state flow boiling CHF on Fe-13Cr-6Al, Inconel600, and Zircaloy-4, as well as pulsed-power transient (1 s width and 8088.78 W peak power) flow-boiling CHF on FeCrAl. The configuration of the flow loop and the cross-sectional view of the test section are shown in Figure 11. The test section features a tubular flow channel with 9.252 mm outer diameter and 5.08 cm heated length. The tests were intentionally repeated on the same sample to investigate the effects of surface conditions on flow CHF.

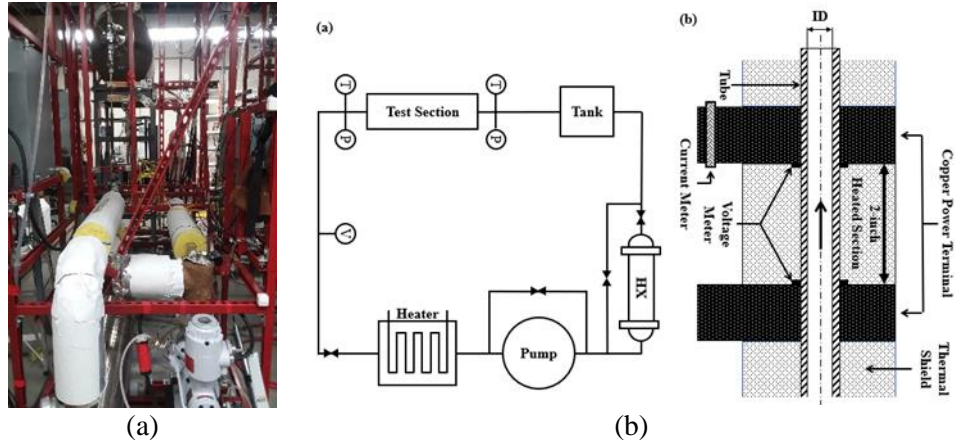(a)   (b)

Figure 11. (a) Flow loop diagram, (b) test section cross-sectional view (UNM).

Figure 12 (a) shows several steady-state CHF values on FeCrAl. Note that the standard deviation is less than 10% of the average value, confirming the repeatability of the tests. Figure 12 (b) shows the average experimental CHF values of three tested materials compared to the 2006 CHF lookup table at corresponding equilibrium qualities. The CHF value measured on the FeCrAl tube is higher than the CHF measured on Zircaloy and Inconel and the value reported in the Groeneveld lookup tables. This finding suggests that FeCrAl could lead to larger safety margins—i.e., a higher departure from nucleate boiling (DNB) ratio.
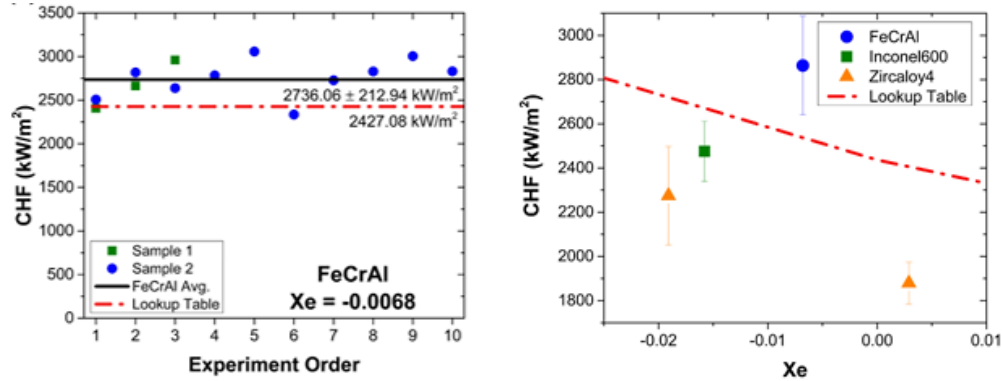
Figure 12. (a) Repeated CHF measurements on the FeCrAl alloy, (b) CHFs compared to the look-up table at corresponding equilibrium quality (UNM).

To address the change in surface characteristics after several experiments on the same tube, UNM measured surface roughness and wettability on post-steady-state CHF surfaces, which showed an increase in both roughness and CA compared to the as-received surfaces, as shown in Table 3. The results suggest that the effect of surface roughness in the range of ~0.2–5 µm and CA in the range of 50–80 degrees has

limited influence on flow-boiling CHF. This also suggests that, unless materials with extreme roughness or CA are used, the influence on flow-boiling CHF is likely limited for most engineered materials.

Traditionally, thermal parameters (e.g., thermal effusivity, activity, and diffusivity) were used to explain observed CHF differences; however, given the limited range of thermal parameters from three materials, no clear relation of thermal parameters to measured CHF values was observed under the same reference flow condition. UNM plans to carry out material-sensitivity studies in flow-boiling conditions to evaluate the impact of thermal parameters over a broader range. The effect of mass flow on flow-boiling CHF will also be investigated.

In addition to the steady-state tests, transient CHF experiments were also conducted on the Fe-13Cr-6Al tube under the same pressure and mass-flow conditions. The inlet quality was set to that of the steady-state CHF point, assuming that the thermodynamic quality at the instant of DNB does not change significantly in transient condition. By matching every condition (i.e., pressure, flow rate, and quality), a clear comparison between steady-state and transient CHF could be made. Nevertheless, due to limitation of the power supply, the pulsed power input is a much longer pulse than a super-prompt-critical power jump (>$1 of reactivity) or any hot zero-power RIA.

In UNM's tests, CHF and post-CHF phenomena are detected through estimates of the cladding inner temperatures. In this aim, UNM used a transient energy balance to calculate heat flux from measured power and outer surface temperature. Then the cladding inner surface temperature was obtained by solving the transient conduction equation with an implicit finite-difference scheme. The experimental results are shown in Figure 13.

As shown in Figure 13 (b), a sharp increase in the temperature is observed at 1.36 s. The heat flux starts to decrease with a cladding-temperature overshoot, which corresponds to the occurrence of CHF. As the power is cut at CHF, the cladding temperature decreases, and the vapor film is no longer sustained. This is the rewetting point shown in Figure 13 (c), coinciding with a sudden temperature drop at the inner cladding wall.
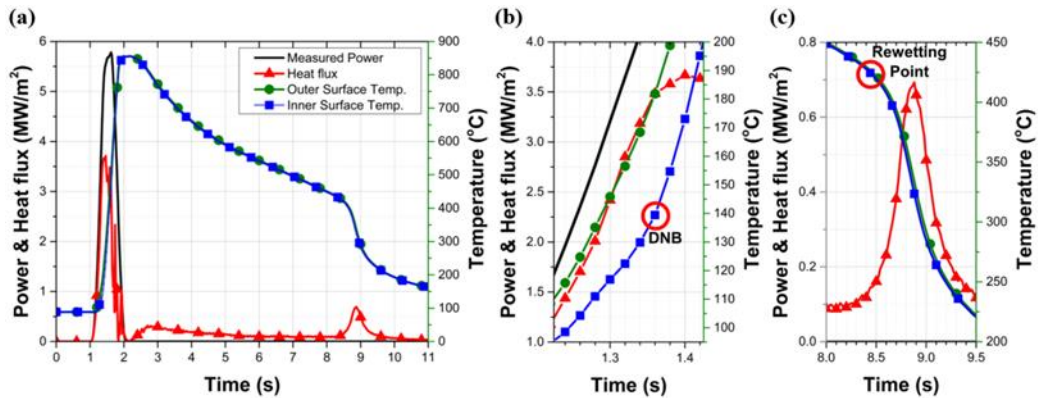
Figure 13. (a) Experimental measurement of transient pulsed power input, (b) CHF determination, and (c) rewetting-point determination (pulsed power: 1 s width and peak at 8088.78 watts, FeCrAl alloy) (UNM).

Based on the analysis, UNM has proposed a modeling approach for transient boiling that can be implemented in reactor-analysis code, as shown in Figure 14. UNM also found that transient CHF is 39% and 23% higher than the lookup table prediction and the steady-state condition experimental result, respectively.
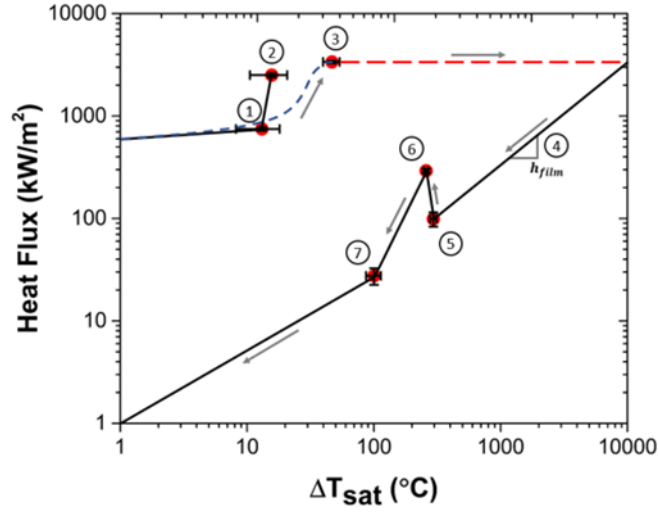
Figure 14. FeCrAl: obtained boiling curves for steady-state (①ONB, ②CHF) and transient flow boiling (300 kg/m^2-s mass flow, Xe = -0.0068, dashed line to ③CHF, then to ⑦) (UNM).

UWM-2 developed and fabricated directly heated rods using ATF material and standard Zircaloy cladding to study flow boiling at atmospheric-pressure conditions. The finished heater rod in the assembly jig is shown in Figure 15 (top). They also collaborated with Stern Labs to design internally heated rods with a cosine power profile for high-pressure flow-boiling tests, as shown in Figure 15 (bottom).
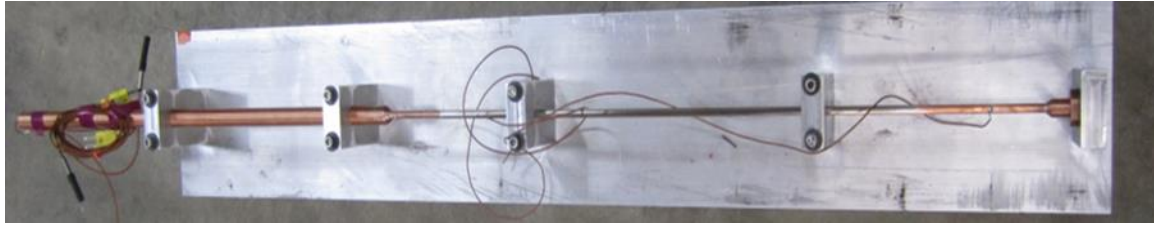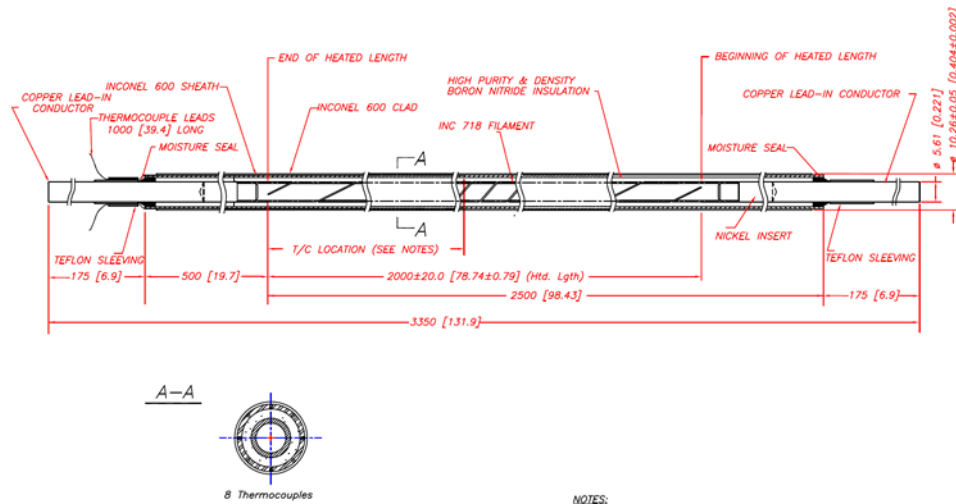
Figure 15. Image of heater rod for low-pressure tests (top), and the design of an internally heated rod for high-pressure tests (bottom) (UWM).

UWM-2 constructed a low-pressure loop and designed a high-pressure loop for flow-boiling tests at different pressures. Until now, UWM-2 has conducted low-pressure tests only while the high-pressure capability is still in the design and construction stages. In the low-pressure test, water with specific subcooling is pumped through an annular flow channel formed by a quartz test section and a directly heated rod located in the center, as shown in Figure 16 (left). The quartz window allows for flow visualization of boiling phenomena and the CHF event via high-speed photography. In steady-state flow-boiling tests, the imposed power across the rod is slowly increased until CHF is achieved.
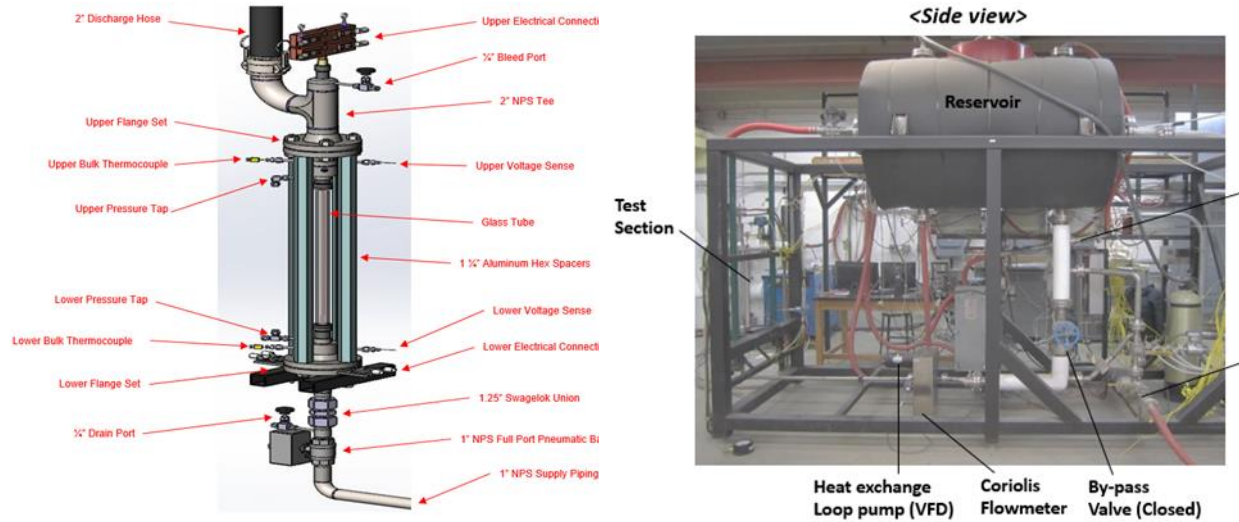
Figure 16. Low-pressure test section (left) and low-pressure flow loop (right) (UWM-2).

To measure the temperature profile along the heated rod, UWM-2 designed and fabricated an optical-fiber sensor and the accompanying data-acquisition system for distributed-temperature measurement. UWM-2 operated the optical-fiber sensor in flow-boiling experiments using Cr-coated and bare Zircaloy heater rods. UWM found that the Cr-coated heater rod has a slightly (~10%) higher heat-transfer coefficient (HTC) than Zircaloy heater rod, as shown in Figure 17.
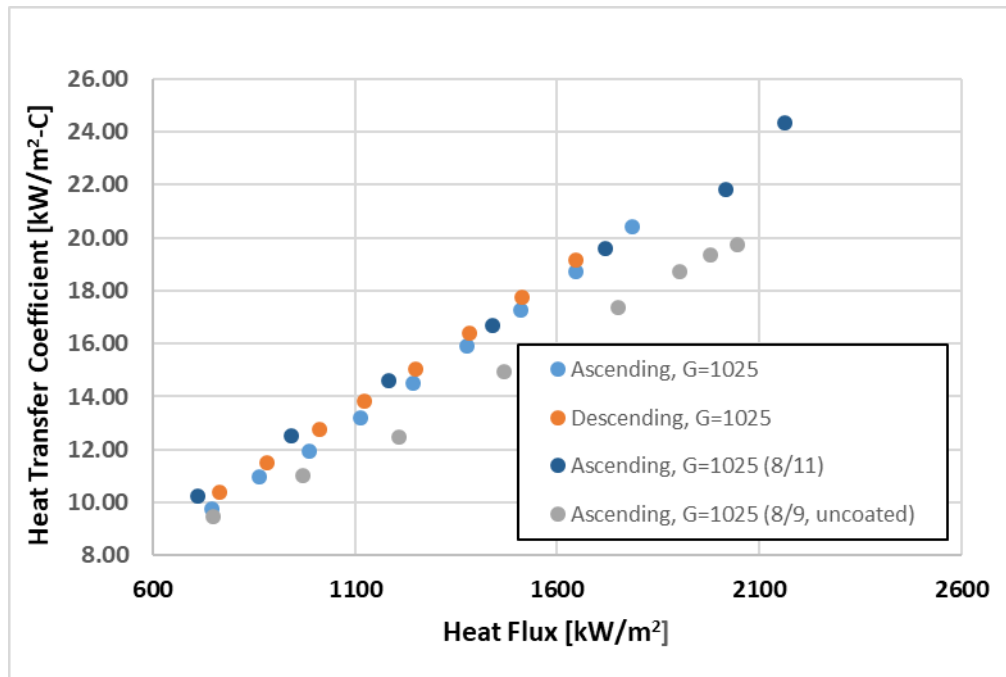
Figure 17. Comparison of rod-average HTC of Cr-coated (PVD) and bare Zircaloy heater rods (UWM-2). Pressure, subcooling, and mass flux are maintained at constant values of 115 kPa, 75°C, and 1025 kg/m^2-s, respectively. HTCs were studied in both ascending and descending heat flux to check for the presence of hysteresis effects; none were found. The Cr-coated rod exhibits ~10% improvement in HTC compared to uncoated rods (gray dots).

UWM-2 has finished initial testing of CHF for bare Zircaloy rods and two types (PVD and cold spray) of Cr-coated rod. Due to power-supply limitations, CHF tests were performed at mass flux of 750 kg/m²-s, 75°C subcooling, and 115 kPa pressure. CHF testing under these conditions (moderate mass flux and high subcooling) results in extreme temperature excursions, which typically destroy the heater rod. The bare zircaloy rod was destroyed during the first CHF test. Both Cr-coated rods survived their first CHF test and a second test was repeated on both, yielding similar CHF values (within 1.7% of the first CHF result). Figure 18 shows the heat-flux values at CHF, and Figure 19 shows the boiling curves for the three heater rods.
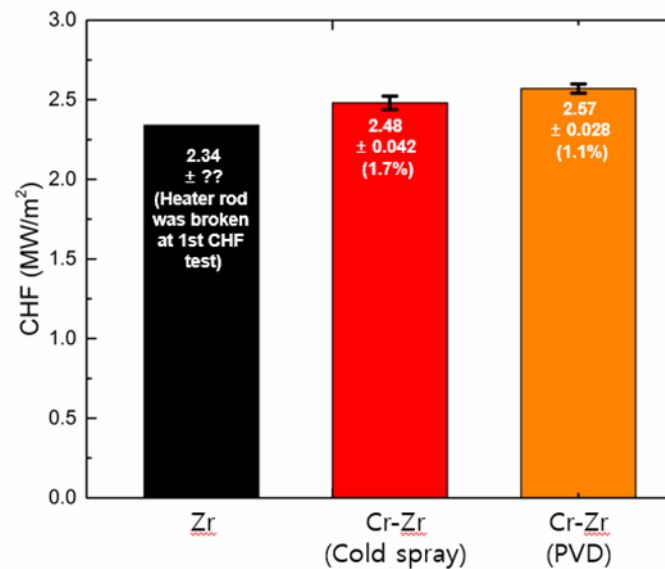

Figure 18. Heat flux values at CHF for bare Zircaloy and two types (PVD and cold spray) of Cr-coated Zircaloy.
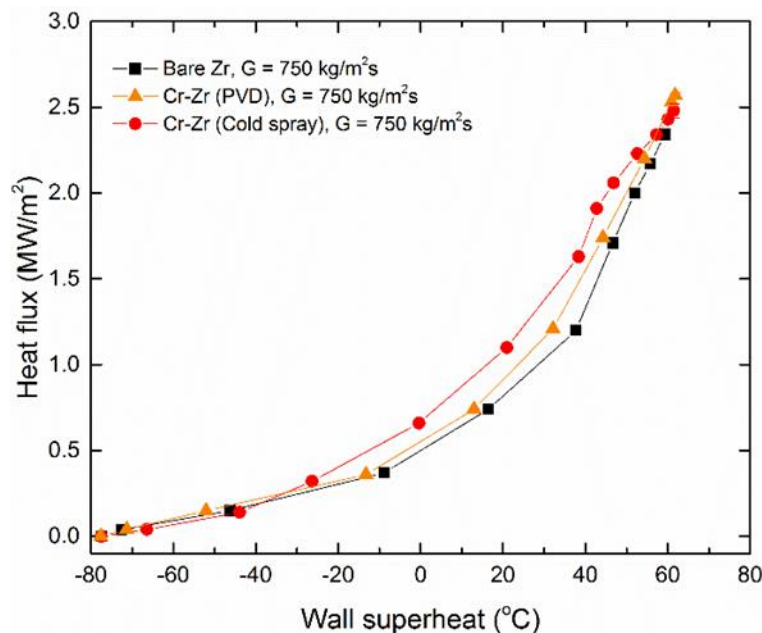

Figure 19. Boiling curves for bare Zircaloy and two types (PVD and cold spray) of Cr-coated Zircaloy. Pressure and subcooling were maintained at 115 kPa and 75°C, respectively.

Both UNM and UWM-2 have conducted flow-boiling experiments under atmospheric pressure. Their results provide a precious first look into the performance of ATF material in flow-boiling heat transfer and CHF. However, due to the non-prototypical operating pressure and temperature, it is still unclear whether their conclusions can be directly applied to actual reactor conditions. The main issue comes from the change of thermohydraulic properties—such as surface tension (and thus contact angle), two-phase density ratio, latent heat, thermal diffusivity, thermal effusivity—when pressure and temperature increase.

WEC conducted flow-boiling CHF tests at full PWR pressure and temperature. The coolant used during the CHF tests simulates water chemistry in an actual PWR. It contained 1000 ppm boric acid and 2.2 ppm LiOH, made from high-purity deionized water. WEC believes that water conductivity has a minimal impact on CHF results. The configuration of the flow loop, also known as the WALT loop, is shown in Figure 20. The main parameters of the WALT loop are summarized in Table 5. As shown in Figure 20 (right), the test section features an annular flow channel, which is formed by a direct-heating rod with OD of 9.5 mm and a test section shroud with inner diameter of 20.96 mm. The heated length is 330 mm.
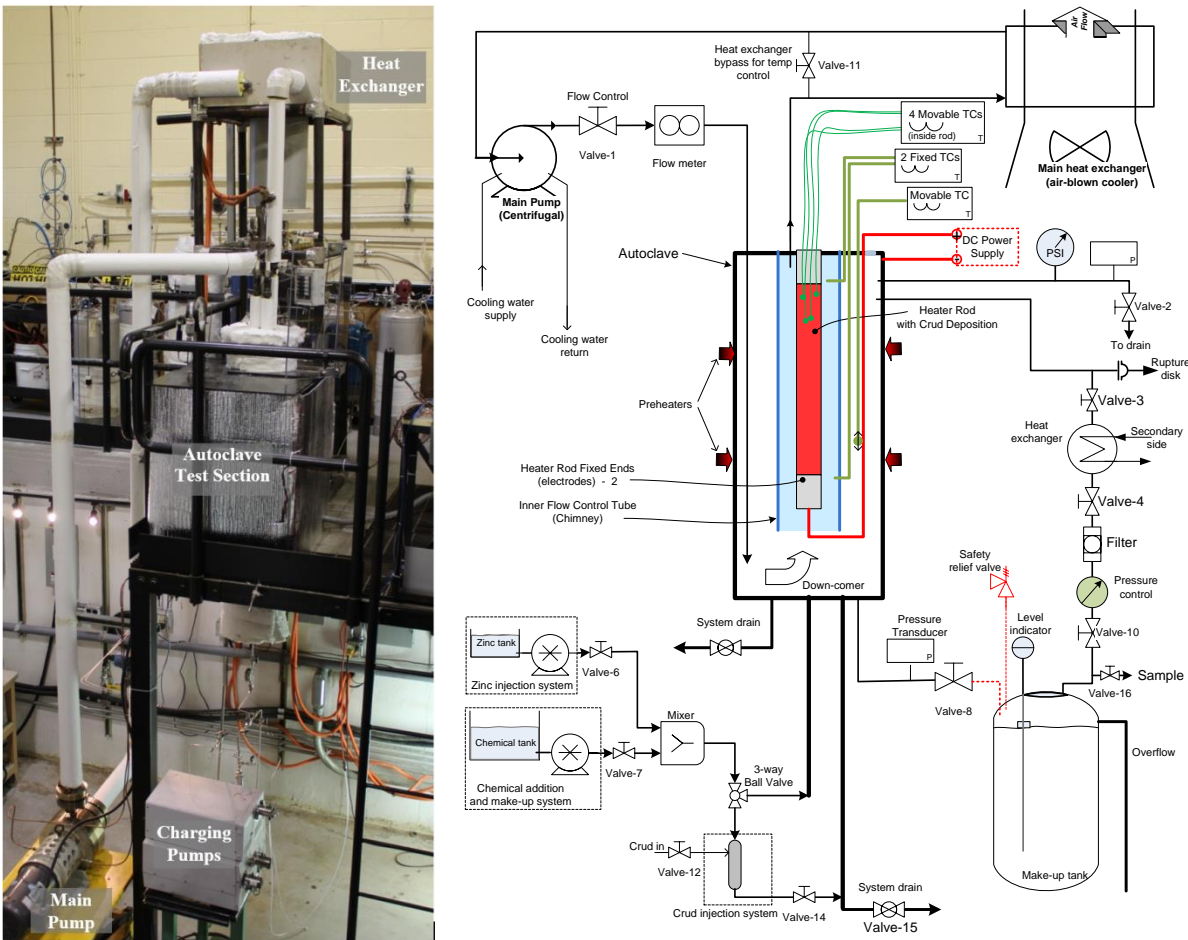

Figure 20. Photograh (left) and schematic representation (right) of WALT loop (WEC).

Table 5. Key parameters of the WALT loop (WEC).

Parameters	Upper Limits
System pressure, MPa	17.22
DC power supply, kW	90
DC power supply, A	1800
DC power supply, V	100
Heat exchanger, kW	31.8
Flow velocity, m/s	6.00
Inlet temperature, °C	<Tsat
Axial Power Shape	Uniform
Heater rod materials	Inconel, Zr-4, Zirlo®
Heater rod length, m	<1.35 (0.33 heated typical)
Heater rod OD, mm	9.50
Heater rod ID, mm	8.35~9.2
Test section shroud ID, mm	20.96
Test section flow area, mm^2	274.0

WEC has tested flow-boiling CHF in the WALT loop using uncoated Zirlo cladding, Cr-coated Zirlo cladding, and Cr-coated Zirlo cladding with crud. They generated crud deposits to the Cr-coated Zirlo by adding FeEDTA, NiEDTA, and colloidal crud precursors in the loop. All CHF test results and associated test conditions are summarized in Table 6.

The CHF test results shown in Table 6 were regrouped according to thermohydraulic conditions of inlet temperature, flow, and pressure, as indicated by yellow, green, and orange colors. Therefore, the separate effect of cladding surfaces, such as Cr-coating and crud deposit, can be examined within the same color group. As shown in Figure 21, the change of CHF due to the Cr-coating and/or crud deposit seems to be within the CHF variation measured from the uncoated surface. The CHF variation in each group is approximately ±6%.

Table 6. Summary of CHF test results (WEC).

Rod	Run	Cr Coating	Average Crud Thickness (microns)	Inlet Temperature (°C)	Flow (m³/hr)	Pressure (bars)	CHF (W/cm²)	Relative Change in CHF Compared to Average
198	1a	No	0	336.8	2.42	152.63	233.12	4.74
198	1b	No	0	339.5	2.37	154.05	208.94	-6.12
198	1c	No	0	338.7	2.42	156.58	221.22	-0.60
193	1a	Yes	0	338.1	2.38	148.78	231.16	3.86
193	1b	Yes	0	338.1	2.40	158.99	218.37	-1.86
Average				**338.2**	**2.40**	**154.21**	**222.56**	

28

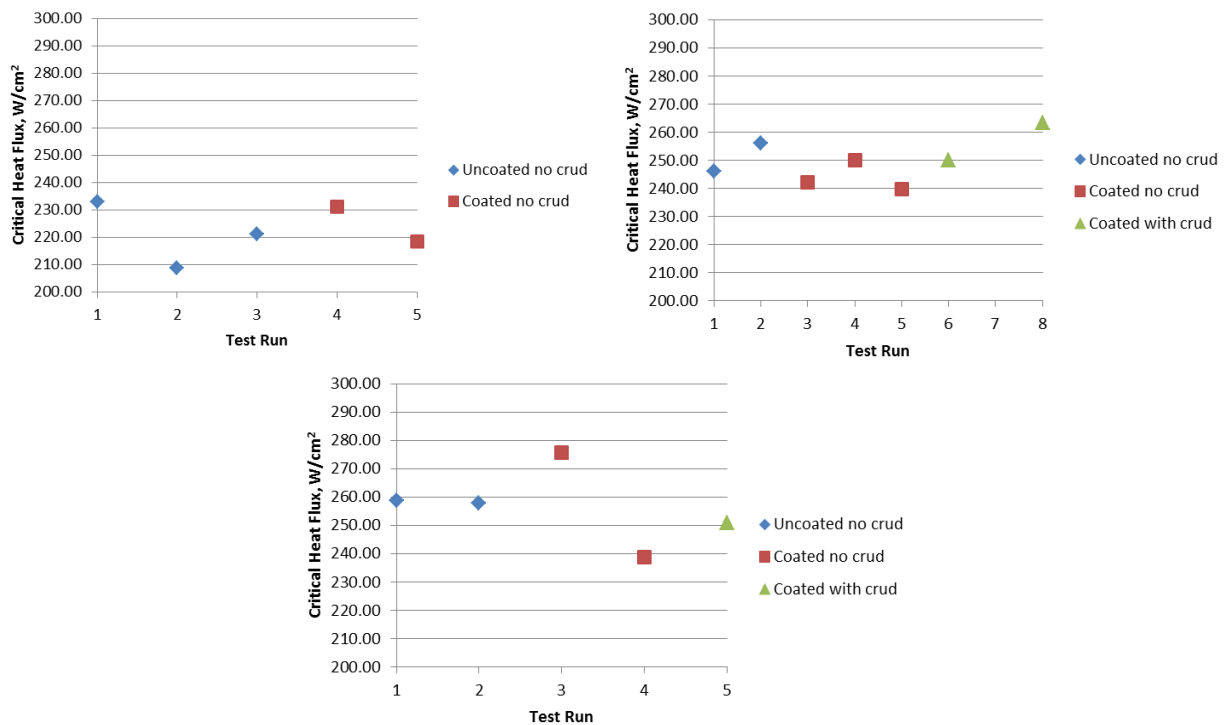| Rod	Run	Cr Coating	Average Crud Thickness (microns)	Inlet Temperature (°C)	Flow (m³/hr)	Pressure (bars)	CHF (W/cm²)	Relative Change in CHF Compared to Average
198	2a	No	0	333.9	3.49	156.21	245.91	-1.37
198	2b	No	0	340.6	3.49	156.72	256.16	2.74
194	1a	Yes	0	339.9	3.39	153.88	241.95	-2.96
195	1a	Yes	0	339.6	3.37	151.78	249.99	0.26
200	1a	Yes	0	338.8	3.39	153.46	239.53	-3.93
200	1b	Yes	43	341.7	3.38	155.16	249.97	0.26
201	1a	Yes	0	339.2	3.38	156.94	247.82	-0.61
201	1b	Yes	40	339.4	3.41	156.86	263.32	5.61
Average				**339.9**	**3.41**	**155.13**	**249.33**	
198	3a	No	0	329.1	3.34	128.57	258.74	0.92
198	3b	No	0	328.3	3.41	125.08	257.88	0.58
199	1a	Yes	0	328.7	3.22	126.78	275.70	7.53
202	1a	Yes	0	330.6	3.00	127.90	238.65	-6.92
202	1b	Yes	21	331.1	3.25	130.52	250.97	-2.11
Average				**329.5**	**3.24**	**127.77**	**256.39**	

Figure 21. Comparison of CHF values from different surfaces at similar thermohydraulic conditions. Top left: yellow group; top right: green group; bottom: orange group (WEC).

3.4 Modeling and Simulation

UTK simulated the UNM experiment using RELAP5-3D and CTF, finding significant discrepancies between calculation and experimental data in terms of CHF and post-CHF tube temperatures for

Inconel 600, stainless steel 316, and FeCrAl. Parametric studies were carried out to understand the sensitivity of CHF and the post-CHF temperature excursion from HTCs, material thermophysical properties, and a transient CHF multiplier. Sensitivity studies were performed using a RELAP5-3D model of the UNM experiment and the uncertainty quantification code RAVEN. The range of input parameters used in sensitivity studies was chosen based on the measuring uncertainties in material properties and HTCs, as well as the differences in experimentally measured HTCs and the HTCs predicted from the RELAP5 model. Results from the sensitivity study were used to highlight fundamental differences between how CHF is modeled and empirical findings.

The sensitivity cases that best matched the experimental results in terms of maximum heat flux (MHF), integral heat flux, and peak cladding temperature (PCT) were determined, as was a case that gave the minimum RMS error for the three figures of merit. Table 7 summarizes the relative error of the RELAP5 results from the sensitivity case that gave the minimum RMS error.

Table 7. Error from the minimum RMS error sensitivity case.

Figure of Merit	MHF	PCT	Energy Deposition	RMS Error
Relative Error (%)	1.24	27.02	1.70	27.10

The parametric study showed that even when the simulated MHF and energy deposition were closely matched with the experimental results, the model still overpredicted PCT. The reason for this remaining discrepancy is attributed to differences in how CHF phenomena are being modeled versus what occurs in reality. Figure 22 (a) shows the experimental heat flux and FeCrAl outer surface temperature around the CHF point. The plot shows that the CHF, determined by an increase in the rate of change in the tube temperature, differs from the MHF. It is possible that this is a product of measurement uncertainty, but it is clear that there is a transition period during which the heat flux remains elevated post-CHF. Computer codes always consider the MHF and CHF to be equivalent, as shown in Figure 22 (b). Once CHF is reached in the models, the heat flux instantaneously and rapidly declines. This leads to a much narrower heat-flux pulse width and the overshoot in PCT predictions.
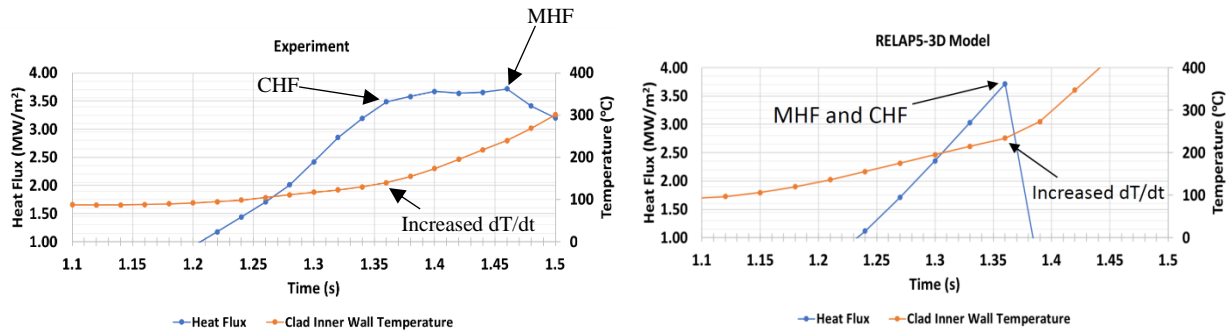

Figure 22. (a) Experimental heat flux and tube temperature and (b) simulated heat flux and tube temperature. (UTK)

Motivated by reducing the high cost of running CHF tests that cover a wide range of operating conditions, UNM explored a machine-learning algorithm for practical interpolation and extrapolation of experimentally measured CHFs so as to inform a strategic scheme of CHF experiment for such technology implementation. Figure 23 demonstrates the capitalization on sparingly distributed experimental data. Machine learning (support vector machine [SVM]) shows the capability to accelerate the development of CHF look-up tables or correlations with high accuracy ($R^2 \geq 0.95$). The rationales behind the CHF predictability of SVM are that the kernel function can map the nonlinear relation of CHF to pressure and mass flux into a linear relation of high-dimensional space. The automatic determination of support vectors can provide the importance weights of training data, and then the prediction of CHF will

be provided by locally calculating the similarities among the prediction target, training data, and globally summed weighted CHF of training datasets.
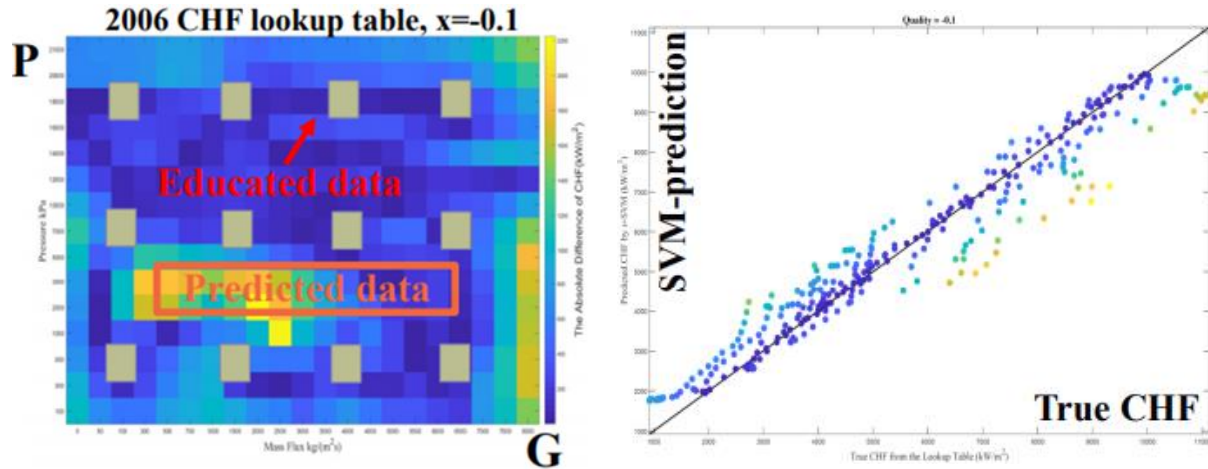

Figure 23. (a) CHF prediction with 12 evenly distributed educated data and (b) comparison of machine-learning prediction to true CHF (UNM).

For pressure-dependent CHF behavior, training data in the proximity of the pressure inflection point that characterizes the maximum allowable CHF for different pressures significantly contribute to the prediction accuracy of the SVM. This implies that experimental CHF data should be procured in the proximity of pressure inflection points, and the prior knowledge of pressure-CHF inflection points can enhance the prediction accuracy of the ATF CHF look-up table. Moreover, the linearity of CHF with respect to mass flux determines prediction accuracy in the absence of a good spread of training data.

Another advantage of the SVM application for CHF prediction is that extrapolation to high pressure from low can be effectively achieved with a few data points in the high-pressure range, as shown in Figure 24. This shows the possibility of strategically integrating high- and low-pressure experimental data to construct a new CHF look-up table while reducing the experimental costs associated with the high-pressure testing.
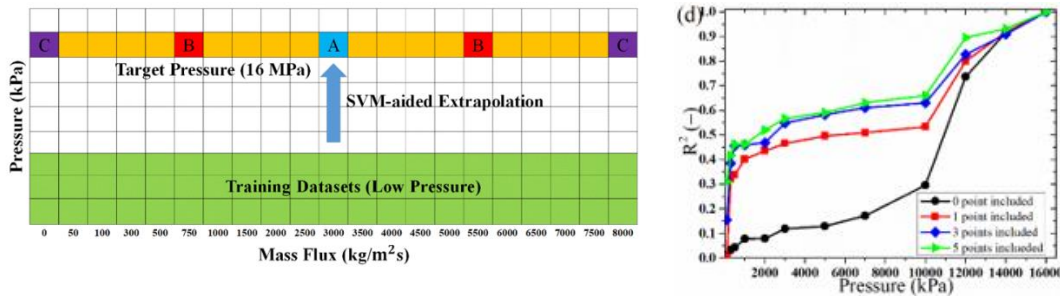

Figure 24. (a) High-pressure extrapolation strategy and (b) SVM supported extrapolation at Xe = - 0.05 (UNM).

3.5 Quenching

Many studies have investigated rewetting of heated samples in reflooding scenarios. Droplet quenching is another important phenomenon that occurs during safety spray cooling—e.g., in a BWR. The spray-cooling system generates tiny droplets on the millimeter scale, which then impinge and quench the fuel-cladding surfaces. Different from pool quenching, droplet quenching is a scarcely investigated phenomenon, especially on ATF materials.

MIT constructed and operated a test facility for droplet-quenching experiments, as shown in Figure 25. The experimental setup enables the use of synchronized infrared (IR) thermometry and high-speed shadowgraphy, which provides high temporal and spatial resolution for quenching heat-transfer measurement. The test sample is in direct contact with a heater, which is used to control the sample temperature. A through-hole in the center of both the heater and the supporting insulation structure allows IR measurements of time-dependent test-sample temperature and heat-flux distributions. The side view of the droplet-wall collision is recorded by high-speed video (HSV). The IR camera and HSV are carefully synchronized to record the droplet-collision behavior.
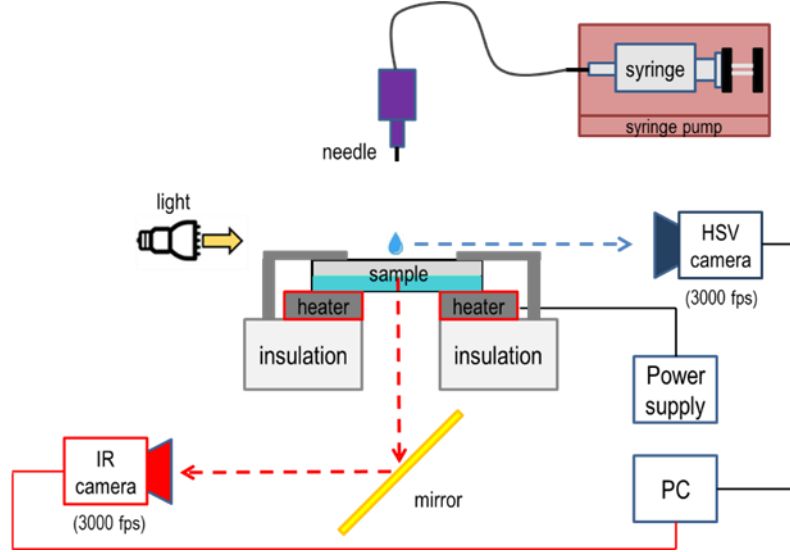

Figure 25. Schematics of the droplet quenching experiment (MIT).

MIT fabricated the test sample by PVD-deposition using different coating materials on circular sapphire substrates. Sapphire is an excellent simulant of Zircaloy, as they have very similar thermal effusivity and diffusivity. In the tests shown in Figure 26 and Figure 27, a 300 nm Cr coating was used. The test temperature ranges typically from 100 to 500°C. After the test sample reaches the desired steady-state temperature, a deionized water droplet, of 2.0 mm diameter, is released from the needle. It falls by gravity and impinges on the sample. In the reported test, a deionized water droplet with a small Weber number (7.3) at room temperature (75 K subcooling) was used.

IR videos from the droplet-quenching test were post-processed with an in-house MATLAB code to reproduce time-dependent temperature and heat-flux distributions of the sample surface. Figure 26 and Figure 27 show temperature profiles (top row) and high-speed video images (bottom row) during the droplet collision at different sample temperatures. The Leidenfrost temperature can be determined based on shadowgraphy images as well as on the temperature and heat-flux distributions. More tests will be run to fully quantify how the LFP temperature depends on Weber number, droplet temperature and, importantly, surface conditions (i.e., material and roughness).
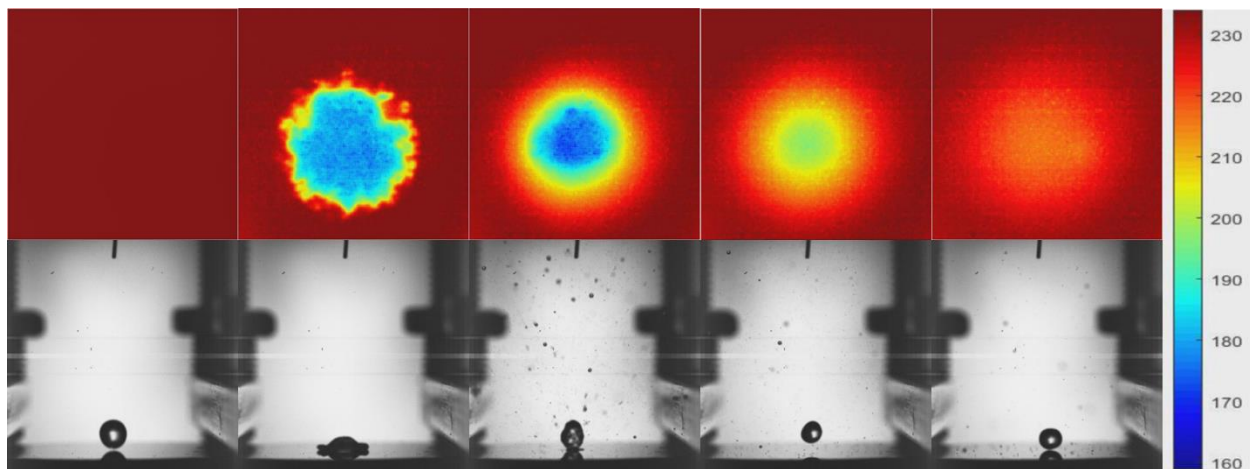
Figure 26. Droplet quenching at transition boiling (240°C). Temperature color scale in °C (MIT).
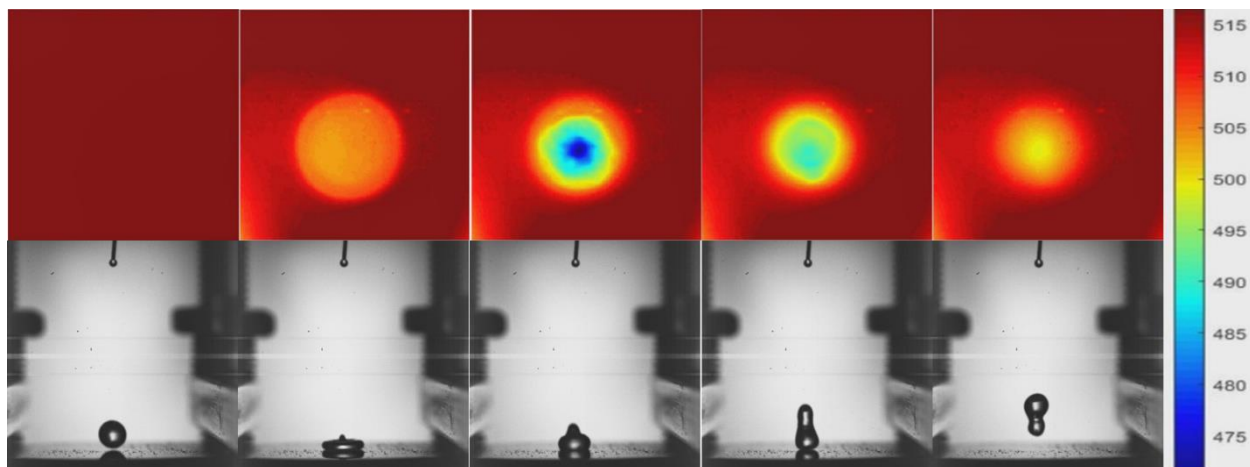

Figure 27. Droplet quenching at film boiling (520°C). Temperature color scale in °C (MIT).

UWM-1 designed and constructed a quenching test facility that was used to demonstrate boiling heat transfer of modified surfaces under high-pressure and subcooled-water conditions. Figure 28 shows a schematic illustration of the facility. UWM proposed to use such a facility to study the effect of ATF materials' surfaces on the minimum film boiling point and the associated heat-transfer processes.
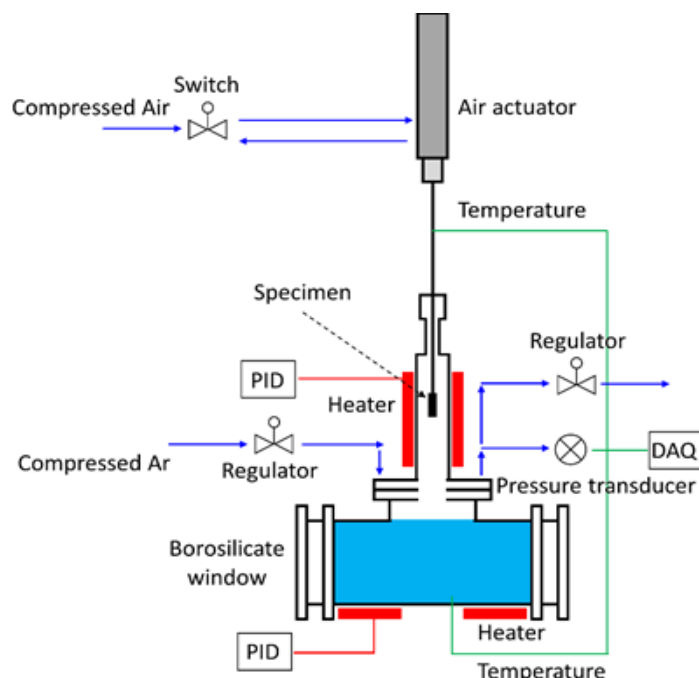
Figure 28. Schematic illustration of the quench-test facility to evaluate boiling heat transfer of various ATF cladding surfaces under high-pressure and subcooled-water conditions (UWM).

4. CONCLUSIONS

This report discusses the main achievements of four NEUP projects aimed at investigating the thermal-hydraulic behavior of ATF-cladding materials. Lesson learned and near-term—i.e., to be carried out within the last year of the four NEUP projects—activities are summarized hereafter.

4.1 Surface Characterization

Many groups have measured the CAs of ATF materials in the air at atmospheric pressure. However, there seems to be some disagreement on the measured CA from the same material with similar surface roughness. These differences may arise from the sample-cleaning protocol or the surface itself. To address and potentially clarify this issue, samples could be circulated and analyzed by more than one organization.

The CA varies significantly from ambient pressure and temperature to LWR operating conditions. Such variation has been partially clarified by MIT's tests. Systematic CA measurements on ATF materials (from the four projects) with different surface roughness could be conducted under LWR conditions using the MIT facility. The effect of surface degradation during the high-pressure measurements should be evaluated to better understand the CA hysteresis observed with some materials.

4.2 Boiling

An analysis of the impact of surface characteristics on CHF has been conducted. However, more experiments should be run before definite conclusions can be drawn.

In pool-boiling conditions at atmospheric pressure, the CHF values measured by UWM-1 suggest that Zirlo, FeCrAl, and Cr-coated Zirlo have very similar CHF and that the CHF limit can be captured by a modified version of the Kandlikar correlation.

However, UNM performed flow-boiling CHF tests at atmospheric pressure and observed that FeCrAl has a higher CHF limit compared to Zircaloy or Cr-coated Zircaloy at the same operating conditions.

UNM also observed that surface degradation, e.g., the increase of surface roughness and wettability, does not affect the CHF limit. UNM also conducted a test with a transient power pulse on FeCrAl tubes and observed that the transient CHF value is higher than the steady-state value.

UWM-2 has carried out studies on steady-state flow boiling on Cr-coated and bare Zirlo cladding, and has observed that the Cr-coated cladding has a higher boiling HTC and a slightly higher CHF compared uncoated claddings.

WEC conducted several flow-boiling CHF tests at PWR operating conditions, showing no difference in the CHF values of bare, Cr-coated, and crud-coated Zirlo claddings.

More tests will be carried out in the third year of the project by WEC and UWM-2, with a specific focus on high pressures, ideally covering both PWR (15.5 MPa, 344°C) and BWR (7.6 MPa, 291°C) conditions.

4.3 Modeling and Simulation

UTK has generated a computational framework to simulate flow boiling until post-CHF. UTK quantified the uncertainty and sensitivity of the CHF value and the post-CHF temperature excursion. According to the UTK analysis, there is a need to improve the modeling of post-CHF heat transfer during power transients. However, the development and validation of these models require more experimental data, particularly for high-pressure conditions.

4.4 Quenching

MIT has developed a facility to study droplet quenching, producing demonstrative results on Cr-coated surfaces. A systematic study will be carried out to quantify the LFP temperature of potential ATF materials. For each material, different surface finish from nanosmooth to PWR-cladding roughness should be tested. The impact of droplet Weber number and subcooling should also be investigated.

Appendix A

Program:
Thermal-Hydraulics of ATF Cladding Materials

Appendix A

Program:
Thermal-Hydraulics of ATF Cladding Materials

Thermal-hydraulics of Accident Tolerant Fuel cladding materials
NEUP-ATF meeting

Room 24-213
MIT, 77 Massachusetts Avenue, Cambridge, MA 02139
August 13, 2019

Opening 9 AM – Closure 5 PM

9:00 **Welcome + coffee**

9:05 AM
Introductory remarks
P. Sabharwall

9:15 AM
Critical Heat Flux Studies of Advanced Accident Tolerant Fuel Cladding Concepts
S. Yeom, K. Sridharan, M. Corradini

9:45 AM
ATF testing in UW-Madison flow loops
B. Elward, M. Anderson

10:15 AM
Flow CHF with various tube materials
Y. Lee, N. Brown

10:45 AM **Coffee break**

11:00 AM
Sensitivity of Critical Heat Flux for ATF FeCrAl Alloy
N. Brown, J. Gorton

11:30 AM
Wettability of ATF cladding materials in nuclear reactor conditions
A. Jena, A. Kossolapov, B. Phillips, M. Bucci

12:00 PM
Progress on the surface characterization of ATF and preliminary results on CHF
J.R. Marin

12:30 PM

Investigation of Droplet Quenching on Accident Tolerant Coatings Using Infrared Thermometry

H. Kim, W. McGee, A. Kossolapov, B. Phillips, M. Bucci

1:00 PM

WALT Loop CHF testing for ATF Cladding

G. Wang, Z. Karoutas

1:30 PM **Lunch break**

2:15 PM

Tour of The Red Lab and other "ATF" facilities in NSE

The Red Lab

- **PEThER loop**: 10 bar, 180 °C, 2000 kg/m^2/s
- **LWR loop**: full PWR pressure, temperature and mass flux
- **Autoclave CA facility**: up to 221 bar at steam saturated environment
- **Quenching facility**: up to 500 °C

The Green Lab

- **Oxidation Column**: superheated steam up to 1500 °C
- **KAPL loop**: all flow regimes up to annular flow

3:30 PM

In-Pile CHF Experiments at TREAT and related Activities.

C. Folson, C. Jensen

4:00 PM

Coordination of NEUP projects and proposal for joint publications

P. Sabharwall, M. Bucci

4:15 PM

Discussion

Moderated by P. Sabharwall, M. Bucci

5:00 PM **Adjurn**

Participants

Mark Anderson	UWM	manderson@engr.wisc.edu
Nick Brown	UTK	nbrown49@utk.edu
Matteo Bucci	MIT	mbucci@mit.edu
Barret Elward	UWM	elward@wisc.edu
Charlie Folsom	INL	charles.folsom@inl.gov
Jake Gorton	UTK	jgorton@vols.utk.edu
Zeses Karoutas	WEC	karoutze@westinghouse.com
Haeseong Kim	MIT	haeseong@mit.edu
Youho Lee	SNU	leeyouho@snu.ac.kr
Bren Phillips	MIT	bren@mit.edu
Jessika Rojas Marin	VCU	jvrojas@vcu.edu
Piyush Sabharwall	INL	piyush.sabharwall@inl.gov
Kumar Sridharan	UWM	kumar.sridharan@wisc.edu
Guanyu Su	MIT	gysu@mit.edu
Daniel M. Wachs	INL	daniel.wachs@inl.gov
Guoqiang Wang	WEC	wangg@westinghouse.com
Sung Yeom	UWM	hyeom@wisc.edu

WebEx

Christian Deck	GA	christian.deck@ga.com

Appendix B

Critical Heat-Flux Studies of Advanced Accident-Tolerant Fuel-Cladding Concepts

Appendix B

Critical Heat-Flux Studies of Advanced Accident-Tolerant Fuel-Cladding Concepts

CRITICAL HEAT FLUX STUDIES OF ADVANCED ACCIDENT TOLERANT FUEL CLADDING CONCEPTS

Hwasung Yeom, Emilio Guiterrez, Kumar Sridharan, Hangjin Jo, Yimin Zhou, Michael Corradini*

Nuclear Engineering & Engineering Physics
University of Wisconsin, Madison WI

NEUP-ATF Meeting at MIT

August 13th, 2019

1

41

Presentation Outline

1. Introduction
   - Project Overview
   - Surface Effects on CHF
2. Experimental
3. Results
   - Coated Zirlo Samples
   - SiC Samples
4. Concluding Remarks
5. Publications

Acknowledgement

Introduction

Project Overview

- **Objective**
  - Investigating CHF for surfaces of ATF cladding materials that are presently being considered for implementation jointly by industry, utilities, and DOE.

- **Tasks**
  - Task 1: Preparation of candidate ATF cladding materials' heat transfer surfaces
  - Task 2: Surface characterization of candidate ATF cladding materials
  - Task 3: Pool boiling tests of candidate ATF cladding materials
  - Task 4: Flow boiling tests of ATF cladding materials under prototypical reactor conditions
  - Task 5: Modeling of boiling and CHF for ATF cladding surfaces

- **Material of Interest**
  - **Zirlo®, Cr coatings, FeCrAl coatings, CVD SiC, SiC-SiC$_f$ composite**

Boiling and Critical heat flux (CHF)

Parameters: Fluid, Pressure, Subcooling, mass flow rate **& surface/material effects**

[wettability, thermal-physical properties, surface structure/roughness]

Boiling curve with ONB, CHF, and MHF
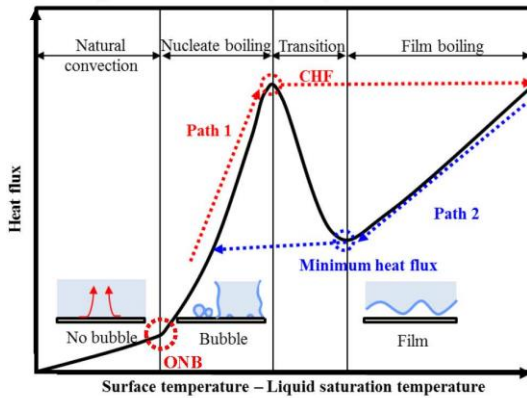
High speed camera visualization (near CHF)
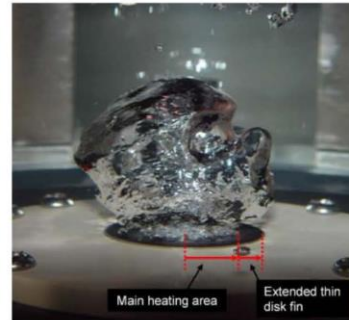
Kim et al., JHT, vol. 132, pp. 061501 (2010)

The surface change could affect boiling associated with TH nuclear reactor limits

6

Surface parameters with CHF :
1. Wettability

In prior work, heated surface wettability effect has been studied. Receding contact angle (dynamic contact angle) would be the representative contact angle for CHF

SiO_2 smooth 63° SiO_2 nanostructure ~10° Teflon smooth 120° Teflon nanostructure ~170°

Ahn et al., APL, vol. 98, pp. 071908 (2011)
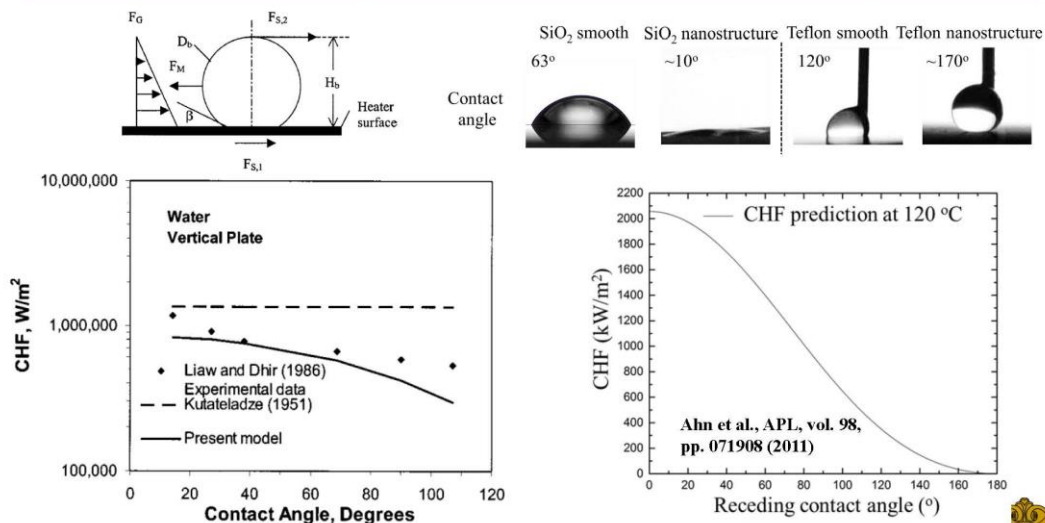
7 **Kandlikar, J. Heat Transfer, Vol. 123, pp. 1071 (2001)**

Surface parameters associated with CHF:
2. Thermophysical Properties of Heater

**Larger surface thermal conductivity inhibited formation of hot spots, increasing CHF**
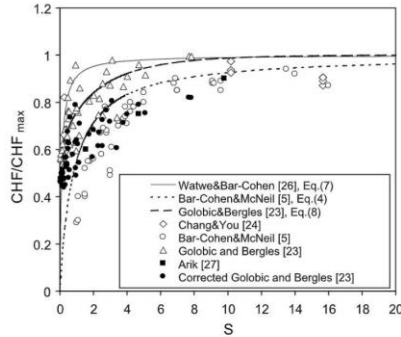
Fig. 9. Variation of the non-dimensional experimental pool boiling CHF values with thermal activity parameter.

IR images of heating surfaces at boiling at 98% of the CHF of the bare silicon surface

Bare Si

Graphene coated Si

Thermal activity = Thickness x √thermal effusivity

$$S = \delta_w \sqrt{\rho_w C_{p.w} k_w} \qquad \frac{q''_{CHF}}{q''_{max}} \propto \frac{S}{S+C}$$

Arik, M. & Bar-Cohen, A. Int. J. Heat and Mass Trans. 46, 3755–3764 (2003).
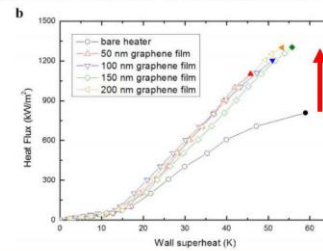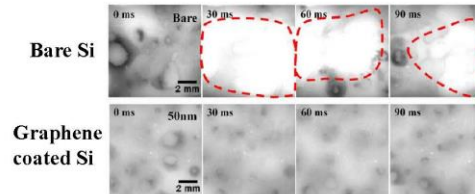
8

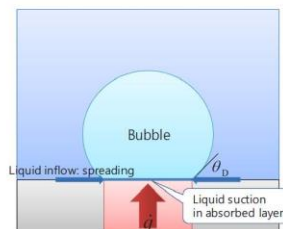Ahn et al., Scientific Reports, vol. 4, pp. 6276 (2014)

Surface parameters associated with CHF:
3. Surface Morphology (nano/micro-structure)

Capillary wicking phenomena enhances CHF on nanostructured surfaces

Nano/Micro (NM)
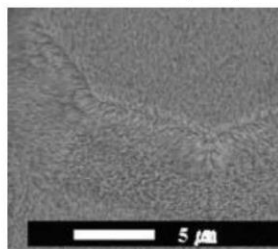
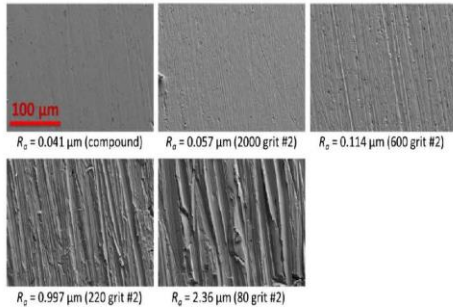Capillary wicking
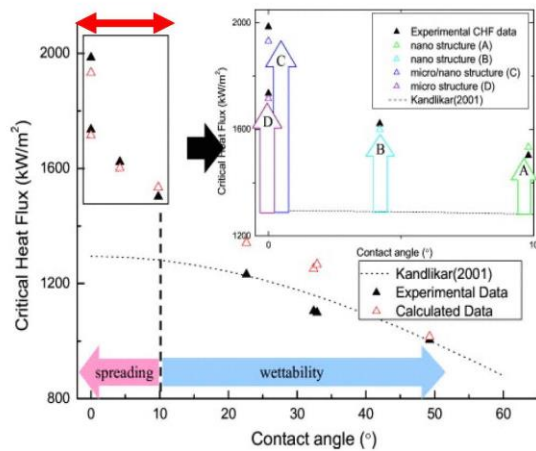
9

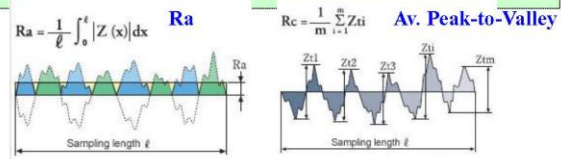Ahn et al., APL, vol. 98, pp. 071908 (2011)

Increasing surface roughness enhanced CHF, possibly due to capillary wicking effect and enhanced nucleation site density

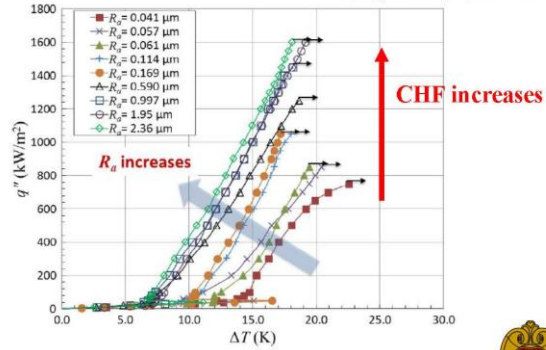**Roughness is a subset of surface morphological parameters**

$$Ra = \frac{1}{\ell} \int_0^\ell |Z(x)| dx \qquad \textbf{Ra}$$

$$Rc = \frac{1}{m} \sum_{i=1}^{m} Zti \qquad \textbf{Av. Peak-to-Valley}$$

https://www.olympus-ims.com

100 μm

$R_a = 0.041$ μm (compound) $R_a = 0.057$ μm (2000 grit #2) $R_a = 0.114$ μm (600 grit #2)

$R_a = 0.997$ μm (220 grit #2) $R_a = 2.36$ μm (80 grit #2)

Copper surfaces polished by sand papers

Copper blocks of size 10 mm x 10 mm x 3 mm

- $R_a = 0.041$ μm
- $R_a = 0.057$ μm
- $R_a = 0.061$ μm
- $R_a = 0.114$ μm
- $R_a = 0.169$ μm
- $R_a = 0.590$ μm
- $R_a = 0.997$ μm
- $R_a = 1.95$ μm
- $R_a = 2.36$ μm

CHF increases

R_a **increases**

10

Kim et al., IJHMT, vol. 101, pp. 992-1002 (2016)

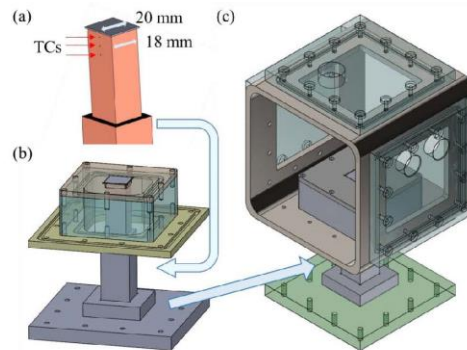# Pool Boiling Experiment and Surface Characterization at Univ. Wisconsin-Madison

11

Pool boiling facility
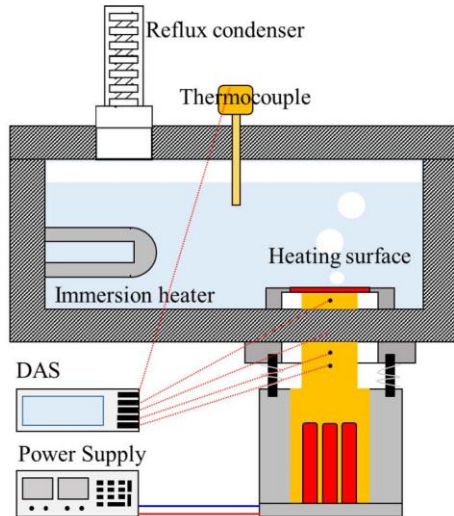
**Heater block and sample (2 x 2 cm)**

Pool chamber (14 x 14 x 14 cm³)

12

- Heating deionized water in the boiling pool at atmospheric pressure (degassing for one hour)

- Cartridge heaters generate heat embedded in a copper block, transferring heat to a sample flat

- Three thermocouples installed in the copper block measure temperature for heat flux calculation

- The power level was step-wisely increased until the thermocouple temperature abruptly increases and the measured heat flux decreases
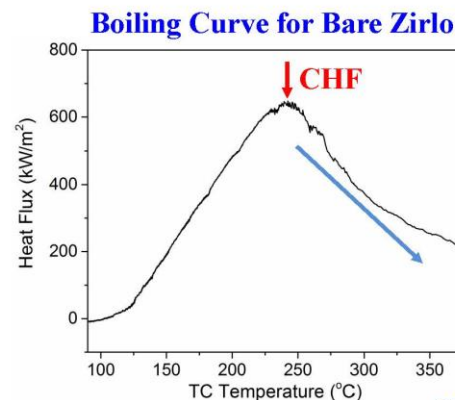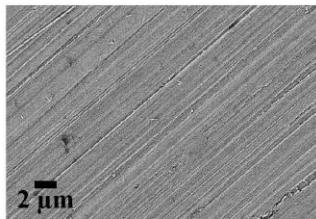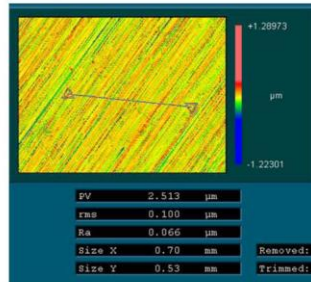

Boiling Curve for Bare Zirlo

13

47

Surface Characterization

Scanning electron microscope (SEM)

Optical profilometer

Contact angle measurement

PV	2.513	µm	
rms	0.100	µm	
Ra	0.066	µm	
Size X	0.70	mm	Removed:
Size Y	0.53	mm	Trimmed:

14

Experimental Results

Coated Samples
SiC Samples

15

Coating Fabrication (Cold Spray Process)

ZIRLO | Cold spray Cr coated ZIRLO | Cut samples | Polished sample

Cr

Before spray | **After spray**
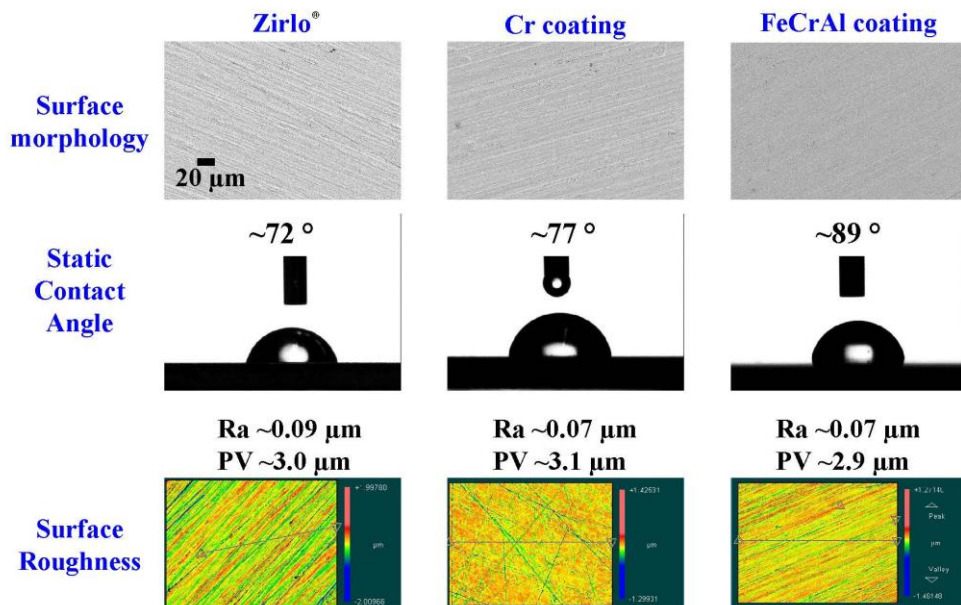
FeCrAl
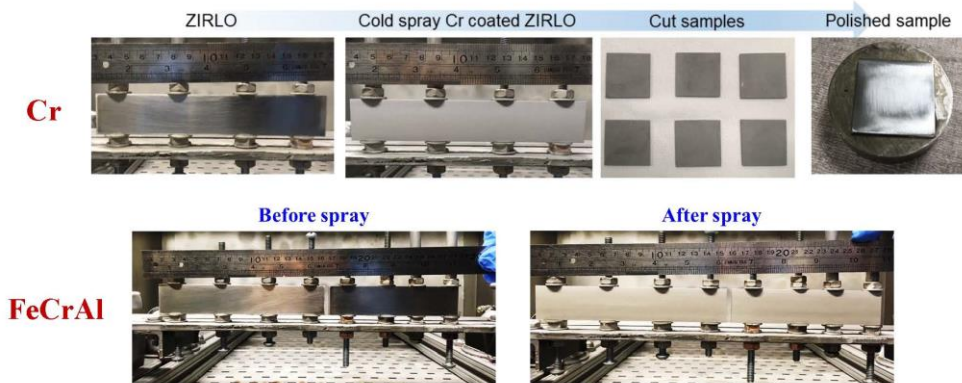
- Substrate: 0.8 mm Zirlo® Sheet
- Pure Cr powder and Fe20Cr5Al powder
- Surface finishing
  - Thickness down to 30 and 70 μm using <u>600 grit SiC abrasive paper</u>

16

Surface Characteristics of Coated Zirlo® Samples

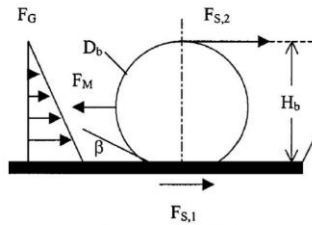|	Zirlo®	Cr coating	FeCrAl coating
Surface morphology	20 μm		
Static Contact Angle	~72°	~77°	~89°
Surface Roughness	Ra ~0.09 μm PV ~3.0 μm	Ra ~0.07 μm PV ~3.1 μm	Ra ~0.07 μm PV ~2.9 μm

17

49

Summary of CHF Data

Results for smooth surfaces were well described with contact angle effect on CHF

$$q''_{CHF\_Kandlikar} = \rho_g^{0.5} h_{lg} \left(\frac{1+\cos\beta}{16} \right) \cdot \left[\frac{2}{\pi} + \frac{\pi}{4}(1+\cos\beta) \right]^{0.5} [\sigma g(\rho_l - \rho_g)]^{0.25} * S \; (=0.823)$$

Modified Kandlikar's model based on Ahn et al., APL, 2011

Kandlikar, J. Heat Transfer, Vol. 123, pp. 1071 (2001)
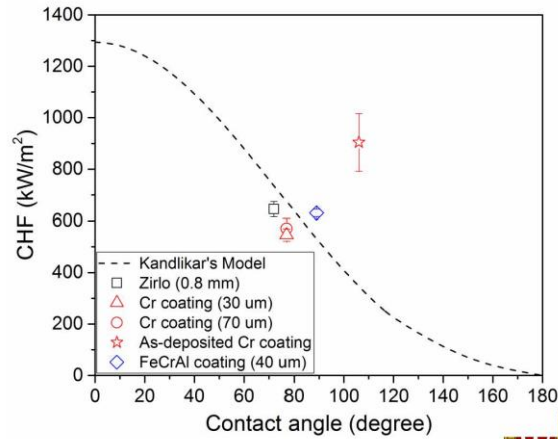
18

Thermo-Physical Measurement

- **No significant change of thermo-physical properties due to the thin surface coating**
  - Substrate: 0.8 mm Zirlo® Sheet
  - Cr coating thickness was ~ 100 μm

| Material	Temperature (°C)	Thermal conductivity (W/mK)	Heat capacity (Cal/gK)	Density (g/cc)
Zirlo®	24	13.5-13.6	0.065	6.552
Zirlo®	200	15.4-15.7	0.075	6.552
Cr coated Zirlo®	24	15.0	0.075	6.606
Cr coated Zirlo®	200	15.7-16.0	0.081	6.606

- **Thermal conductivity: Laser flash thermal conductivity method**
- **Density: Archimedes Principle**
- **Heat capacity: Differential scanning calorimetry (DSC)**

19

50

CHF as a function of heater thermo-physical properties

Thermo-physical properties of heater affect CHF values
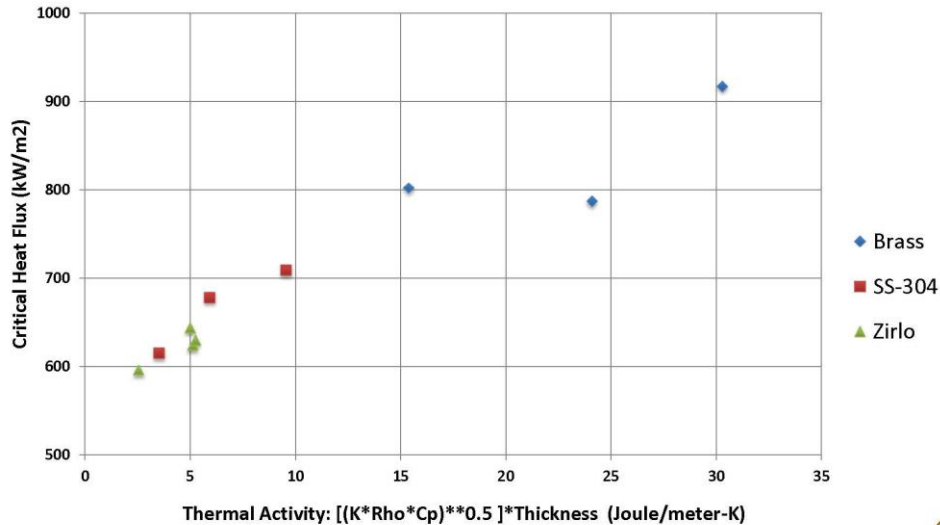
H. Jo, et al, ANS Transactions, Minneapolis MN (2019)   H. Jo, et al, ANS Transactions, Orlando FL (2018)

Comparison with Literature (Pool Boiling Test at DI Water)

Other factors (e.g., surface condition, base material, heater size) should be also considered

Authors	Materials (Coating/Substrate)	Coating technique	CHF change	Note
UW	Cr/Zirlo flat	Cold spray	-15%	30 μm coating Conduction heating
UW	FeCrAl/Zirlo flat	Cold spray	-2%	40 μm coating Conduction heating
Seo et al, 2016	FeCrAl/SS316 flat	DC sputter	+40%	1 μm coating Joule heating Coating cracks
Son et al., 2017	Cr/SS316 flat	DC sputter	+79%	1 μm coating Joule heating Superhydrophilicity
Son et al., 2019	Cr/SS316 tube FeCrA/SS316 tube (L: 10cm)	DC sputter	+27% (Cr) +34% (FeCrAl)	1.5 μm coating Joule heating Near zero contact angle
Kam et al., 2014	SiC/Zircaloy flat Cr/Zircaloy flat	DC sputter (SiC) Electroplating (Cr)	+56% (SiC) -30% (Cr)	1 μm coating Joule heating

21

51

Conventional PVD Cr Coatings

Sputter Cr coating process leaves inherent micron-scale surface structure resulting from coating growth mechanism, likely influencing CHF

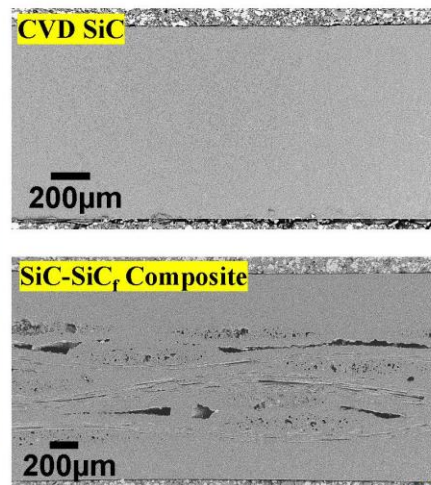**SEM images of as-deposited PVD Cr coating developed at UW**
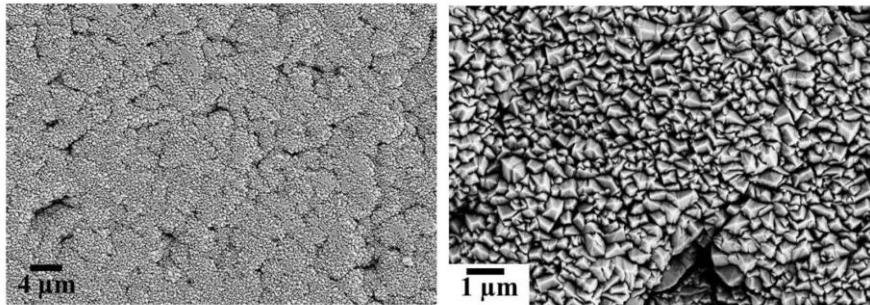
22

CVD SiC and SiC-SiC$_f$ Samples

CHF tests for CVD SiC and SiC-SiC$_f$ composite are undergoing

Material	Static contact angle (°)	Roughness (PV, μm)	Thickness (mm)
Zirlo®	72	4.1	0.8
CVD SiC A	57	2.6	1
CVD SiC B	36	3.1	1
CVD SiC C	32	5.0	1
SiC-SiC$_f$ A	67	11	1.4
SiC-SiC$_f$ B	51	6	1.4
SiC-SiC$_f$ C	66	23	1.4

CVD SiC

200μm

SiC-SiC$_f$ Composite

200μm

23

Do not distribute

Surface Morphology of As-prepared SiC Surfaces

CVD SiC A (PV~2.6μm)   CVD SiC B (PV~3.1μm)   CVD SiC C (PV~5.0μm)

20 um

SiC-SiC$_f$ A (PV~11μm)   SiC-SiC$_f$ B (PV~6μm)   SiC-SiC$_f$ C (PV~23μm)
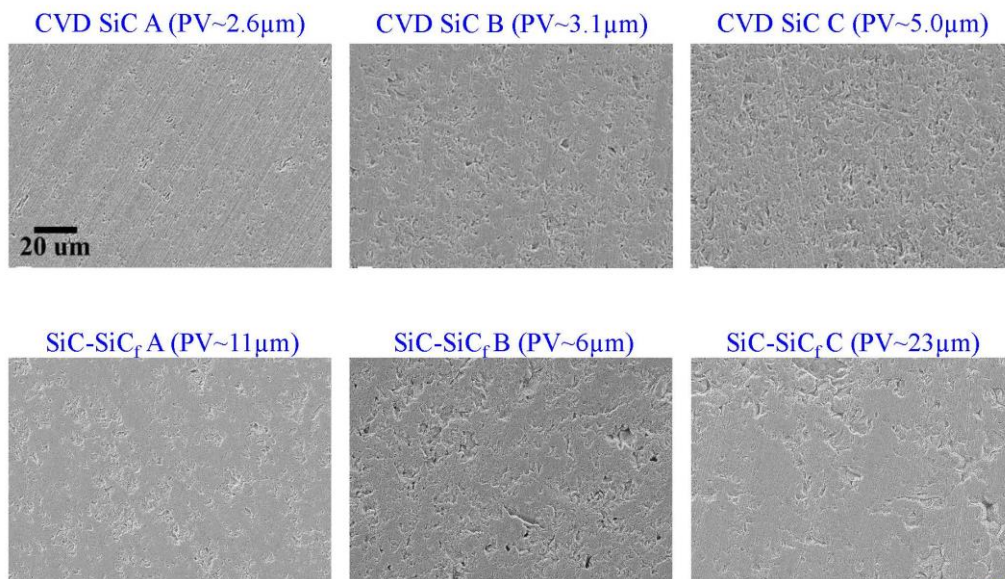
24

Do not distribute


Immediate Future Work

- Complete pool boiling tests of SiC samples and comprehensive understanding of the results

- Investigation of corrosion effects on boiling performance of cladding materials

- CHF test of coated Zirlo fuel cladding and SiC-SiC$_f$ composite cladding in prototypical flow boiling conditions (Westinghouse WALT Loop Test)

Roughness change during water autoclave test [UW]

25

53

DEPARTMENT OF
ENGINEERING PHYSICS
COLLEGE OF ENGINEERING UNIVERSITY OF WISCONSIN-MADISON
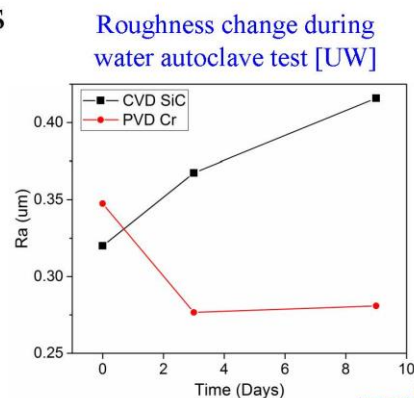
Pool boiling experiments used to screen results for subsequent flow boiling tests

26

DEPARTMENT OF
ENGINEERING PHYSICS
COLLEGE OF ENGINEERING UNIVERSITY OF WISCONSIN-MADISON
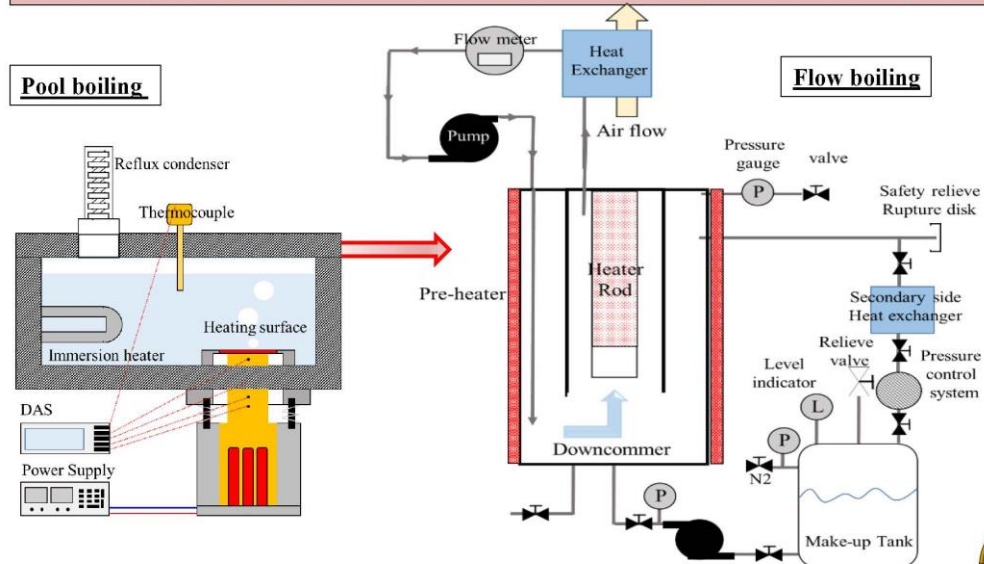
Concluding Remarks

- Pool boiling experiment for potential ATF cladding materials has been performed
- Thermal physical properties and surface characteristics of coated cladding were very similar to uncoated cladding, resulting in insignificant change of CHF values
- Effect of evolution of surface characteristics (due to corrosion/oxidation) under prototypical normal operating conditions on boiling behavior would be considered
- This study will be extended for prototypical flow boiling test to describe the LWR hydraulics conditions

27

- Journal Publication
  - H. Jo, H. Yeom, E. Gutierrez, K. Sridharan, M. Corradini, Evaluation of Critical Heat Flux of ATF Candidate Coating Materials in Pool Boiling, *Nuclear Engineering and Design*, accepted (in press), 2019
- Conference proceedings
  - H. Jo, H. Yeom, E. Gutierrez, K. Sridharan, M. Corradini, "Characterization of boiling characteristics of accident tolerant fuel (ATF) cladding surfaces, *Proc. 2018 ANS Winter Meeting and Nuclear Technology Expo, Orlando, FL, 2018*
  - H. Jo, E. Gutierrez, H. Yeom, K. Sridharan, M. Corradini, "Critical Heat Flux Study with Different Substrate Conditions for Accident Tolerant Fuel Cladding Development", *Proc. 2019 ANS Annual Meeting, Minneapolis, MN, 2019*

28

Back-up Slides
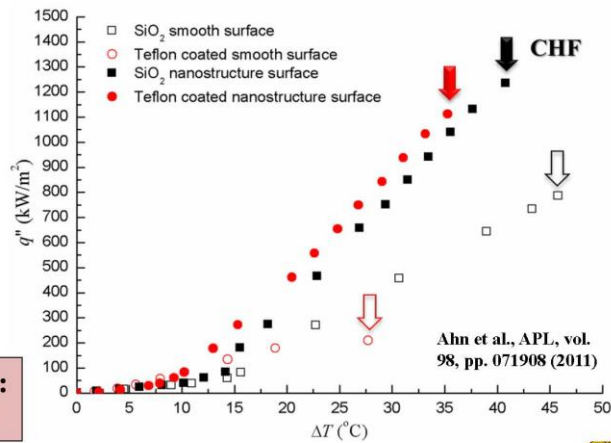
29

ATF and Boiling Heat Transfer

Surface/material changes can affect boiling heat transfer limits on heating surfaces

Prior work indicates:

- Surface wettability

- Thermophysical properties

- Surface morphology (roughness, capillarity)

Ahn et al., APL, vol. 98, pp. 071908 (2011)

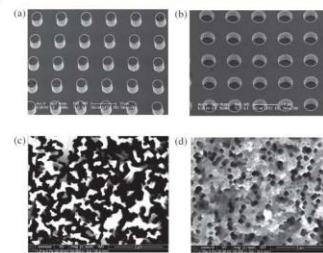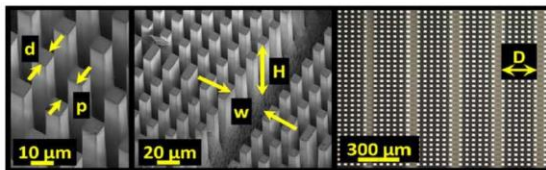**Current work funded by DOE: ATF effects on boiling & CHF**

30

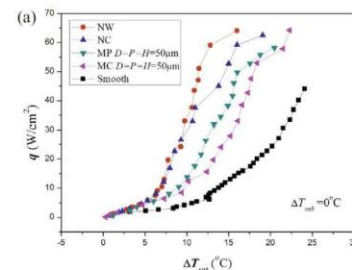# Surface parameters associated with CHF:
3. Surface Morphology

Bubble dynamics is altered by **surface structures**

Micro/nano-structures on Si surface
[Dong et al., IJHM, 2014]

Micro-pin–fin-array structured Si surface
[Coso et al, J. Heat Transfer, 2012]
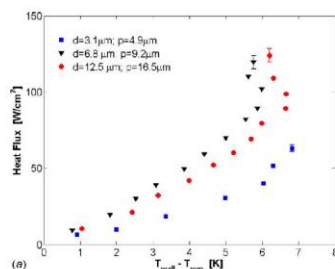
(a) micro-pillars (MP), (b) micro-cavities (MC), (c) nanowires (NW), and (d) nano-cavities (N
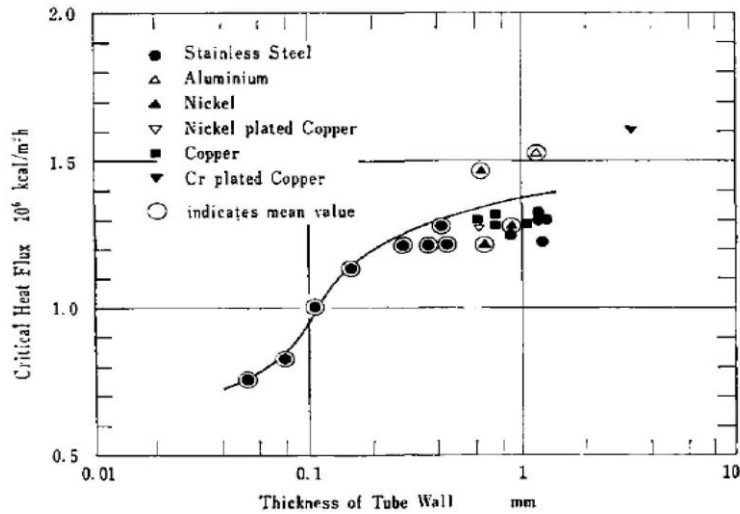
31

56

Thickness Effect on CHF

Fig. 2 Critical Heat Flux *vs.* Thickness of Tube Wall

32 **Arik, M. & Bar-Cohen, A. Int. J. Heat and Mass Trans. 46, 3755–3764 (2003).**

Heater Size Effect on CHF

Table 1
Summary of experimental results.

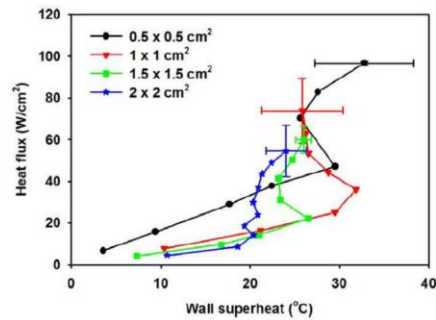|		Heater size			
		0.5×0.5 (cm^2)	1×1 (cm^2)	1.5×1.5 (cm^2)	2×2 (cm^2)
SiNW	CHF (W/cm^2)	223.90 ± 5.61	150.67 ± 12.42	124.85 ± 16.21	125.52 ± 3.06
	HTC (W/cm^2 K)	9.06 ± 1.60	4.68 ± 0.23	3.89 ± 0.64	4.84 ± 0.72
	Conduction loss (%)	7.03	7.96	5.80	4.26
Plain Si	CHF (W/cm^2)	81.48 ± 0.87	67.40 ± 15.52	46.82 ± 6.46	44.22 ± 12.33
	HTC (W/cm^2 K)	2.98 ± 1.01	2.80 ± 0.47	1.82 ± 0.29	1.93 ± 0.73
	Conduction loss (%)	16.21	13.46	17.88	10.08

Fig. 8. Boiling curves on plain Si surfaces for different sizes of heaters, which shows that CHF increases as heater size reduces.

33 **Lu et al., IJHMT, vol. 54, pp. 5359-5367 (2011)**

57

Appendix C

Summary of ATF Testing at the University of Wisconsin

Appendix C

Summary of ATF Testing at the University of Wisconsin

SUMMARY OF ATF TESTING AT THE UNIVERSITY OF WISCONSIN

ATF Testing Objectives

- Understand the characteristics and functions of ATF cladding materials
  - Overall performance
  - Failure modes and CHF performance
  - Film stability
  - Reflood/rewet conditions
- ATF cladding materials to investigate
  - FeCrAl Alloys (APMT and C26M)
  - SiC and SiC-SiC Composites
  - Coated Zirconium Alloys (PVD and Cold Spray)
  - Compare to Zirconium Alloy standard
- Test plan
  - Flow visualization, HTC, and CHF measurements at atmospheric pressure
  - HTC and CHF performance at prototypic BWR and PWR conditions

UW Madison Team

- UW's ATF research is a collaboration with MIT, VCU, and industry partners
- Principal Investigators
  - Dr. Matteo Bucci (MIT), Dr. Jessika Rojas (VCU), and Dr. Mark Anderson (UW)
- UW Team
  - Barret Elward, Research Assistant
  - Paul Brooks, Instrumentation/Welding Specialist
  - Seth Jones, Machinist/Fabricator
  - Brandon , Ian, Jake, and Sid: Undergraduate Hourly Support

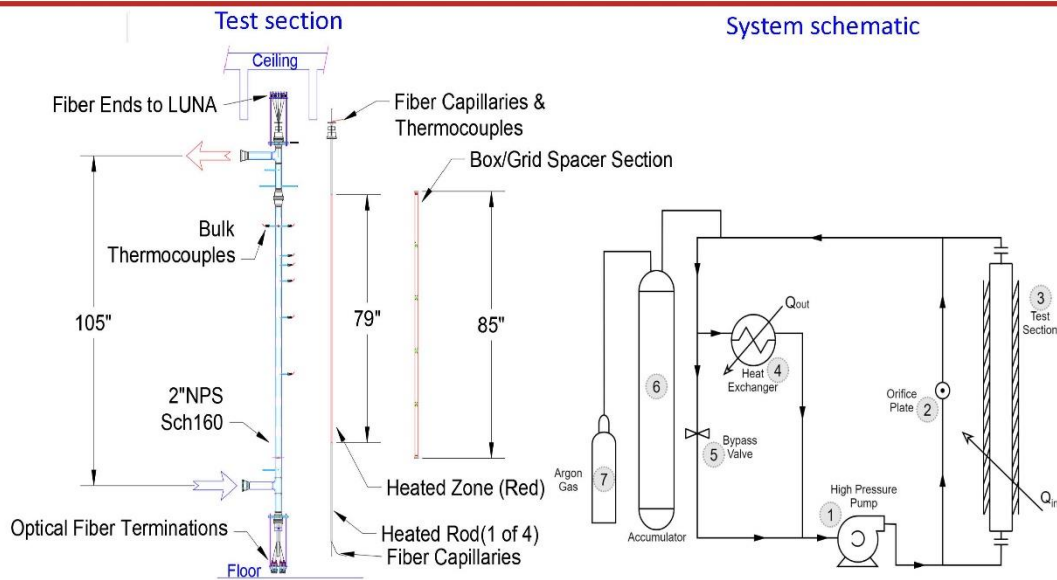# High and Low Pressure Flow Boiling Facilities

High pressure TEST CONDITIONS
Pressure: 8.0 − 25 MPa
Temperature: 25 − 550°C
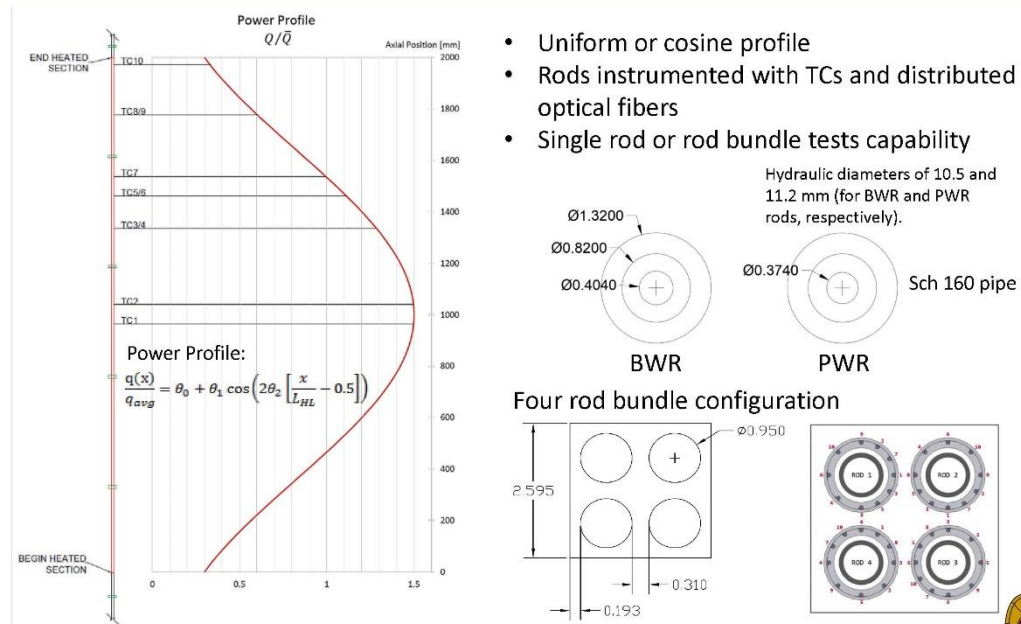Mass Flux: 0 − 5000 kg/m²s

Low pressure TEST CONDITIONS
Pressure: ATM - 200 kPa
Temperature: 10 − 100°C
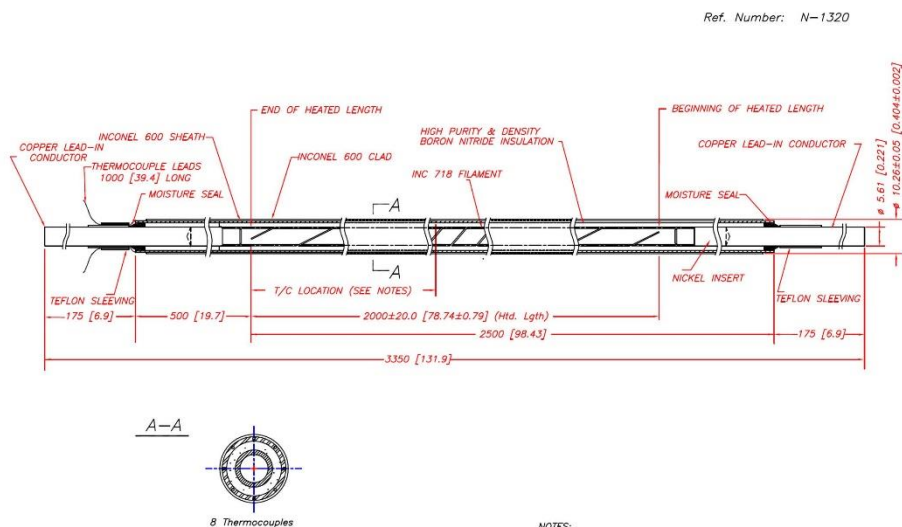Mass Flux: 0− 4000 kg/m²s

High Pressure Heat Transfer and Flow Boiling

Heater Power Profile and Thermocouples

Power Profile
$Q/\bar{Q}$

Power Profile:
$$\frac{q(x)}{q_{avg}} = \theta_0 + \theta_1 \cos\left(2\theta_2\left[\frac{x}{L_{HL}} - 0.5\right]\right)$$

- Uniform or cosine profile
- Rods instrumented with TCs and distributed optical fibers
- Single rod or rod bundle tests capability

Hydraulic diameters of 10.5 and 11.2 mm (for BWR and PWR rods, respectively).

BWR — Ø1.3200, Ø0.8200, Ø0.4040

PWR — Ø0.3740, Sch 160 pipe

Four rod bundle configuration
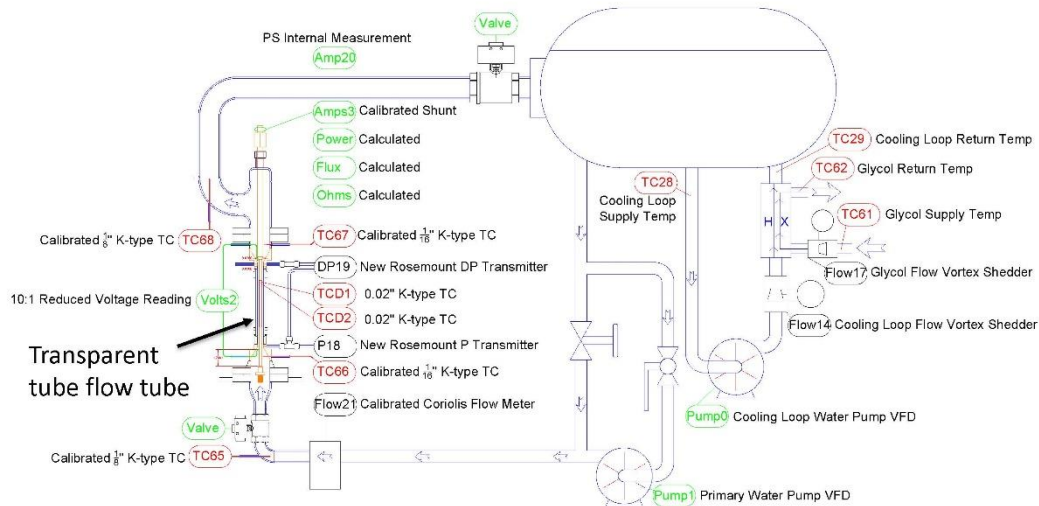
Internally Heated Rod – Stern Labs Design

Ref. Number: N−1320

NOTES:
1. All dimensions in millimeters [inches].
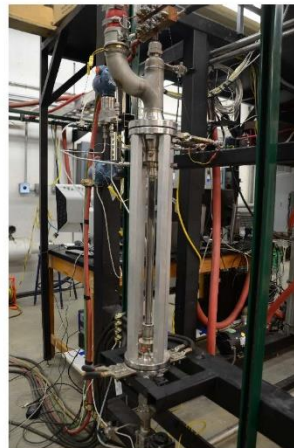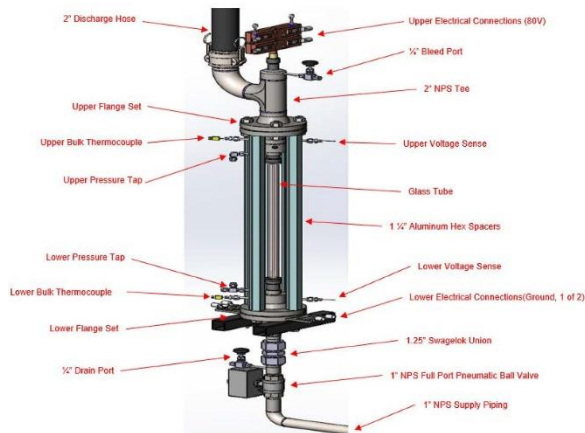2. Upto 10 thermocouples can be embedded in the sheath as shown.

Low Pressure System - Instrument Diagram

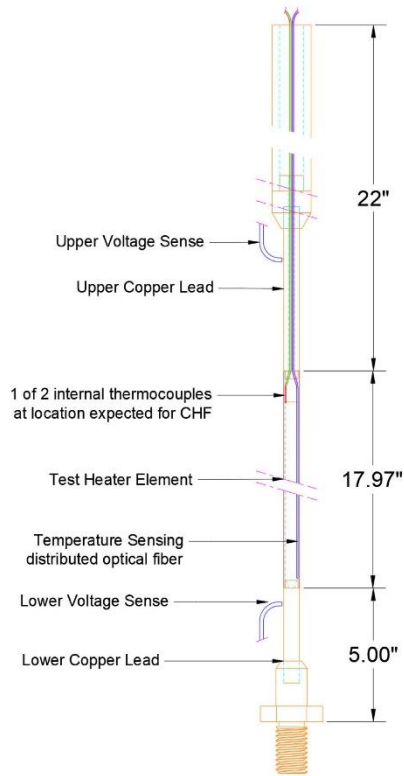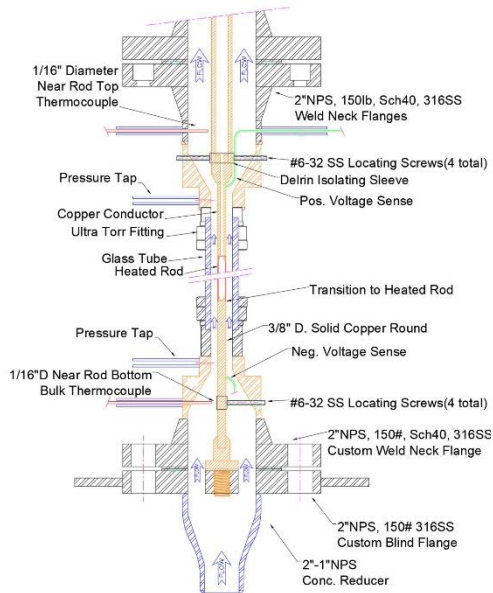# Low Pressure System – Flow Boiling

- Simulated fuel pin heated directly via ohmic dissipation
- Steady Uniform heat fluxes up to 2.1MW/m^2 for Zirlo and 3.8MW/m^2 for FeCrAl alloys

- Process data captured w/ LabView DAQ system and LUNA distributed thermal sensing fiber
- High-speed video (1000Hz) via Redlake MotionPro and Ametek Phantom cameras

Test Section Details

- 1/16" Diameter Near Rod Top Thermocouple
- 2"NPS, 150lb, Sch40, 316SS Weld Neck Flanges
- Pressure Tap
- #6-32 SS Locating Screws(4 total)
- Delrin Isolating Sleeve
- Pos. Voltage Sense
- Copper Conductor
- Ultra Torr Fitting
- Glass Tube
- Heated Rod
- Transition to Heated Rod
- Pressure Tap
- 3/8" D. Solid Copper Round
- Neg. Voltage Sense
- 1/16"D Near Rod Bottom Bulk Thermocouple
- #6-32 SS Locating Screws(4 total)
- 2"NPS, 150#, Sch40, 316SS Custom Weld Neck Flange
- 2"NPS, 150# 316SS Custom Blind Flange
- 2"-1"NPS Conc. Reducer

- Upper Voltage Sense
- Upper Copper Lead
- 1 of 2 internal thermocouples at location expected for CHF — 22"
- Test Heater Element — 17.97"
- Temperature Sensing distributed optical fiber
- Lower Voltage Sense — 5.00"
- Lower Copper Lead

10

Low Pressure System - Instrumentation

- TCs in the cooling water and heater rod provide reference points for the thermal sensing fiber inside the rod
- **Left:** Top-down view of a rod mid-assembly. The rod has been filled and a capillary for the fiber runs its length
- **Right:** Lights and camera positioning for high speed image capture
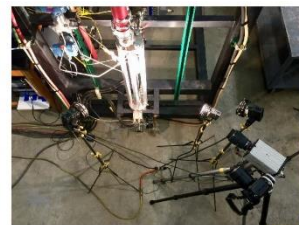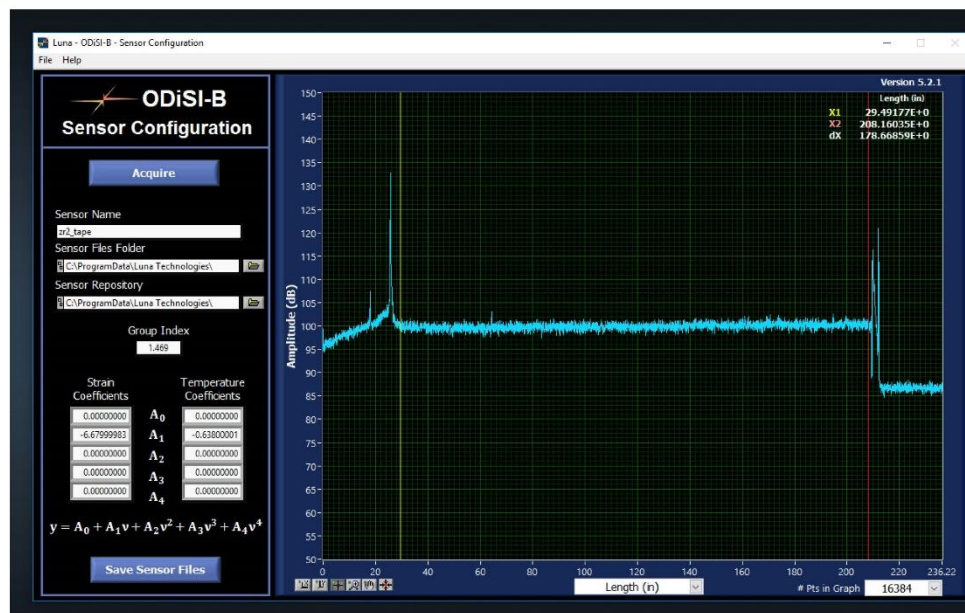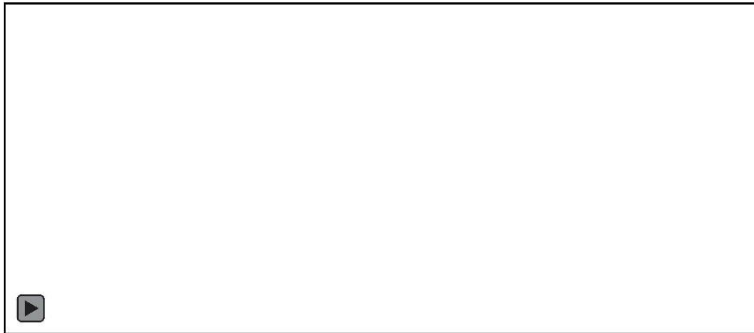
Distributed Thermal Sensing

- LUNA Systems ODiSI-B fiber interrogator uses Rayleigh backscatter of low energy (~1550nm) light to determine temperatures along the length of an optical fiber
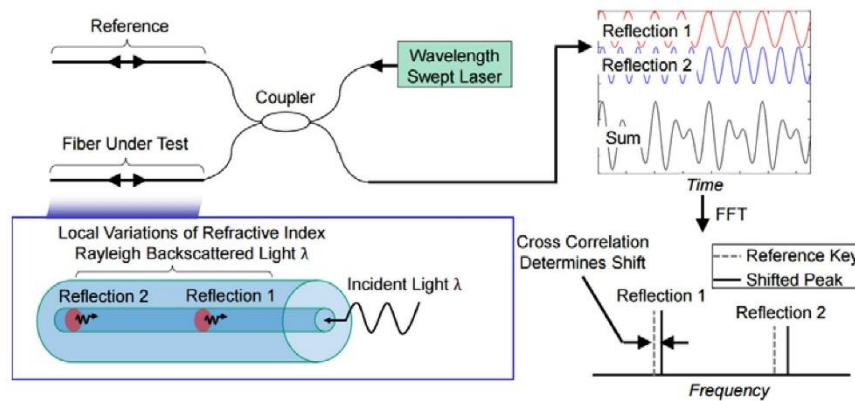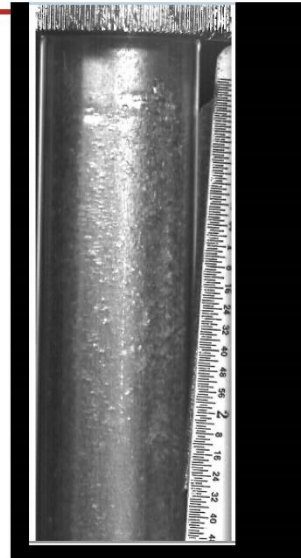

# Distributed Thermal Sensing – Reference Key

Flow Boiling - Atmospheric Pressure

- Example of Flow boiling data from Zirlo rod
- Fiber optic temperature sensor allows determination of HTC and rod temperature as a function of position on the rod.
- End TC is used to confirm fiber temperature
- Mass Flux: 1350 kg/m^2-s
- Heat Flux: 1.55 MW/m^2

Boiling to CHF – Zirconium Alloy

Bubble Formation

Bubble Coalescence

Consistent Vapor Film

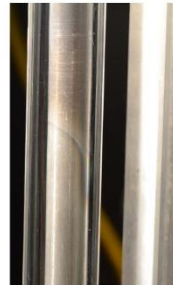CHF Event
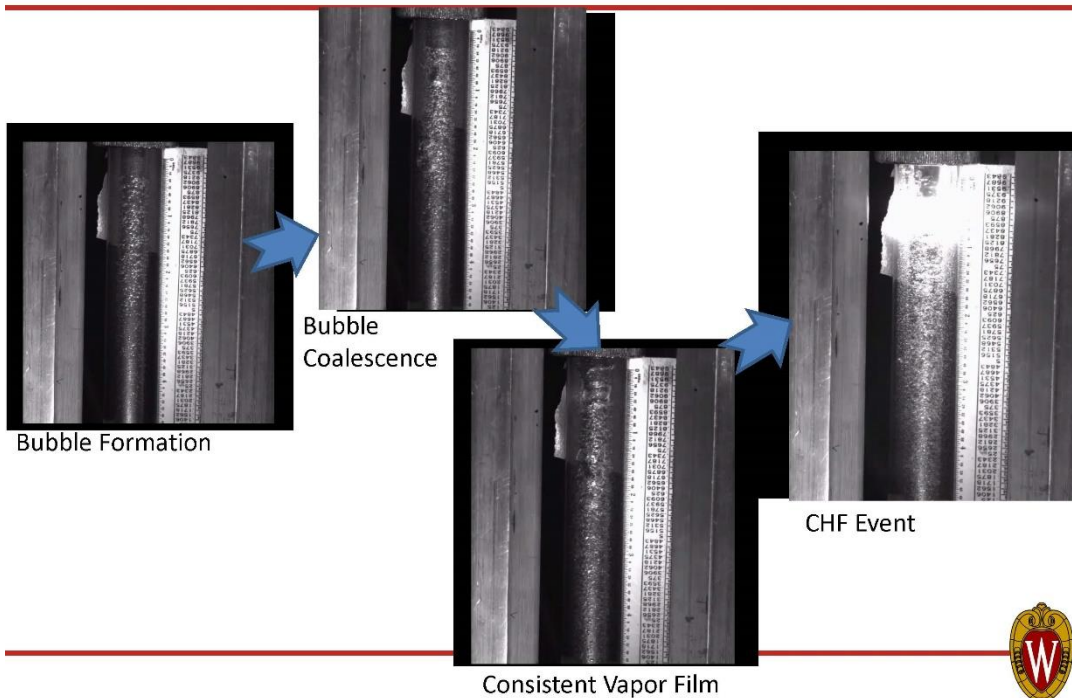
Surface Analysis – ATF Samples
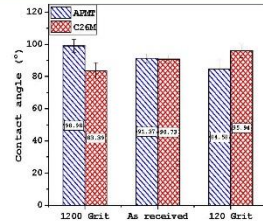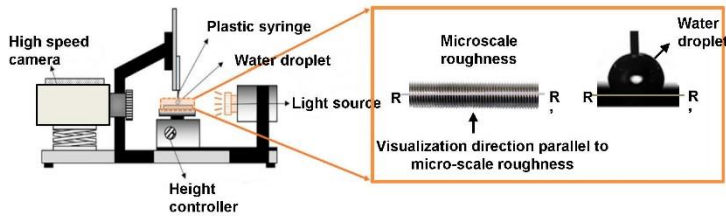
Samples analyzed pre- and post-CHF testing at VCU

- SEM and oxidation measurements
- Surface Roughness
- Wetting angle

CHF oxidation visible on Inconel rod

CHF oxidation visible in top half of image on Zirlo rod

CHF damage in FeCrAl rod

Project Challenges

- Materials acquisition/properties
  - Rare materials
  - Resistivity limits for direct heating
  - Contact/connection for material heating
- Heater rod assembly
  - Preservation of coatings
  - Heat generation/transfer within rod
  - Instrumentation
    - Fiber and TC placement
- Test conditions
  - CHF test conditions are harsh
  - Heater rod attrition is high

67

HTC and CHF Testing – Near and Long Term

- Near term efforts focused on atmospheric pressure testing
- Long term – Internally heated rods for prototypic BWR and PWR testing in high pressure loop

Material	OD	Note
[-]	[mm]	[-]
Zr Alloys	10.26, 9.6, 9.1	-
Coated Zr Alloys	9.6, 9.1	PVD and Cold Spray
FeCrAl Alloys	10.26	APMT and C26M
SiC Ceramics	9.6	-

Experiment Conditons	Heat Flux	Mass Flux	Profile	Data Collected
[-]	[MW/m^2]	[kg/m^2-s]	[-]	[-]
Atmospheric	0-2, 0-4*	500-2000	Uniform	CHF, HTC, Video
BWR	0-2.5	1000-5000	Chopped Cosine	CHF, HTC
PWR	0-2.5	1000-5000	Chopped Cosine	CHF, HTC

Summary

- Working with MIT, VCU, and industry partners, UW has developed testing methods for heater rods using ATF materials at atmospheric pressure and BWR/PWR conditions
- Heat transfer information and boiling/bubble formation have been captured in low pressure test section for materials available
- BWR/PWR reactor tests will use proven Stern Labs design to mimic cosine power profile and provide meaningful data on ATF materials performance
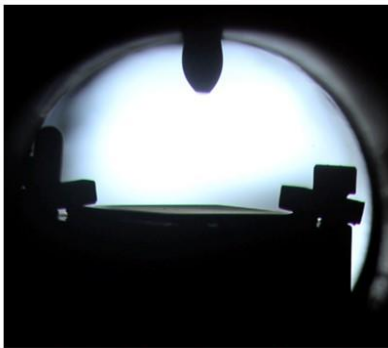
Thank you

- Questions

Appendix D

Wettability of ATF Cladding Materials in Nuclear-Reactor Conditions

Appendix D

Wettability of ATF Cladding Materials
in Nuclear-Reactor Conditions

Droplet falling on Cr-coated Zr-4 surface at 6.7 bar (≈163°C) at 25 fps

Wettability of ATF cladding materials in nuclear reactor conditions

A. Jena, A. Kossolapov, B. Phillips, M. Bucci

G.Y. Su presents on behalf of A. Jena

Massachusetts Institute of Technology
Department of Nuclear Science and Engineering

Motivation

- The surface characteristics have shown to greatly impact both pool and flow boiling heat transfer coefficient and CHF

- There is almost no data available for both the Zr-4 and the candidate ATF cladding materials beyond the atmospheric conditions, nor in a saturated steam environment
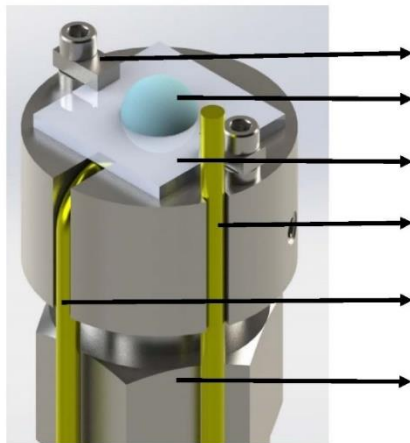
Objective

- Atmospheric Pressure to Critical Pressure (221.1 bar/3206.8 psi, 374°C/705.2°F)

- Saturated Steam Environment
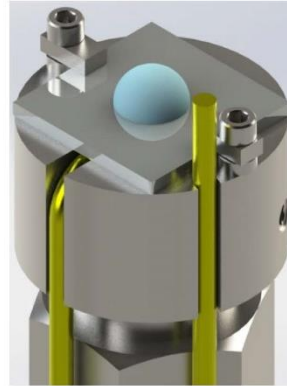
- Static, advancing, and receding contact angle

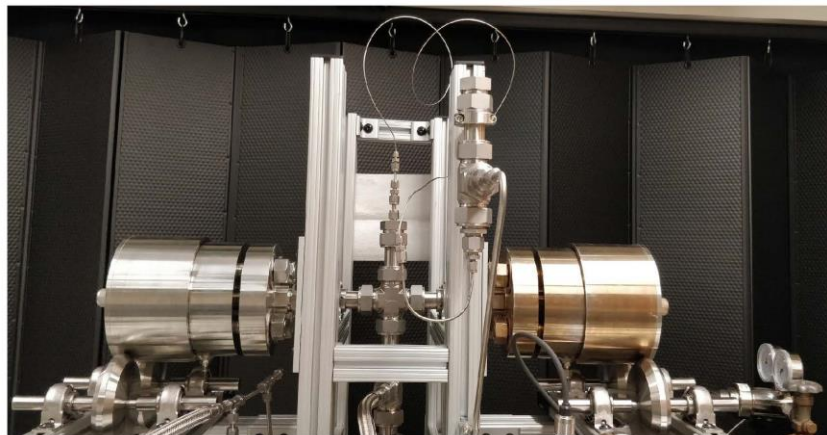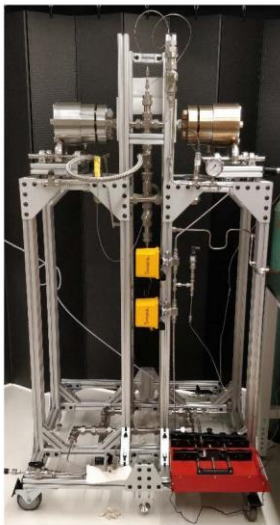# Methodology: Contact Angle Facility
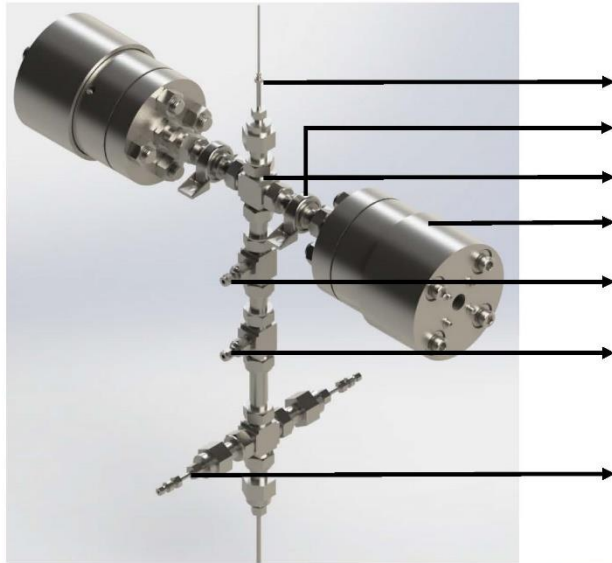
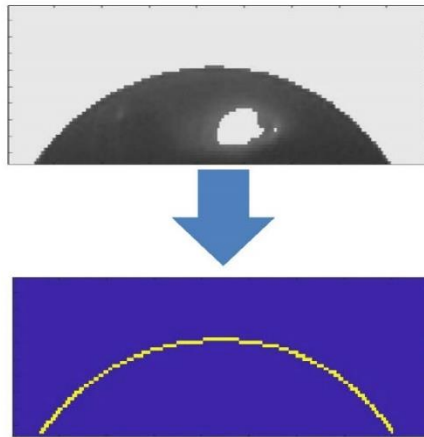## Test Section

Test Section

Experimental Facility

Sample Preparation

- Before each test, the sample is solvent cleaned in sonicated bath using soapy water, DI water, Acetone, Ethanol and DI water in the respective order and mounted on the stage

Tests and Data Processing (Step 1)

Tests and Data Processing (Step 2)

Tests and Data Processing (Step 3)
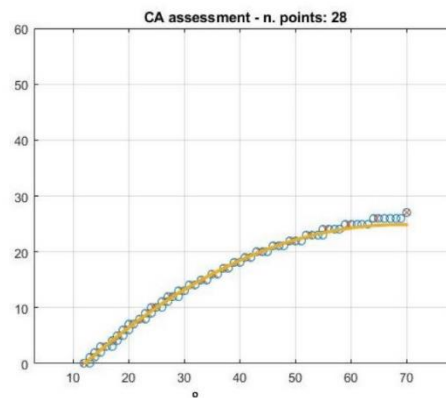
Test Matrix

Material	Surface Finish
Fresh Zr-4	As machined
Fresh Zr-4	Mirror Polished
Oxidized Zr-4	
Cr-coated Zr-4	Mirror Polished
Monolithic SiC	As machined
FeCrAl	Mirror Polished

- Tests were conducted from ambient condition to PWR pressure and temperature

Fresh Zr-4 As Machined
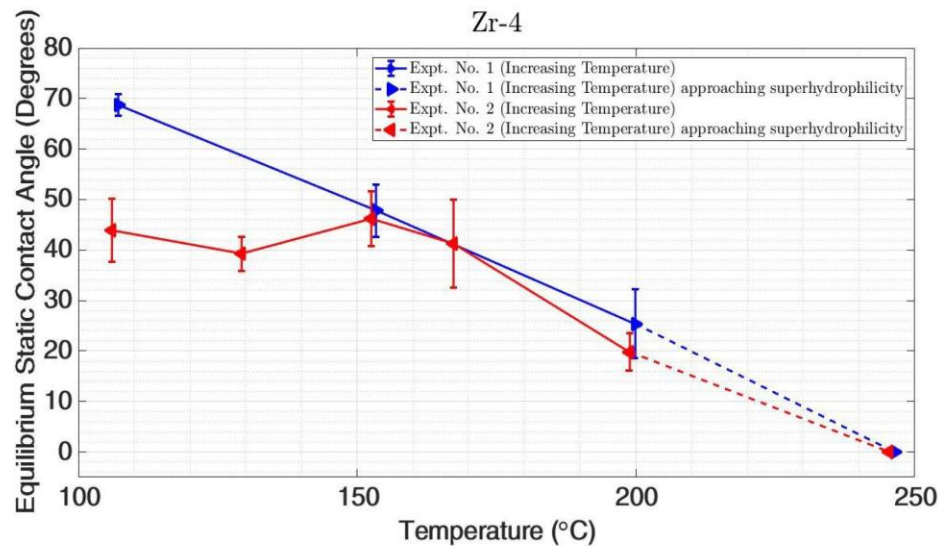
Mirror Polished Fresh Zr-4

Oxidized Zr-4
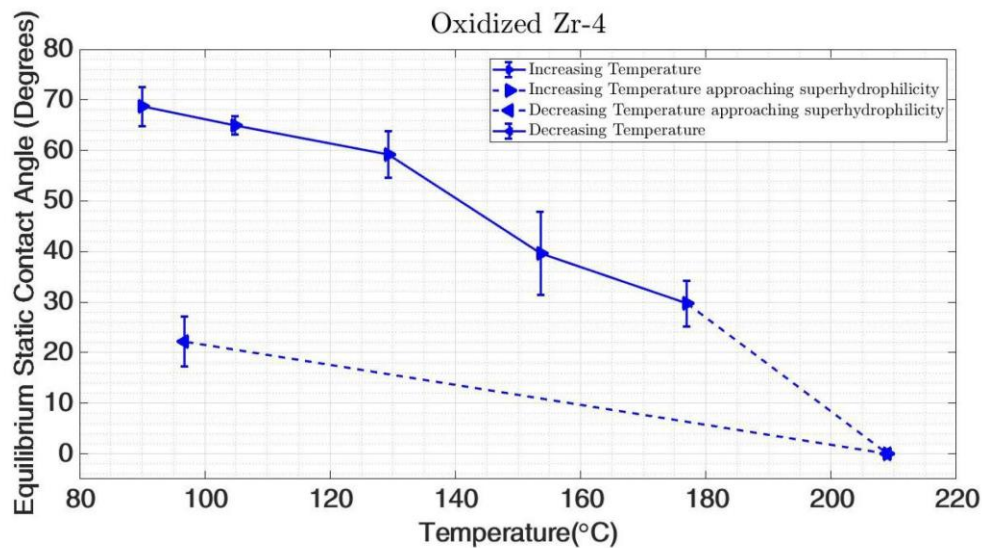
Monolithic SiC As Machined
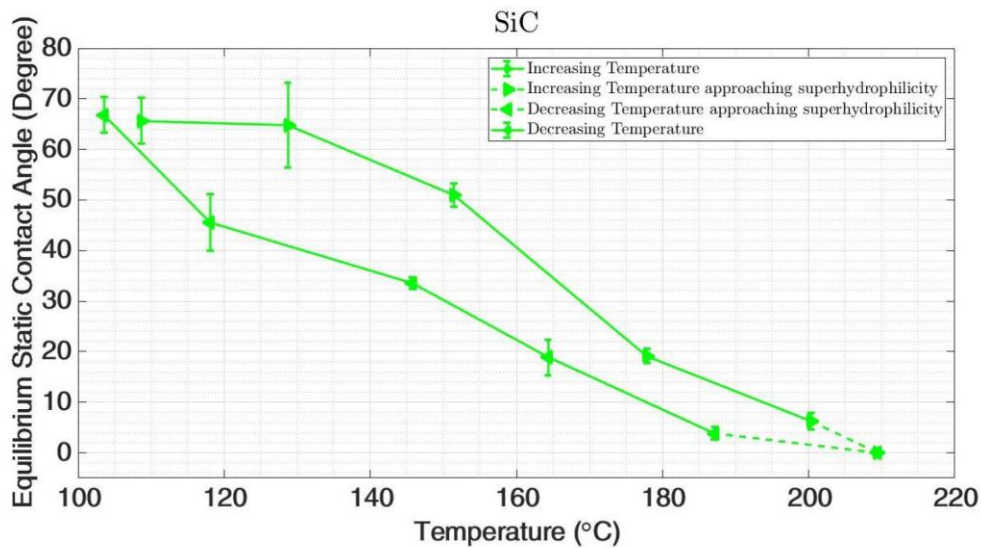
FeCrAl Mirror Polished
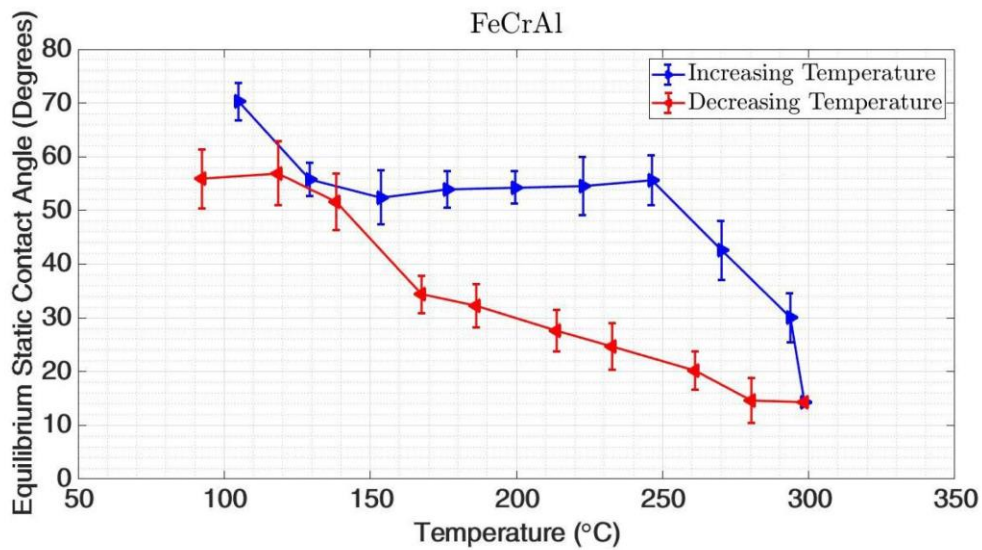
Conclusion

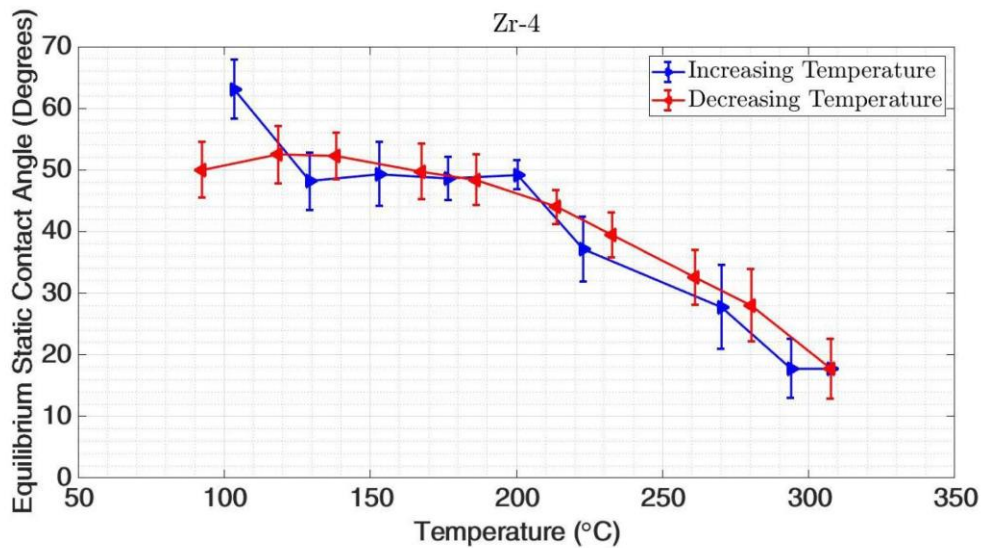- Contact Angle decreases with increasing temperature (in some cases the sample attains superhydrophilicity)

- Roughness and oxication plays an important role in wettability

- Samples get oxidized or corroded at high temperature, and thus may bias the trend

- Repeat measurements on samples with no clear trend

Future Work

Near term:
- Compare data with existing models
- Quantify the effect of roughness on the trend of contact angle
- Figure out the hysteresis (lower contact angle while going down in temperature) and repeat measurements

Long term:
- Measure advancing/receding contact angles
- Measure contact angle of other relevant materials

Appendix E

Sensitivity of Critical Heat Flux for ATF FeCrAl Alloy Using RELAP5-3D and RAVEN

Appendix E

Sensitivity of Critical Heat Flux for ATF FeCrAl Alloy Using RELAP5-3D and RAVEN

Jacob Gorton
Nicholas Brown

THE UNIVERSITY OF
TENNESSEE
KNOXVILLE

Introduction

- Iron-Chromium-Aluminum (FeCrAl) alloys are potential candidates for replacing zirconium alloys in LWRs as part of the Accident Tolerant Fuel (ATF) program

- Experimental data from a flow-boiling apparatus at the University of New Mexico (UNM) show large discrepancies between measured critical heat flux (CHF) and CHF predicted using the systems code RELAP5-3D

- Code-to-experiment discrepancies in post-CHF tube temperatures also observed

- Sensitivity studies were performed to understand the sensitivity of CHF and the post-CHF temperature excursion to heat transfer coefficients, material thermophysical properties, and a CHF multiplier

- Sensitivity studies were performed using a RELAP5-3D model of the UNM experiment and the uncertainty quantification code RAVEN

THE UNIVERSITY OF TENNESSEE KNOXVILLE

Objectives

This study has 3 main objectives:

1. To compare best-estimate CHF and temperature predictions from a widely used system analysis code to a simple, well-understood CHF test for an ATF candidate material

2. To enhance understanding of the sensitivity of these models to the shape of the boiling curve and thermophysical properties of the test section

3. To demonstrate an approach to optimize CHF and post-CHF model predictions while highlighting differences between how CHF is modeled and what occurs in reality

THE UNIVERSITY OF TENNESSEE KNOXVILLE

Experiment Description

- Low-pressure transient testing performed at UNM using water as the working fluid
- Vertically oriented FeCrAl tubes were placed in the internal flow boiling loop shown
- Test sections were thermally insulated on the outer surface
- Voltage transducers imposed a transient power curve on the tubes similar to a subprompt, hot full power RIA power curve
- A fast-response K-type thermocouple located at the axial center of the tube was used to measure outer surface temperature
- Measured power and temperature were used to calculate inner surface temperature and heat flux
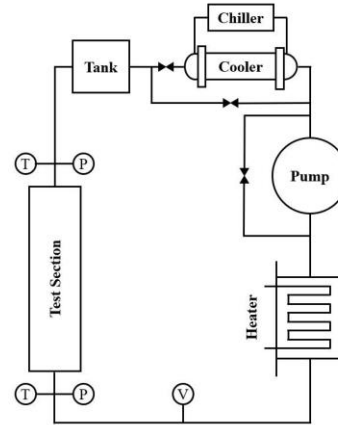
S. K. Lee, M. Liu, N. R. Brown, K. A. Terrani, E. D. Blandford, H. Ban, C. B. Jensen and Y. Lee, "Comparison of steady and transient flow boiling critical heat flux for FeCrAl accident tolerant fuel cladding alloy, Zircaloy, and Inconel," *International Journal of Heat and Mass Transfer*, vol. 132, pp. 643-654, 2019.

THE UNIVERSITY OF TENNESSEE KNOXVILLE

RELAP5-3D Model Description

- The test section portion of the experiment was modeled in RELAP5-3D using the coolant temperature, pressure, and mass flow rate initial conditions controlled in the experiment
- Model consists of a time-dependent volume, time-dependent junction, the FeCrAl pipe and attached heat structure to apply the power curve, a single junction, and a sink volume
- 50 nodes are used in both the pipe and the heat structure, which has been shown to provide stable results through mesh sensitivity studies
- Thermophysical properties of FeCrAl were used in the model
    - Both thermal conductivity and specific heat capacity varied with temperature according to measurements taken at Oak Ridge National Laboratory
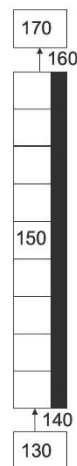
Model nodalization diagram, geometry, and initial conditions

Inner Diameter (in.)	0.345
Outer Diameter (in.)	0.375
Total Length (in.)	20
Entrance Length (in.)	10
Heated Length (in.)	2
Pressure (kPa)	84
Mass Flux (kg/m²-s)	300
Inlet Coolant Temperature (°C)	90

170
160
150
140
130

THE UNIVERSITY OF TENNESSEE KNOXVILLE

Base RELAP5-3D Model Results

- Experimental results for the measured input power, tube surface temperature, and calculated heat flux are shown and compared to the RELAP5-3D results
- Compared to the experiment and for the same input power curve, RELAP5-3D predicted:
  - smaller CHF (2.1 MW/m^2 vs 3.7 MW/m^2)
  - narrower heat flux pulse width
  - greater peak cladding temperature (PCT) (1361°C vs 856°C)
- Discrepancies serve as motivation behind performing sensitivity studies

Experimental Results

RELAP5-3D Results
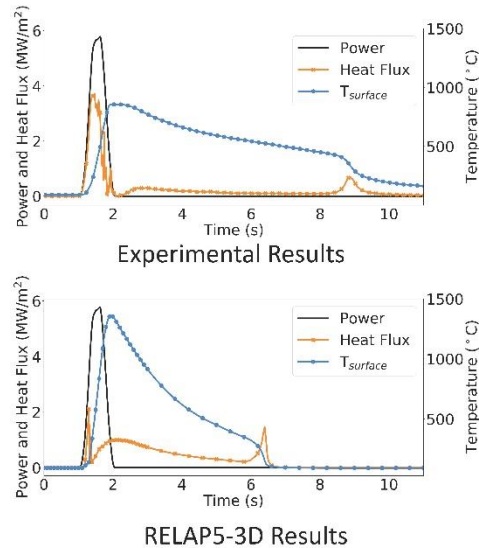
Coupling of RAVEN and RELAP5-3D

- Risk Analysis and Virtual Environment (RAVEN) is an uncertainty quantification tool developed by Idaho National Laboratory
- Used to vary heat transfer coefficient multipliers and CHF multiplier in the first sensitivity study and thermal conductivity (k), volumetric heat capacity (ρCp), and CHF multiplier in the second sensitivity study
- RAVEN acts as a driver to simultaneously vary the desired values in the RELAP5 input deck
- Emphasis is placed in this presentation on the second sensitivity study involving k, ρCp, and CHF multiplier

Sensitivity Study Methodology

- Cp and k were varied within the uncertainties of the measurements taken at ORNL
- ρ was varied within the theoretical limit of possible densities using

$\rho = {}^{1}/_{\sum x_i/\rho_i}$ and $\rho = \sum x_i \rho_i$, where x_i is the weight fraction of each constituent in an alloy and ρ_i is the density of each constituent

- CHF multiplier was varied from 1.0 to 2.0 based on experimental data that showed that transient CHF may be as much double the CHF predicted in steady-state conditions
- Each parameter was varied uniformly within the uncertainty ranges provided by their respective sources
- Impact on CHF and the maximum tube temperature, analogous to PCT in a reactor, was considered
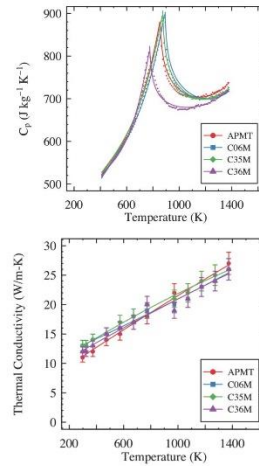
K. G. Field, M. A. Snead, Y. Yamamoto and K. A. Terrani, "Handbook on the Material Properties of FeCrAl Alloys for Nuclear Power Production Applications," ORNL/TM-2017/186, 2017.

Sensitivity of CHF to Material Properties and CHF Multiplier
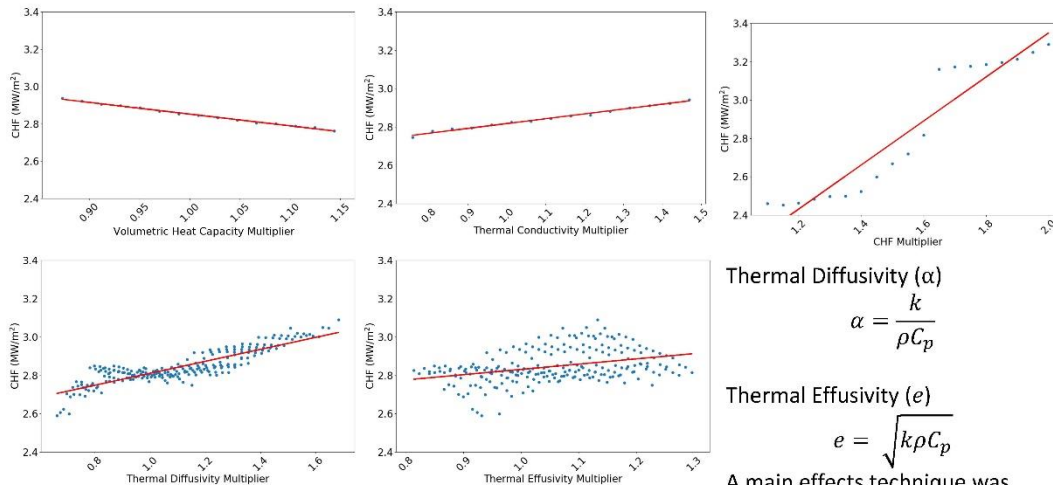
Thermal Diffusivity (α)

$$\alpha = \frac{k}{\rho C_p}$$

Thermal Effusivity (e)

$$e = \sqrt{k\rho C_p}$$

A main effects technique was used in which the output for a single variable was averaged across all other variables

Sensitivity of PCT to Material Properties and CHF Multiplier
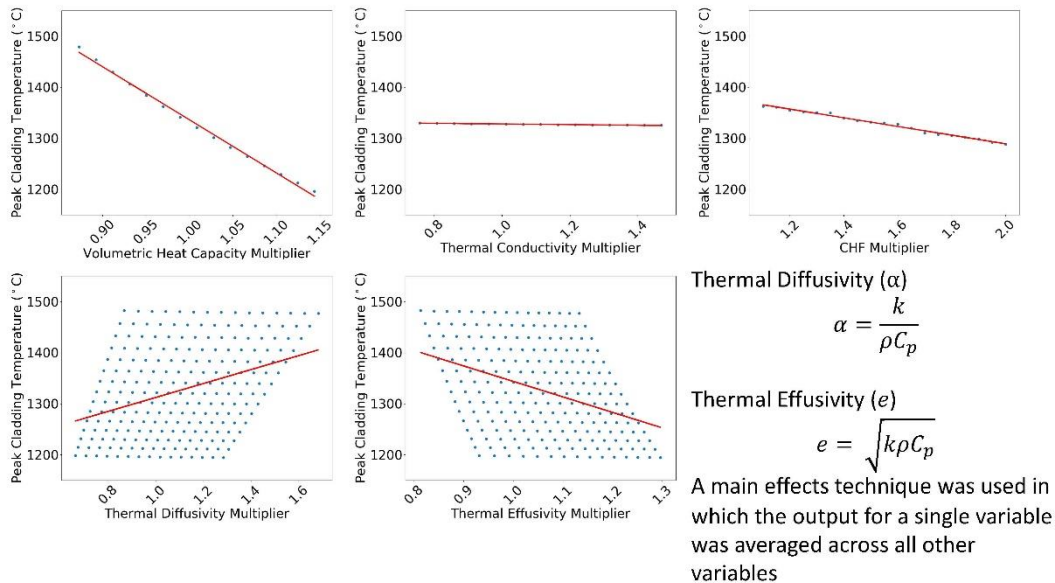

Thermal Diffusivity (α)

$$\alpha = \frac{k}{\rho C_p}$$

Thermal Effusivity (e)

$$e = \sqrt{k \rho C_p}$$

A main effects technique was used in which the output for a single variable was averaged across all other variables

Summary of Material Property and CHF Multiplier Study

- CHF was sensitive to all parameters and increased with each of them except for the volumetric heat capacity
- PCT was insensitive to thermal conductivity, but was sensitive to each of the other parameters

Separation of CHF and Maximum Heat Flux

- From the UNM experimental results, it was shown that CHF was reached at a heat flux value lower than the maximum heat flux (MHF)
  - CHF was determined by the increased rate of change of cladding temperature, which indicates DNB
  - This observation may be caused by uncertainties in the measurements
- Even if the effect is a product of measurement uncertainty, it is clear that the heat flux stays elevated for a period of time before significantly dropping in the experiment
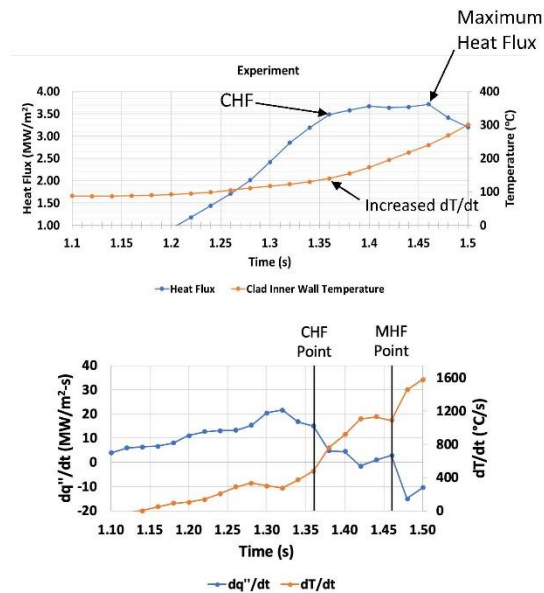
Separation of CHF and Maximum Heat Flux

- By the classic definition, RELAP assumes CHF and MHF are one in the same, and the heat flux drops immediately and at a much faster rate after CHF is reached compared to the experiment
- The more drastic drop in heat flux predicted by RELAP after CHF is reached is a main factor in causing the overprediction of PCT
- Key takeaway: post-CHF phenomena is being modeled differently from what occurs in reality

88
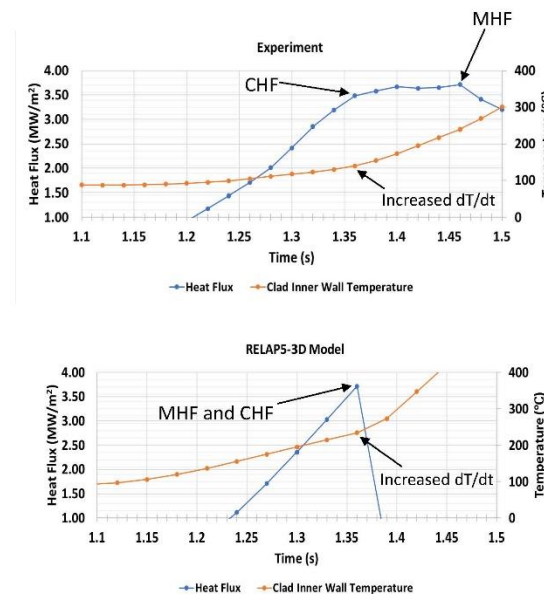
Best Match Parameters

- The combination of parameters from each sensitivity study that provided the best match to the experimental data was determined
- RELAP5 runs with the smallest relative error to the experimental results for each of three figures of merit, MHF, PCT, and integral energy deposition per unit area, were identified
- An overall best match run was identified by finding the run with the minimum RMS value of the three errors

Best Match Parameters – Material Property and CHF Multiplier Study

- The runs with the minimum relative error from the experimental data in terms of MHF, PCT, and integral heat flux were identified
- The run with the minimum RMS of the three error values was also identified

Parameters used in Run #4155
(RMS error of 27.10%)

Parameter	Value
k multiplier	1.06
ρC_p multiplier	1.14
e multiplier	1.10
α multiplier	0.93
CHF multiplier	2.0

Figure of Merit	Relative Error (%)
MHF	1.24
PCT	27.02
Energy Deposition	1.70
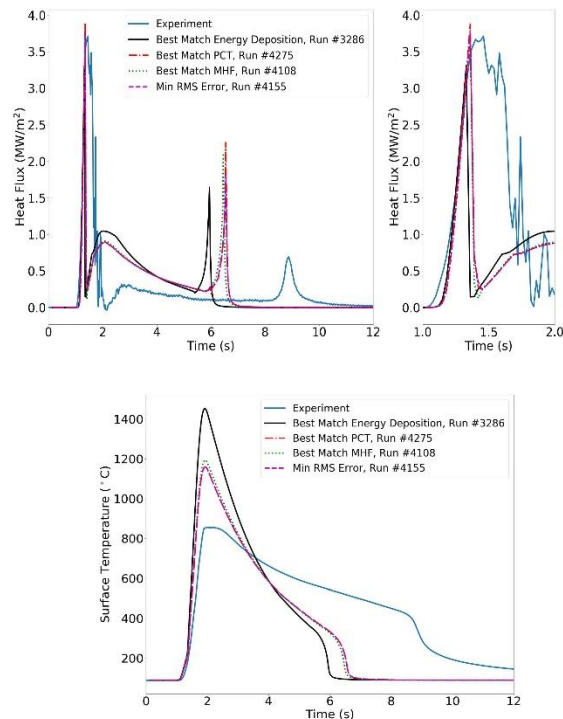
Summary and Conclusions

- Two parametric studies were performed to determine the impact of heat transfer coefficients, material thermophysical properties, and a CHF multiplier on CHF and PCT
- The combination of input parameters that gave the best match to experimental data in terms of MHF, PCT, and integral heat flux
- Even when the experimental MHF and integral heat flux were able to be matched within several percent difference, the PCT was still ~27% greater in the RELAP results
- Differences in PCT are caused by the different pulse widths of the heat flux
  - The pulse width during the transient was much narrower in all RELAP runs compared to the experiment, meaning less heat is able to be transferred from the tube to the coolant
- Current modeling of post-CHF phenomena differs from phenomena recorded in experiments

THE UNIVERSITY OF
TENNESSEE
KNOXVILLE

Acknowledgments

THE UNIVERSITY OF
TENNESSEE
KNOXVILLE

QUESTIONS?

**BACKUP:
HEAT TRANSFER COEFICIENT
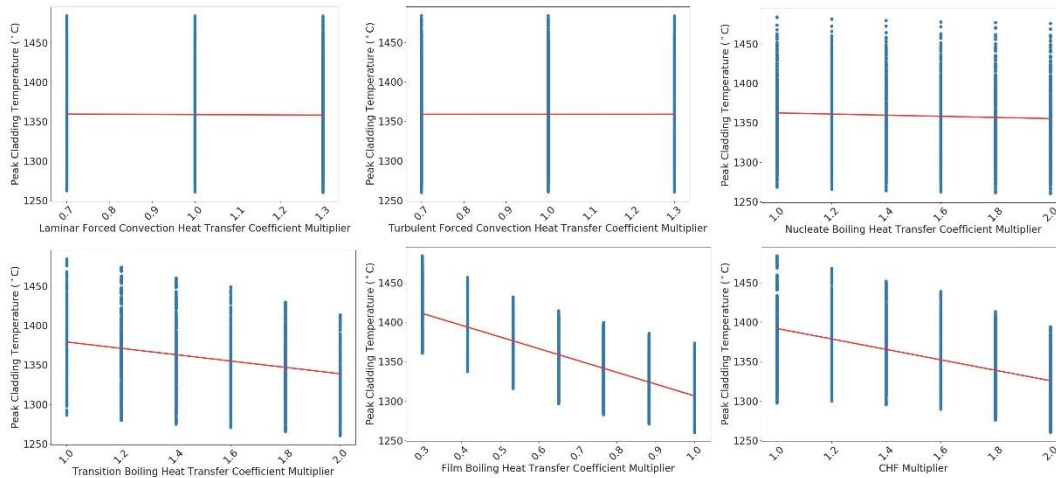AND CHF MULTIPLIER
SENSITIVITY STUDY**

Sensitivity Study Methodology

- Heat transfer coefficients were varied based on the data collected by UNM or from the experiments from which the correlations were developed
  - The following flow regimes are entered during the transient:
    - Forced Laminar Flow (no impact expected; arbitrarily varied from 0.7 to 1.3)
    - Forced Turbulent Flow (no impact expected; arbitrarily varied from 0.7 to 1.3)
    - Nucleate Boiling (UNM measured h_{nucl} to be double the h_{nucl} predicted by the RELAP5-3D base model; varied from 1.0 to 2.0)
    - Transition Boiling (The Chen-Sundaram-Ozkaynak correlation used in RELAP5-3D is based on experimental data with an error up to approximately 100%; varied from 1.0 to 2.0)
    - Film Boiling (UNM measured h_{film} to be approximately 1/3 the h_{film} predicted by the RELAP5-3D base model, varied from 0.3 to 1.0)

Sensitivity of CHF to Heat Transfer Coefficient and CHF Multipliers
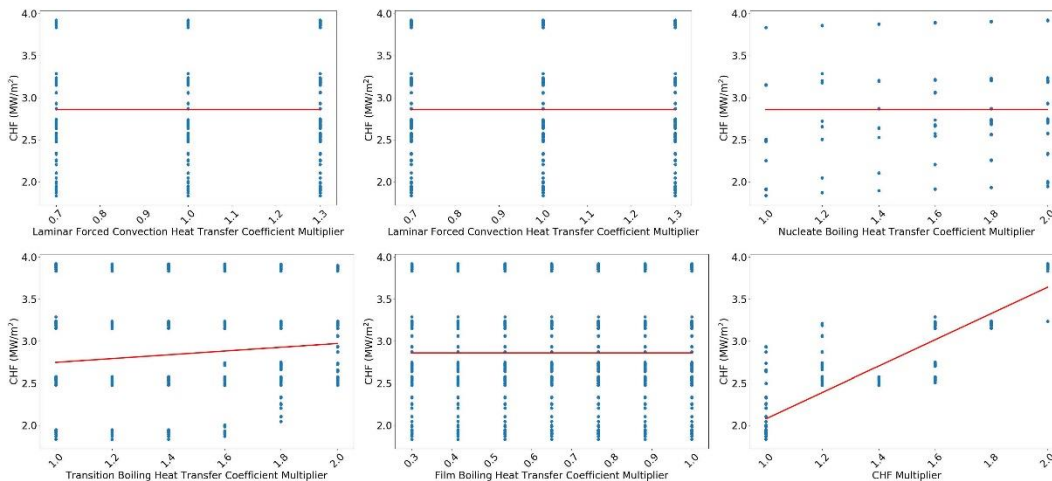
Sensitivity of PCT to Heat Transfer Coefficient and CHF Multipliers

Summary of Heat Transfer and CHF Multiplier Study

- Results confirm there is no sensitivity of CHF or PCT on the laminar or turbulent heat transfer multiplier since these regimes are entered prior to the transient
- CHF is most sensitive to the CHF multiplier and somewhat sensitive to the h_{trans} multiplier
- PCT decreases slightly as h_{nucl} increases and more noticeably so when h_{trans}, h_{film}, and CHF multipliers increase

Best Match Parameters – Heat Transfer Coefficient and CHF Multipliers Study

- The runs with the minimum relative error from the experimental data in terms of MHF, PCT, and integral heat flux were identified
- The run with the minimum RMS of the three error values was also identified

Parameters used in Run #756 (RMS error of 36.74%)

Parameter	Value
$h_{laminar}$ multiplier	1.3
$h_{turbulent}$ multiplier	0.7
$h_{nucleate}$ multiplier	1.0
$h_{transition}$ multiplier	2.0
h_{film} multiplier	1.0
CHF multiplier	2.0

Figure of Merit	Relative Error (%)
MHF	3.22
PCT	36.52
Energy Deposition	2.52
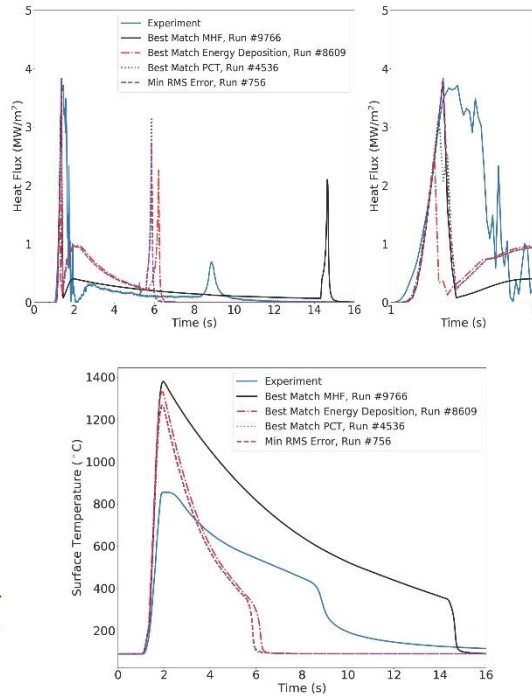
Appendix G

Progress on the Surface Characterization of ATF and Preliminary Results on CHF

Appendix G

Progress on the Surface Characterization of ATF and Preliminary Results on CHF

Overall Goal

This project will perform separate-effects tests of several of the ATF concepts under consideration to investigate **the impact of cladding surface characteristics in CHF** under normal and anticipated off-normal conditions. The experimental results will be used to **develop enhanced models or correlations for the prediction of CHF** that will be implemented in the various subchannel analysis **codes currently licensed** for core thermal-hydraulics analysis (VIPRE, LYNXT, FRACG, COBRA) as appropriate

VCU College of Engineering
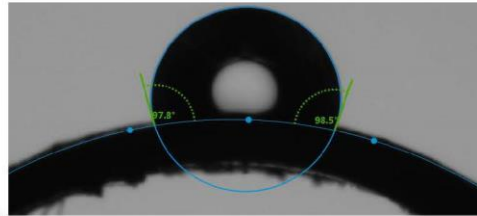
Objectives

- Characterize the surfaces of the ATF concepts under study.

- Conduct CHF experiments to obtain high fidelity qualitative and quantitative measurements for the thermal-hydraulic behavior of the ATF claddings

- Design a series of high fidelity full-scale experiments of the ATF concepts as independent data for the verification and validation of the new CHF models.

- Develop new or enhanced CHF models in accordance with the behavior observed in the CHF experiments

VCU College of Engineering

Team and Tasks

BWXT — BWX Technologies, Inc.

- Conceptual design of an instrument assembly to investigate surface impacts of ATF samples.
- system-scale validation plan intended for future use in pilot-scale T-H experimental facilities
- Robert Martin

VCU

- Surface Characterization of ATF, that includes SEM, profilometry, AFM, contact angle, surface chemistry, before and after CHF.
- Development and Implementation of Models in Suitable Subchannel and System Codes

WISCONSIN — UNIVERSITY OF WISCONSIN–MADISON

- Performing CHF experiments of the ATF concepts using both high pressure vertical forced circulation test loop and Atmospheric pressure test section
- Dr. Mark Anderson

framatome

- Provide Zr-4 cladding material and technical support on coating characteristics
- Provide COBRA-U (university package)
Richard Harne

GE

- Provide FeCrAl tubes, both APMT and C26M grade. Provide technical support on materials characterization
- Dr. Raul Rebak

VCU College of Engineering

Methodology

VCU College of Engineering
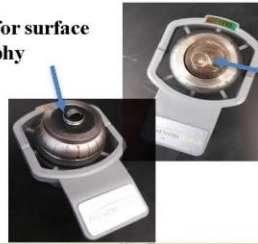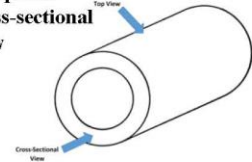
Scanning Electron Microscopy (SEM)

- Phenom ProX Scanning Electron Microscope used to image sample surfaces
- sample preparation
  - Material sectioning
  - Epoxy Molding
  - Grinding & Polishing
  - Ultrasonic Cleaner
- Completed SEM analysis of Zr-2, Zr-4, C26M, and APMT

Sample for surface topography

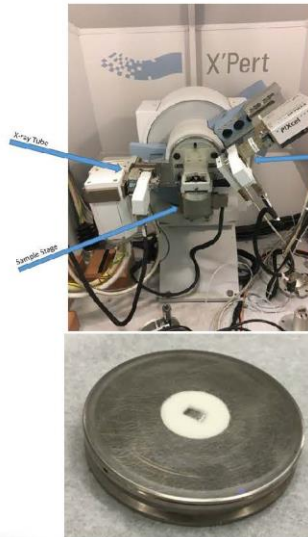Sample for cross-sectional view

VC Phenom ProX SEM

Hitachi SU-70 FE-SEM

X-Ray Diffraction (XRD)

- Finalized sample preparation procedure
  - Polymeric powder (PVP) used with spinner stage
- Completed preliminary XRD scans of Zr-2, Zr-4, C26M and APMT
- Finalized and submitted XRD Test Procedure

PANalytical X'Pert Pro Diffractometer

VCU College of Engineering

99

Contact Angle

Rame-hart Contact Angle Goniometer

- Rame-hart Contact Angle Goniometer is used to measure wettability of surface
- Completed Contact Angle measurements of Zr-2, Zr-4, FeCrAl C26M, and APMT
  - 5 µL droplet was used with plastic needle
  - Followed American Society for Testing and Materials (ASTM Designation D7334-08) standards
  - 50 measurements taken over totality of surface
- Finalized and submitted Test Procedure

Sample stage

Parallel and perpendicular to axial direction
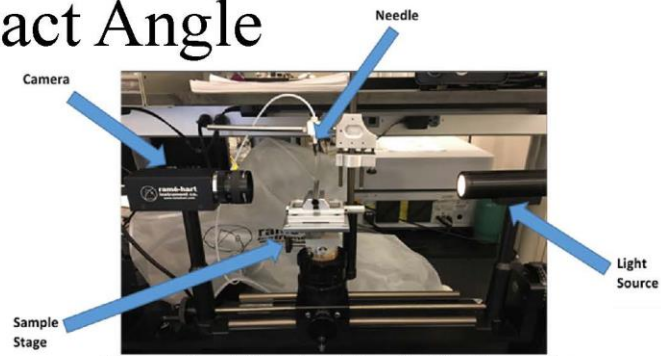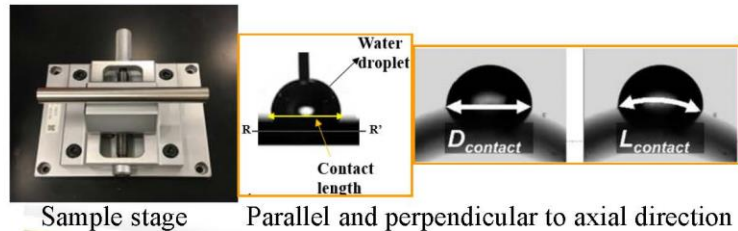
Surface Roughness

- Measure surface roughness parameters
- Completed Surface Roughness measurements of Zr-2, Zr-4, C26M, and APMT
  - 5 mm sampling length measurements
  - Followed the International Organization for Standardization (ISO4288) standards
  - 100 measurements taken over totality of surface
- Finalized and submitted Test Procedure

- Bruker Dimension Icon Atomic Force Microscope used to scan sample surface
- Completed preliminary AFM scans of Zr-2, Zr-4, C26M, and APMT
  - Maximum scan size measured was 90µm x 90µm
  - Tapping Mode used to generate high resolution images, while minimizing damage to the surface
  - Between 3-5 scans for each sample
- Finalized and submitted Test Procedure
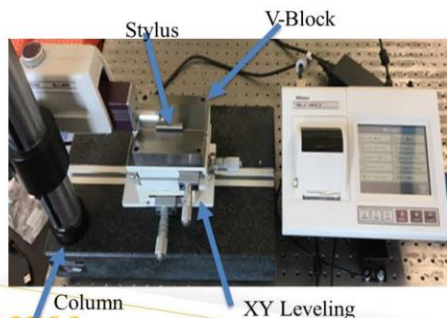
Mitutoyo SJ-410 profilometer
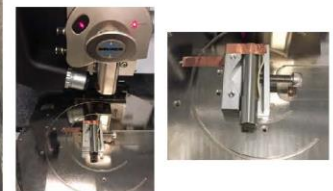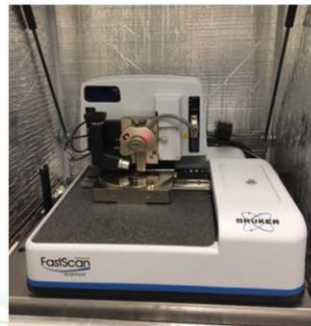
Bruker Dimension Icon Atomic Force Microscope

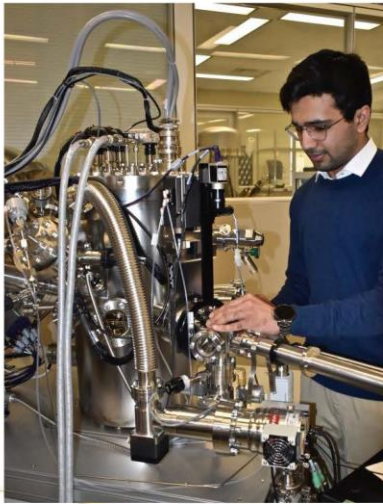# Surface chemistry analysis

PHI VersaProbe III Scanning XPS Microprobe

- Micro-focused, scanning x-ray source which provides excellent large area and superior micro-area spectroscopy performance.
- Spectroscopy, depth profiling and imaging can all be performed over the full range of x-ray beam sizes including the minimum x-ray beam size of less than 10 µm.

FeCrAl APMT tested at UW. Optical appearance may be associated with surface chemistry

VCU College of Engineering

CHF test facilities

- UW Madison has two facilities for studying CHF
  - Near-atmospheric pressures
  - Pressures up to Supercritical
- Flexible in operating conditions and test section design

High Pressure Loop

Atmospheric Pressure Loop

Courtesy from University of Wisconsin

VCU College of Engineering

101

Modeling and Simulation

- The Modeling and Simulation component of this project is being conducted with computational tools provided by FRAMATOME
  - COBRA-U University package

- Non-Disclosure agreement was signed with the company
- Software transfer and training was conducted (April 2019)
  - This stage was substantially delayed from our original plan as FRAMATOME needed to conduct modifications of their code

- One graduate and one undergraduate student as well as 2 Nuclear Engineering faculty (PI and support faculty) were trained
- Software has already been installed in our computer laboratory and preliminary tests are under process.

VCU College of Engineering

Methodology

Materials → ****Coating processes for Zr-4** → **Surface modification**

from GE and FRAMATOME
1. FeCrAl
   APMT
   C26M
2. Zr-4

Cold spray coating
ASB industries

PVD coating:
VCU and ACREE

- FeCrAl:
- ✓ As-received
- ✓ polished 240 grid SiC
- ✓ polished 600 grid SiC
- Cr-Coated Zr-4 ASB
- ✓ Substrate As-received
- Cr-Coated Zr-4 ASB
- ✓ Substrate as-received
- ✓ polished 240 grid SiC
- ✓ polished 600 grid SiC

Modeling/simulation
- Codes will be developed and tested with experimental work

CHF testing at UW
- FeCrAl: full-length and 60 cm tubes will be tested
- Cr-coated Zr only 60 cm long tubes

**Framatome was going to provide Cr-coated Zr however due to technology disclosure issues, only Zr-4 was provided

Data-QA plan

Following the QA program description document, we are:

1. Providing our students with the necessary training and documenting it.
2. Performing standard characterization of samples received from GE and Framatome as a verification point.
3. Managing documents and records, this includes, characterization and testing raw data, developed tests plans, verifying records keeping continuously. Meeting notes are being created and stored. Encrypted drives are being used to store related information
4. Created an ID system for all the samples received and processed for further characterization and results analysis
5. Tracked all the handling, storing, and shipping processes to avoid materials losses and samples being damaged.
6. Control over services being provided by external parties (ASB, ACREE). Documentation of agreements and warranties are stored as well as technical data provided by company
7. All measurement and testing equipment is being calibrated as needed

VCU College of Engineering

RESULTS
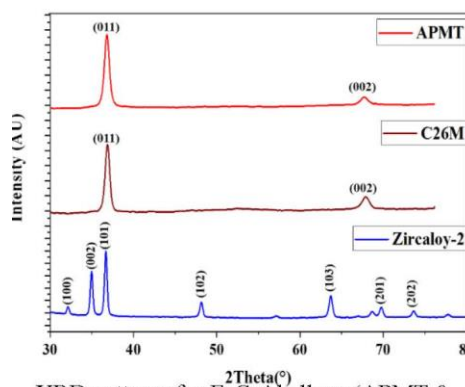
XRD patterns for FeCrAl alloys (APMT & C26M) and Zircaloy-2
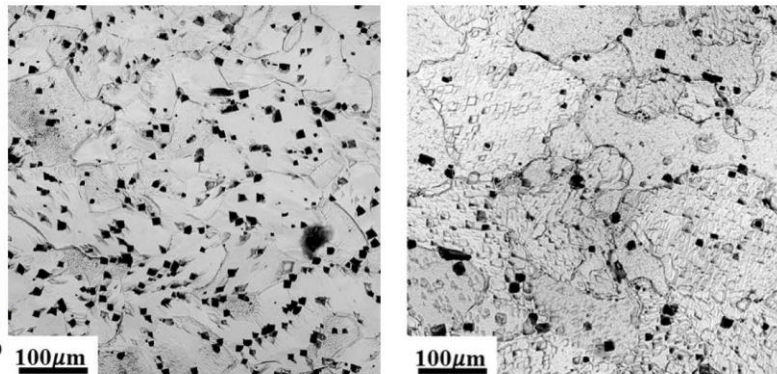
Figure 3. SEM micrographs of etched FeCrAl alloys: a) C26M and b) APMT

Zircaloy-2	Zr	Cr	Fe	Sn	Ni
	96.99	0.24	0.49	1.43	0.85
FeCrAl	Fe	Cr	Al	Mo	Y
APMT	68.54	21.42	5.96	3.43	0.65
C26M	78.49	11.93	6.88	2.29	0.41

EDS analysis of FeCrAl alloys (APMT & C26M) and Zircaloy-2
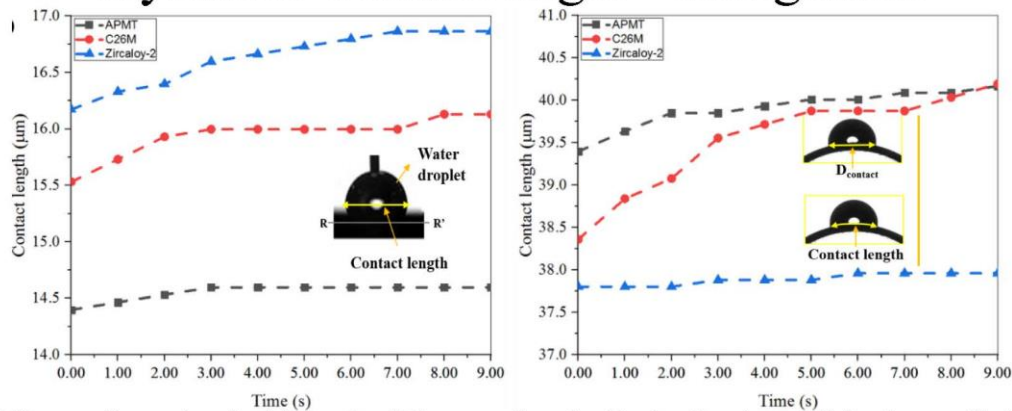
VCU College

Contact angle and SEM
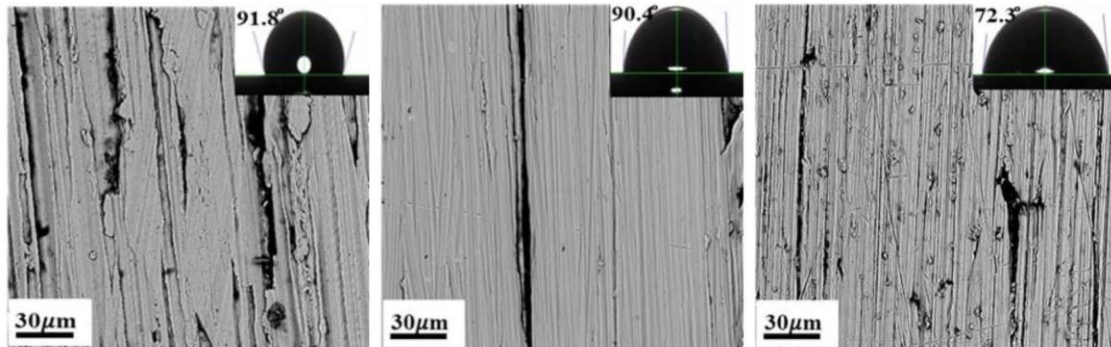
Surface characteristics, including the static contact angle and surface morphologies at microscale for: a) APMT, b) C26M, and c) Zircaloy-2

# Dynamic Contact angle – Roughness

Spreadability test: Contact length with time for all three samples, visualization direction parallel and perpendicular to axial direction

| Material	Roughness						Contact angle (degree)
	SJ-410 Profilometer				AFM		
	Ra (μm)	Rz (μm)	Rsk	Rku	Roughness factor (r)	Rsm (μm)	
Zircaloy-2	0.36±0.04	4.46±1.08	0.01±0.32	4.46±1.79	1.02	0.18	72.33±4.28
APMT	0.68±0.07	5.94±0.84	-0.47±0.12	3.17±0.29	1.07	0.49	91.97±2.78
C26M	0.69±0.07	8.59±1.34	-1.05±0.31	6.23±1.76	1.02	0.38	90.43±2.28

Optical microscopy (APMT)
Surface roughness modification
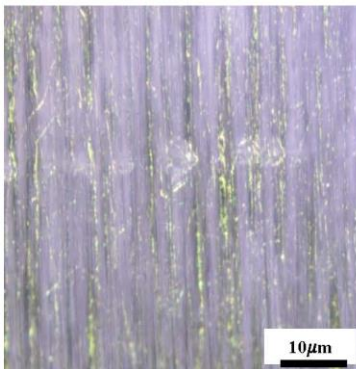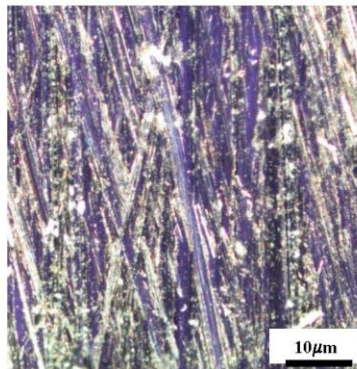

As received   **120 Grit**   **1200 Grit**

VCU College of Engineering
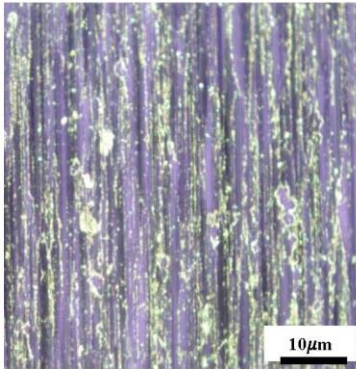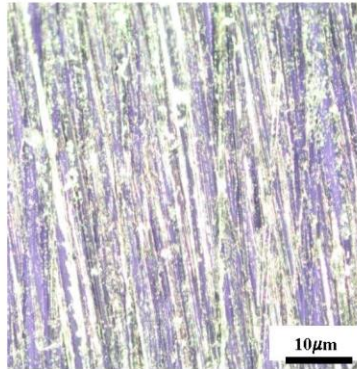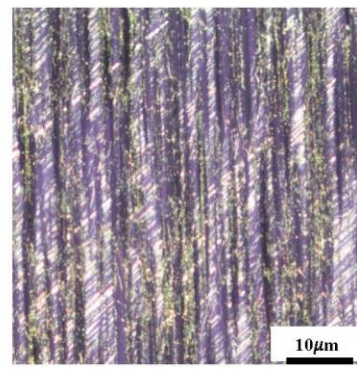
Optical microscopy (C26M)
Surface roughness modification

As received   **120 Grit**   **1200 Grit**

VCU College of Engineering
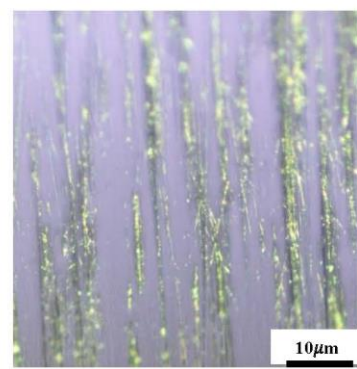
Roughness parameters FeCrAl

Parameters	As received	120 Grit	1200 Grit
Ra (μm)	0.678±0.075	0.889±0.049	0.544±0.074
Rz (μm)	5.941±0.842	11.659±2.372	5.765±1.211
Rsk	-0.466±0.119	-0.712±0.215	-0.647±0.291
Rku	3.172±0.287	5.203±1.358	4.319±2.235
Rsm (μm)	-	221.66±34.827	203.085±29.869
r (AFM)	1.07	-	-

APMT results

- Sample: APMT and C26M
- 100 measurements were taken through out the surface

C26M results

Parameters	As received	120 Grit	1200 Grit
Ra (μm)	0.689±0.072	0.956±0.205	0.572±0.034
Rz (μm)	8.586±1.337	14.570±2.835	7.993±1.010
Rsk	-1.050±0.311	-0.585±0.295	-1.563±0.245
Rku	6.230±1.759	5.843±1.622	8.407±1.745
Rsm (μm)	-	248.750±48.139	372.985±61.089
r (AFM)	1.02	-	-

VCU College of Engineering

AFM characterization of C26M

As received   **1200 Grit**   **120 Grit**
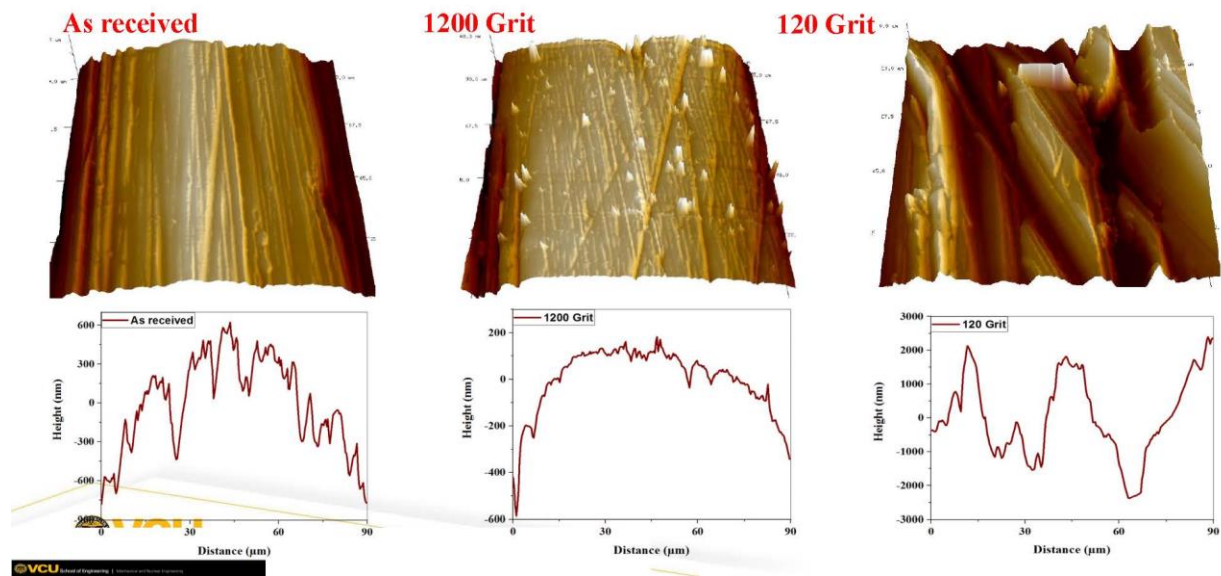
Preliminary results Cr-Coated Zr-4
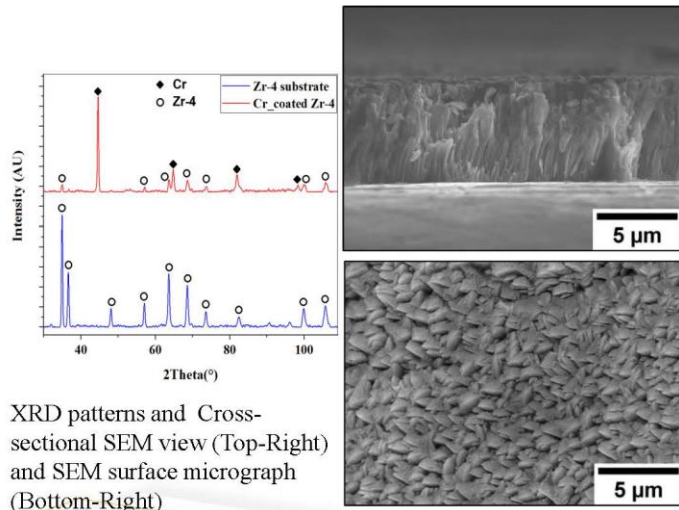
TABLE I. Surface roughness measurements

Roughness Parameters (μm)	Substrate Zircaloy-4	Cr-coated Zircaloy-4
Ra	0.399	0.442
Rsm	31.420	32.260
Rz	2.715	3.245
Rq	0.494	0.551

XRD patterns and Cross-sectional SEM view (Top-Right) and SEM surface micrograph (Bottom-Right)
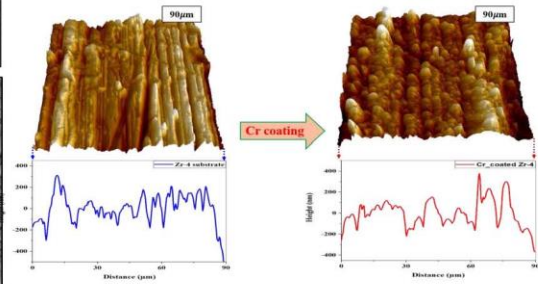
AFM surface morphology and roughness distribution of as received Zircaloy-4 before (Left) and after (Right) Cr coating

VCU College of Engineering

Acree Cr-coating PVD
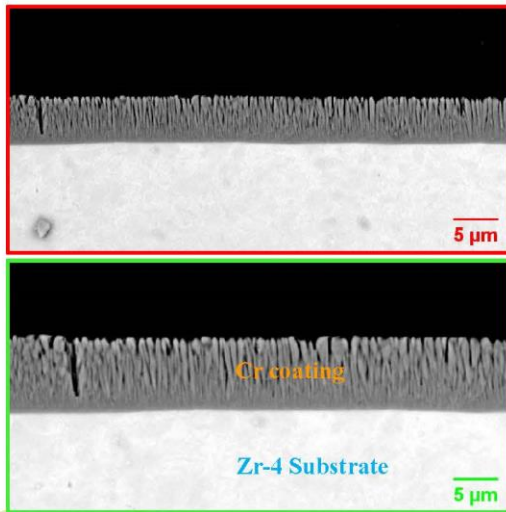
SEM micrographs showing a uniform Cr coating ~ 6.5um thick

Roughness before and after Cr coating
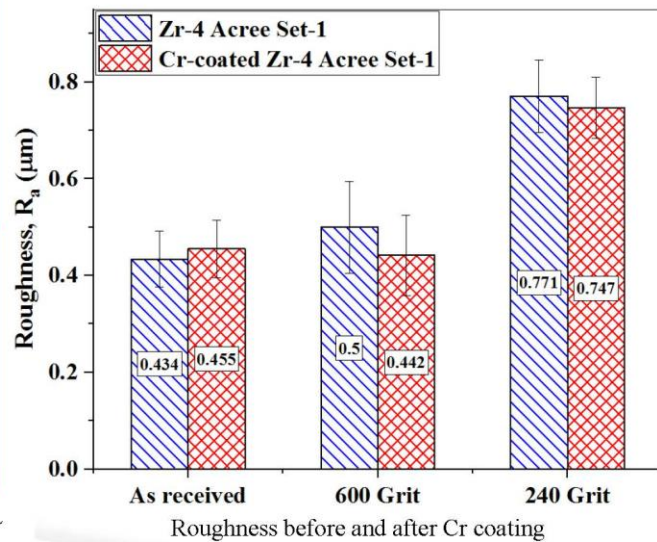
Contact angle Cr-coated Zr-4

Material	Contact angle (°)		
	After Coating	Ultrasonic Cleaning	Plasma Cleaning
Acree	91.95±7.28	127.15±6.12	27.01±3.03
ASB	93.98±6.13	100.95±9.41	41.86±10.17
VCU	21.03±2.71	111.14±7.00	0

Contact angle comparison for As received Samples
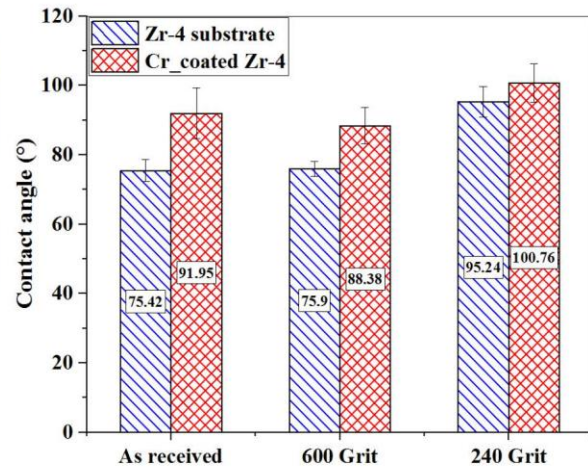
Contact angle before and after Cr coating (PVD (Acree))

Surface behavior with aging
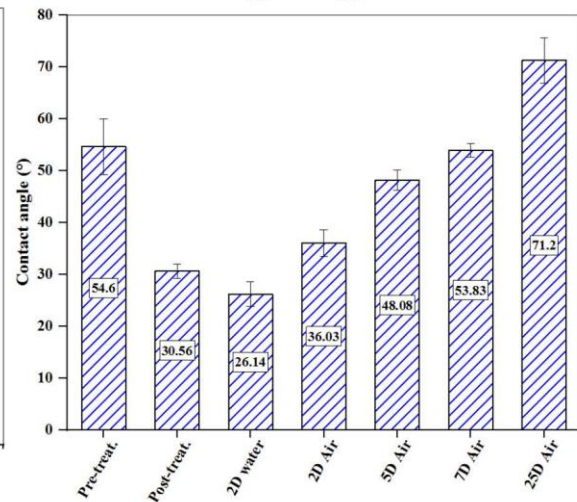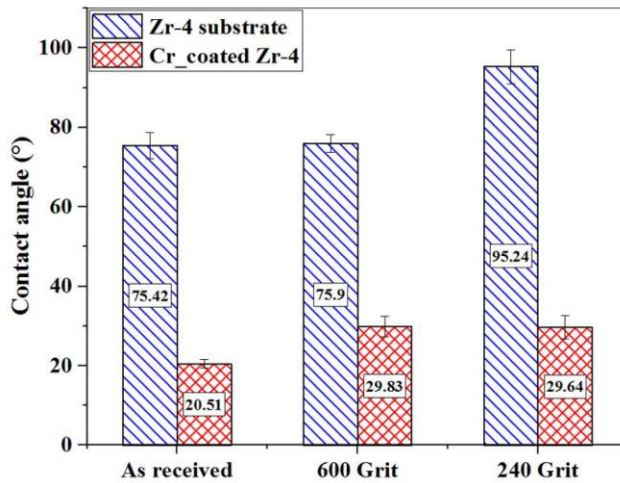
a)Cr-Coated Zr-4, coating performed at VCU and analysis done right after coating b) contact angle evolution with water/air exposure

Surface Chemistry
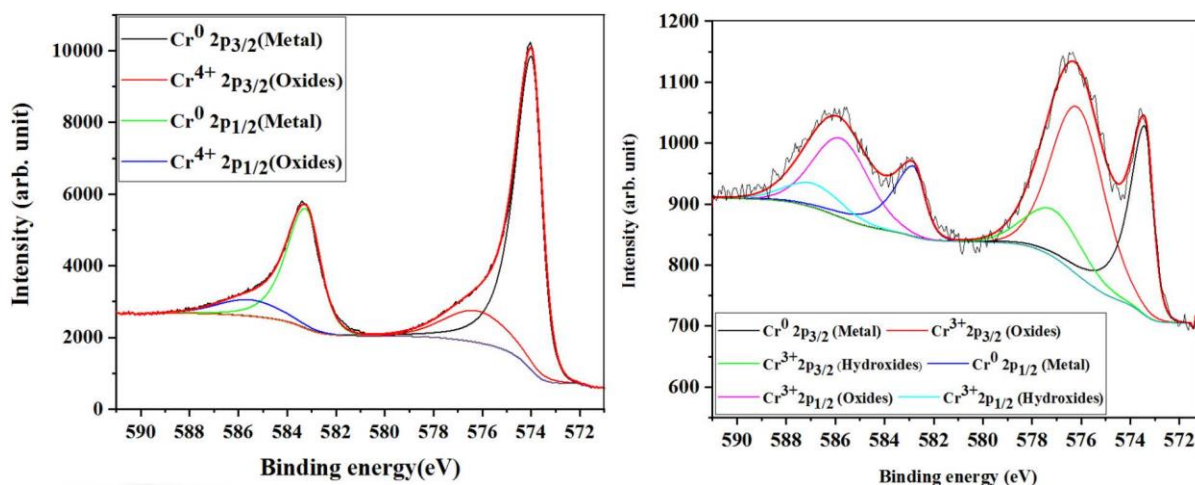
Cr 2p XPS spectrum of 240 grit Cr-coated Zr-4 (a) Reference sample (after coating) and (b) DI Water (2 days) and Air (25 days) exposed

Optical Microscopy (Cr-coated Zr-4-ASB)

Spot Length	Diameter before Spray (mm)			Diameter after Spray (mm)			Final Coating Thickness (μm)
	0 Deg	120 Deg	240 Deg	0 Deg	120 Deg	240 Deg	
5"	9.498	9.501	9.500	9.560	9.556	9.554	28.46
9"	9.501	9.499	9.500	9.565	9.560	9.560	30.84
13"	9.500	9.500	9.501	9.561	9.556	9.558	28.97
17"	9.499	9.499	9.499	9.559	9.573	9.557	28.65

Material	Average roughness, Ra (μm)
Substrate	0.434$\pm$0.058
Cr-coating	1.332$\pm$0.352

Challenges

- The challenges associated with the execution of this work have been mainly associated with delayed materials from our partner companies.
- GE delivered samples for preliminary experiments and test plans in June 2018.
- Framatome decided not to provide the Cr-coated Zr-4 due to technical reasons. This affected our timeline and schedule.
- The team arranged with Framatome the delivery of Zr-4 and VCU will handle coting service from external providers. Acree and ASB were selected. The team received Zr-4 at the beginning of 2019.
- The delivery of COBRA-U was also delayed due to NDA needed to be produced and signed.
- The team received the code in April 2019.

VCU College of Engineering

Future Work

- *Near term efforts (Path Forward)*
- Finalize the surface characterization of the Cr-coated Zr-4. We are planning to benchmark our coatings with the ones being produced by Framatome with regards to thickness.
- VCU has provided bare Zr-4 and Cr-coated Zr to UW. The next step in this work will focus on preparing and running CHF test in the atmospheric pressure loop.
- Acquire full length FeCrAl tubes from GE. Once they are sent, their surface will be modified following the procedures developed previously.
- *Long term efforts (Path Forward)*
- Start modeling and simulation efforts as we continue with our experimental work.

VCU College of Engineering

Publication and students involved

Graduate students:
- At VCU: Rajnikant Umretiya: 3rd Year PhD student (already passed QE)
- At UW: Barret Elward

Undergraduate students:

Robert Uhorchuk: Junior student in Mechanical and Nuclear Engineering, funded partially by the Dean Undergraduate Research Initiative (DERI)

Publications:

2019 ANS Winter Meeting & Expo
1. Surface Characterization of Chromium Coated Zircaloy-4 Accident Tolerant Fuel Cladding Material.
Rajnikant Umretiya, Robert Uhorchuk, Santiago Vargas, Carlos E. Castano, Jessika Rojas
2. Aging Effect of Chromium Coated Zircaloy-4 Accident Tolerant Fuel Cladding Material
Authors: Rajnikant Umretiya, Santiago Vargas, Robert Uhorchuk, Carlos E. Castano, Jessika Rojas
3. Evaluation of Surface Characteristics of FeCrAl alloy Accident Tolerant Fuel Cladding Material after Critical Heat Flux Testing under Atmospheric Pressure. Rajnikant Umretiya, Robert Uhorchuk, Mark Anderson, Barret Elward, Sama Bilbao y Leon, Raul B. Rebak, Jessika Rojas

Publications:

NURETH 2019
Surface Characteristics od Accident Tolerant Fuel Claddings and their potential impact in Critical Heat Flux **Rajnikant Umretiya, Daniel Ginestro, Sama Bilbao y Leon, Barret Elward, Mark Anderson, Raul B. Rebak, Jessika Rojas.**

TMS 2020 (149th Annual Meeting & Exhibition) (Submitted)
1. Evaluation of Surface Characteristics of Cr-coated Zr-4 Accident Tolerant Fuel Cladding Material after Critical Heat Flux Testing under Atmospheric Pressure. Rajnikant Umretiya, Mark Anderson, Barret Elward, Sama Bilbao y Leon, Raul B. Rebak, Jessika Rojas. Status: **Under Review**

2. Surface Characterization of FeCrAl Accident Tolerant Fuel Cladding Material after Flow Boiling Testing under Atmospheric Pressure. Rajnikant Umretiya, Mark Anderson, Barret Elward, Sama Bilbao y Leon, Raul B. Rebak, Jessika Rojas. Status: **Under Review**

3. Surface Characterization and Mechanical Properties of Cr-coated Zr-4 Accident Tolerant Fuels Cladding prepared using different Coating Techniques. Authors: Rajnikant Umretiya, Santiago Vargas, Carlos E. Castano, Reza Mohammadi, Jessika Rojas. Status: **Under Review**

Summary

- The issues with materials availability were resolved
- The team has carried out an extensive characterization and analysis of surface medication on FeCrAl alloys.
- We received the Cr-coated Zr-4 from both ASB and Acree and materials characterization is in process.
- Preliminary results on CHF for APMT were produced at UW and VCU has started identifying changes associated with surface characteristics related to both morphology and chemistry.
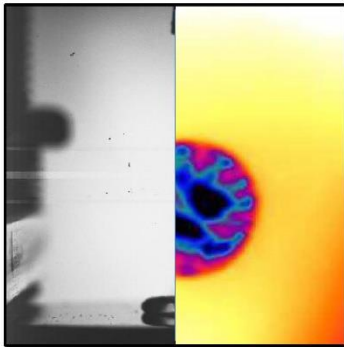
VCU College of Engineering

Questions?

VCU College of Engineering

Appendix H

Investigation of Droplet Quenching on Accident-Tolerant Coating Using Infrared Thermometry

Appendix H

# Investigation of Droplet Quenching on Accident Tolerant Coating Using Infrared Thermometry

Investigation of Droplet Quenching on Accident Tolerant Coatings Using Infrared Thermometry

Understanding Leidenfrost phenomena on ATF materials

H. Kim, W. McGee, A. Kossolapov, B. Phillips, M. Bucci
Massachusetts Institute of Technology
Department of Nuclear Science and Engineering

Introduction and significance of the work

- Spray cooling (BWR)
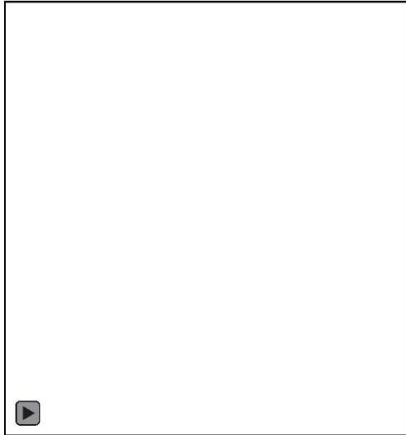
$$D_{avg} = 1{\sim}2 \ mm$$

$$We_n = \frac{\rho v_n^2 D}{\sigma} < 30$$
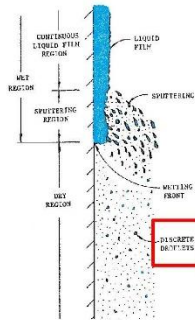
- Boiling curve

  Leidenfrost temperature
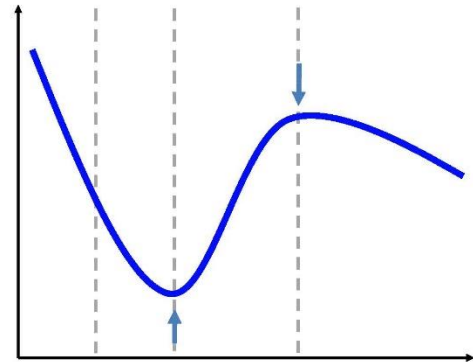
Background

- ATF quenching experiments and T_{MFB}
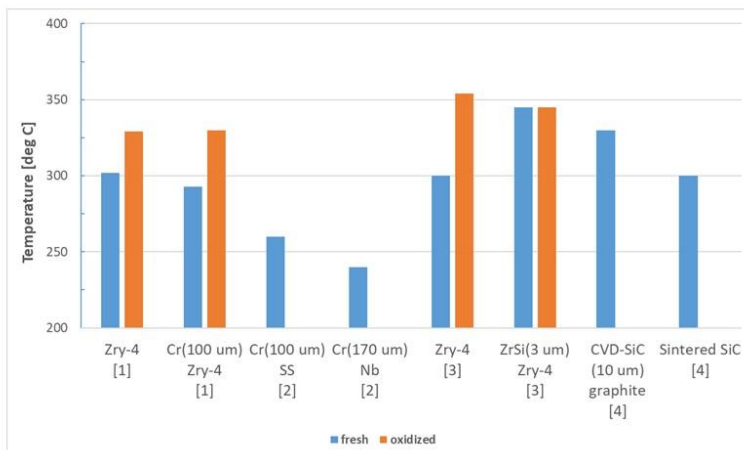
Reference	Type	Definition
Seshadri (2018) [1]	Pool (~100 ˚C)	Dynamic
Lee (2017) [2]	Pool (~100 ˚C)	Dynamic
Lee (2019) [3]	Droplet (~25 ˚C)	Static
Wang (2019) [4]	Droplet (~25 ˚C)	Hydro-dynamic

3

Background

Quenching Experiments	Pool	Droplet
ATF material	• Materials Zry, Cr, FeCrAl, SiC … Effect of oxidation • Surface parameters thermal properties, roughness, wettability, porosity … • System parameters pressure, subcooling …	• Few available ZrSi (Lee, 2019) SiC (Wang, 2019) This work
Other material		Various materials (Si, metal, …) Micro/nano structured surfaces

Objectives

• Quantify Leidenfrost temperature of potential ATF coating materials under BWR spray quenching conditions:

  Surface material: unoxidized and oxidized Zircaloy, SiC-, Cr-, and FeCrAl-coated
  Surface finish: nano-smooth and rough (same as PWR claddings)

  as a function of droplet subcooling and droplet Weber number

• Develop ATF-material-specific correlations to be implemented

Methodology: sample preparation

Simplified - Not to Scale

- PVD sputtering
  Ti (~100 nm) and Cr (~300 nm) layer

- Change in colors

As fabricated   After heated up to ~ 500 ˚C
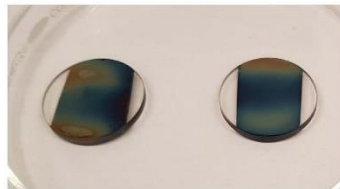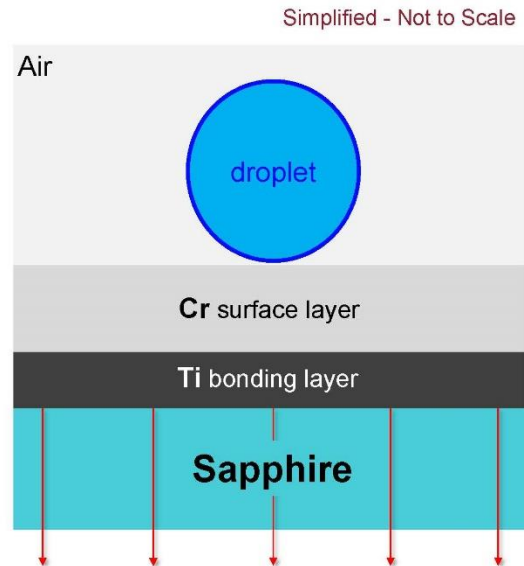
Air

droplet

Cr surface layer

Ti bonding layer

Sapphire

Methodology: Droplet quenching facility

- 2 mm droplet
  Weber number ~ falling height
- Up to ~ 500 ˚C
- Target area ~ 0.6×0.6 cm^2
  IR field of view
- IR and HSV diagnostics
  IR: 30 um/pixel, 3000 fps
  HSV: 20 um/pixel, 3000 fps
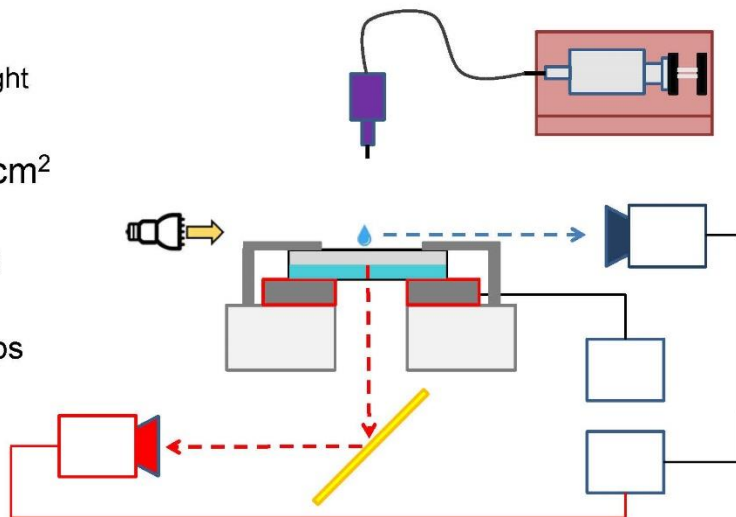
Methodology: Droplet quenching facility

- 2 mm droplet
  - Weber number ~ falling height
- Up to ~ 500 °C
- Target area ~ 0.6×0.6 cm^2
  - IR field of view
- IR and HSV diagnostics
  - IR: 30 um/pixel, 3000 fps
  - HSV: 20 um/pixel, 3000 fps
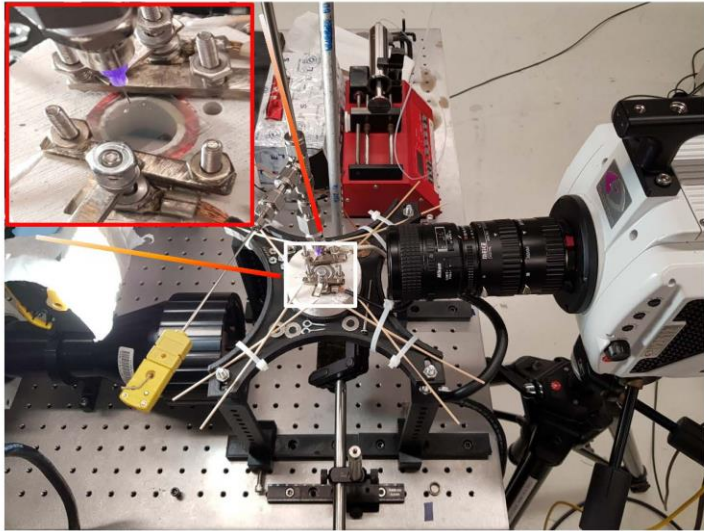
Methodology: IR data post-processing

- T, HTC
- $\alpha_\lambda, \rho_\lambda, \tau_\lambda$
- k, ρ, c_p
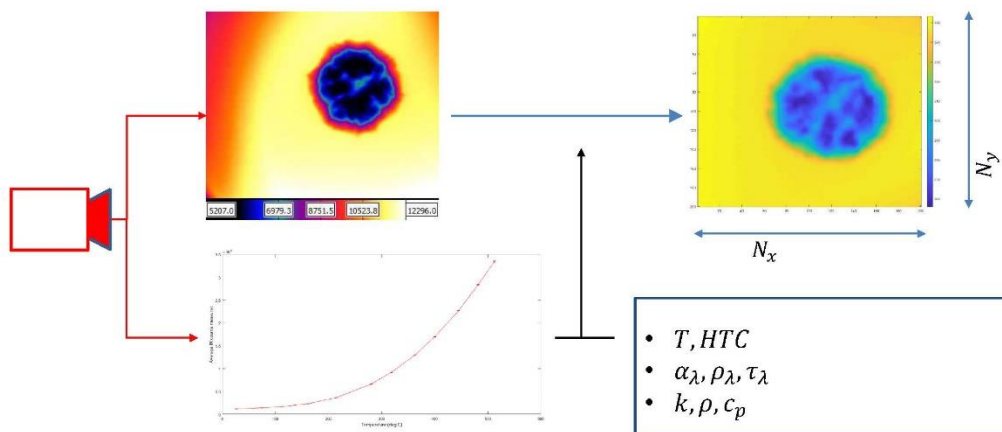
Result

- Nucleate boiling (~ 140 °C)

HSV   Surface temperature
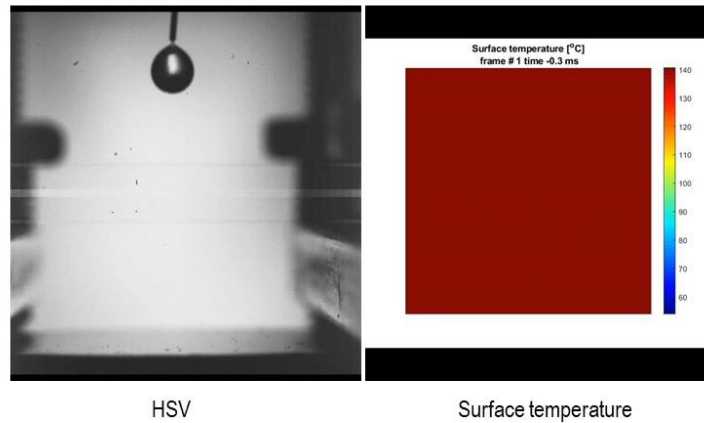
Result

- Transient boiling (~ 240 °C)

HSV   Surface temperature
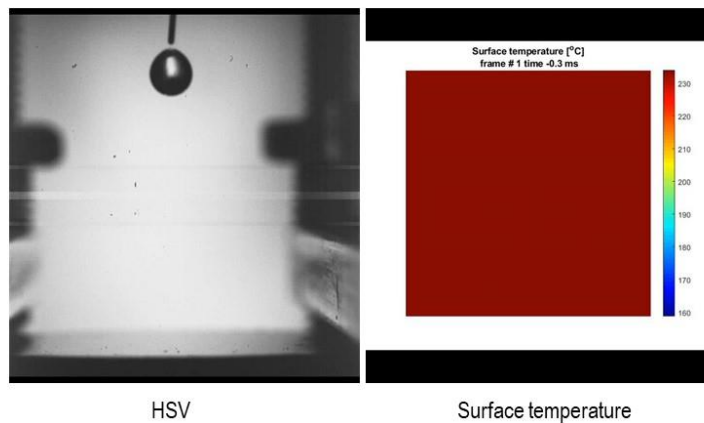
Analysis

- Leidenfrost temperature (hydrodynamic)

150 °C   235 °C   380 °C

400 °C   435 °C   525 °C

$$We = 7.3$$
$$T_{sub} = 75\ K$$

Surface temperature

550 °C
525 °C

400 °C
380 °C

235 °C
150 °C

Weber number

Subcooling

13
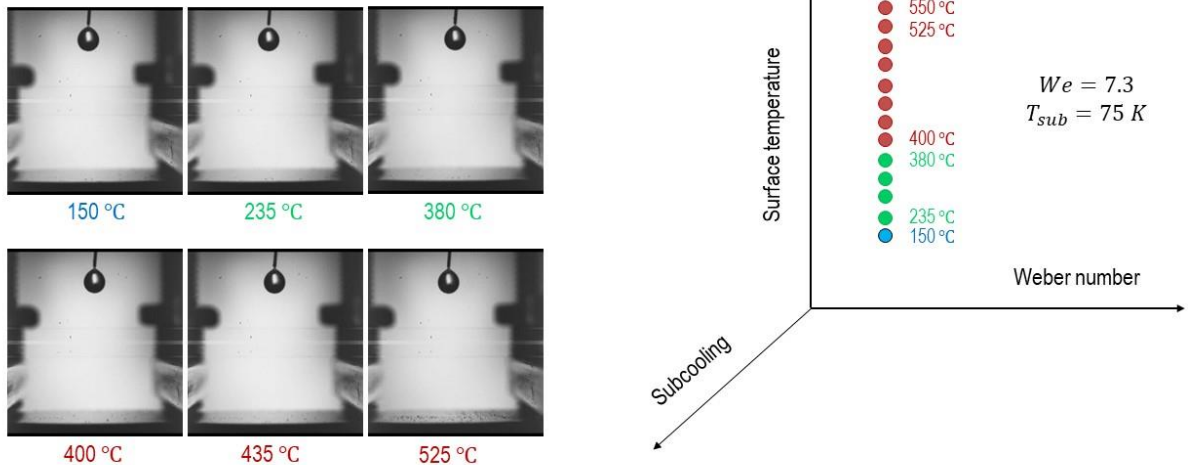
Result

- Film boiling (~ 520 °C)

Surface temperature [°C]
frame # 1 time -0.3 ms

HSV   Surface temperature

12

120
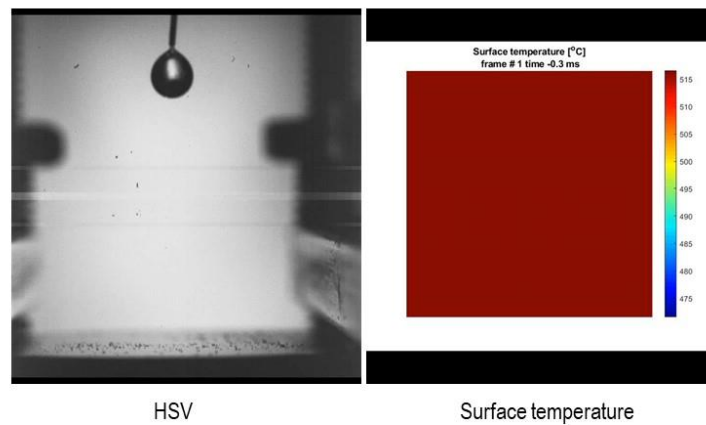
Methodology: further IR data post-processing

Raw data   Temperature / Heat flux

- Macro- quantities
  - Heat transfer efficiency
  - Spreading area
  - Contact time
- Micro- quantities
  - Intermittent contacts
    $(N, t, f, D \dots)$

- Surface parameters
  $k, \rho, c_p, R_a, \theta, r_{pore} \dots$
- System parameters
  T_{sub}, We

T_{MFB}
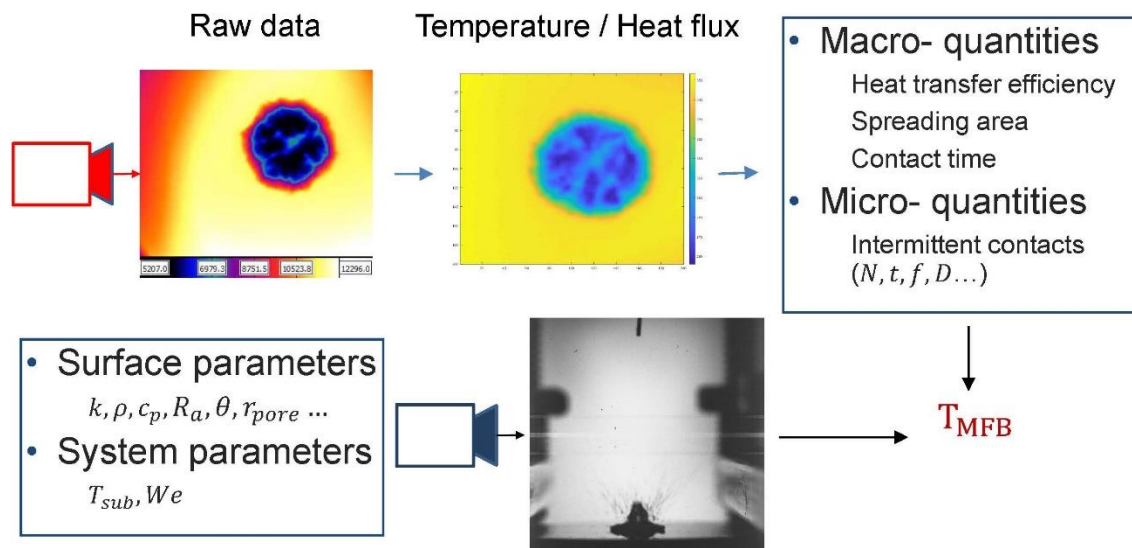
Path forward

Quantify Leidenfrost temperature of potential ATF coating materials under BWR spray quenching conditions:

Surface material: unoxidized and oxidized Zircaloy, SiC-, Cr-, and FeCrAl-coated
Surface finish: nano-smooth and rough (same as PWR claddings)
as a function of droplet Weber number and droplet subcooling

Priority
1. Surface material
2. Surface finish
3. Droplet subcooling
4. Droplet weber number

Backup slides

Star CCM+ calculation
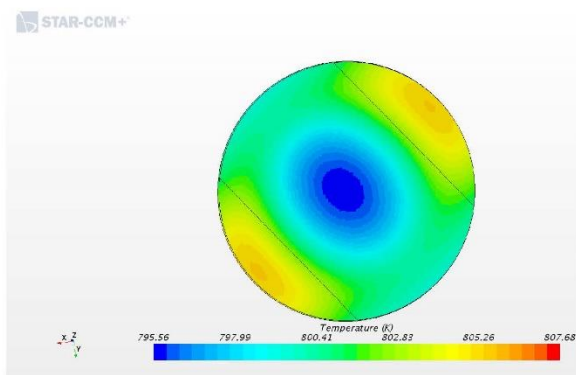
Top view
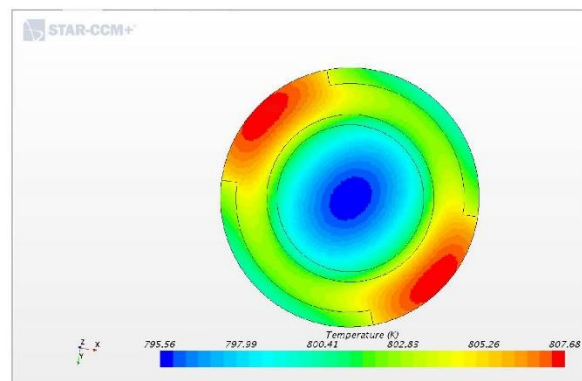
Bottom view

Heat flux = 10 W, HTC = 20 W/m^2 K
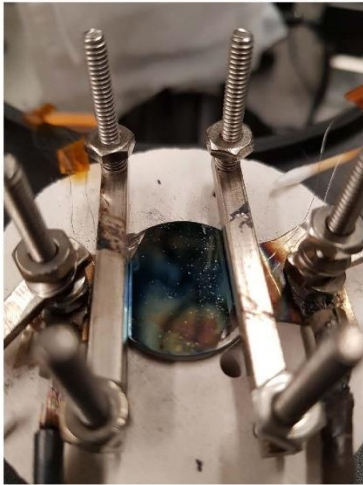
Thermocouple installation
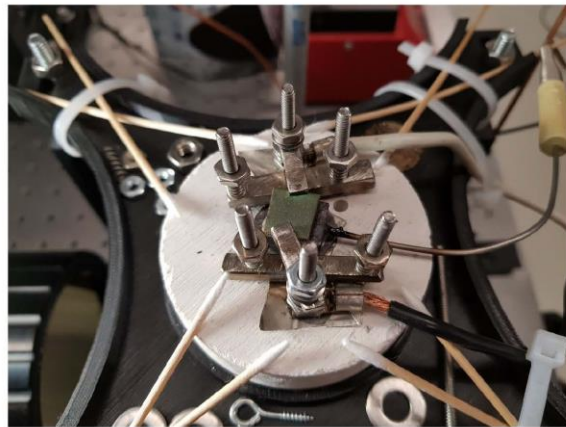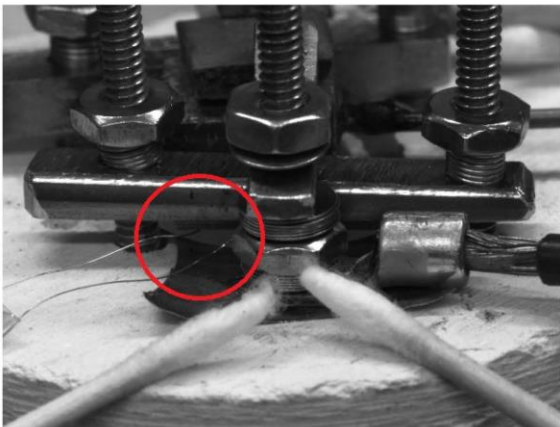
Appendix I

CHF and CRUD WALT Loop Measurements
for Westinghouse Accident-Tolerant Fuel

Appendix I

CHF and CRUD WALT Loop Measurements for Westinghouse Accident-Tolerant Fuel

CHF and CRUD WALT Loop Measurements for Westinghouse Accident Tolerant Fuel

Zeses E. Karoutas, Guoqiang Wang, William A. Byers

[1]Westinghouse Electric Company, LLC
NEUP ATF CHF Meeting at MIT, August 13, 2019
Boston, MA

Westinghouse

1

Outline

- Introduction
- Westinghouse [1]Encore® Fuel
- Description of WALT Loop Test Facility
- WALT CHF Test Method and Procedure
- WALT Loop CHF Test Results
- CRUD Adherence Testing
- Conclusions and Recommendations

Westinghouse

2

Introduction

- Westinghouse is developing ATF fuel products which change the cladding surface
  - Chromium coated cladding and SiC cladding

- Testing has begun in the WALT loop to evaluate the heat transfer and CHF performance with and without coating and CRUD relative to current cladding materials

- Testing also being performed to assess adherence of CRUD deposits

Tests performed in Westinghouse WALT Loop Facility

Westinghouse

3

Westinghouse's EnCore® Fuel

EnCore® includes both incremental and game changing products to enable a sensible path to achieve full ATF benefits.

EnCore® Products:

✓ Advanced Cladding
  ✓ Cr-coated zirconium
  ✓ SiC
✓ Advanced Fuel
  ✓ ADOPT™ doped fuel pellets
  ✓ U_3Si_2 pellets

Chromium-Coated Zr Cladding

Silicon Carbide (SiC) Composite Cladding

Photo courtesy of General Atomics

Product Evolution

ADOPT™ Pellets

Uranium Silicide (U_3Si_2) Pellets

Photo courtesy of Idaho National Labs

Westinghouse

4

Description of WALT Loop Test Facility – Simulate Top Grid Span of PWR Fuel
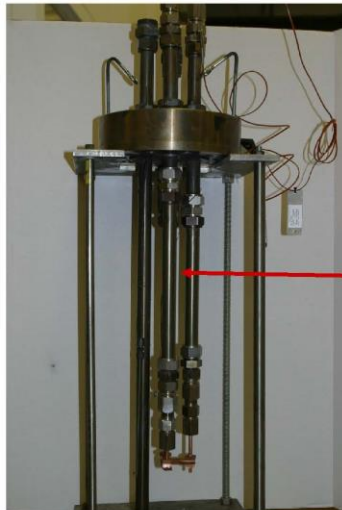
Heater Rod in the WALT Test Loop

Westinghouse

WESTINGHOUSE FUEL USER'S GROUP
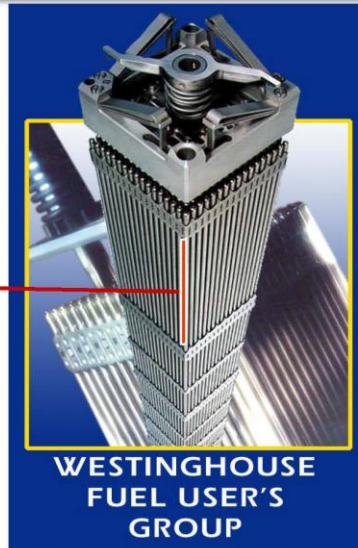
PWR Fuel Assembly

5

Description of WALT Loop Test Facility – Loop Layout
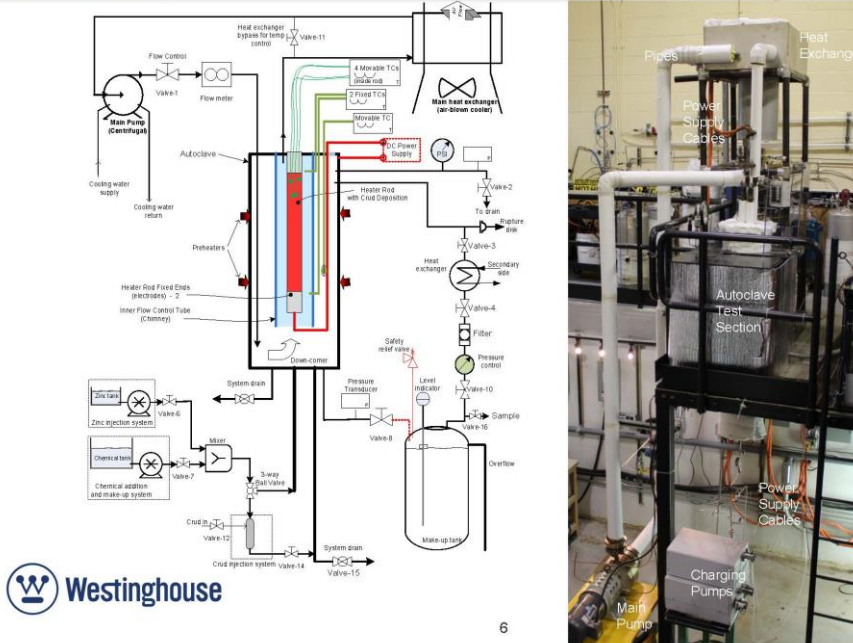
6

Heater Rod Design – Direct Heating

NOT TO SCALE
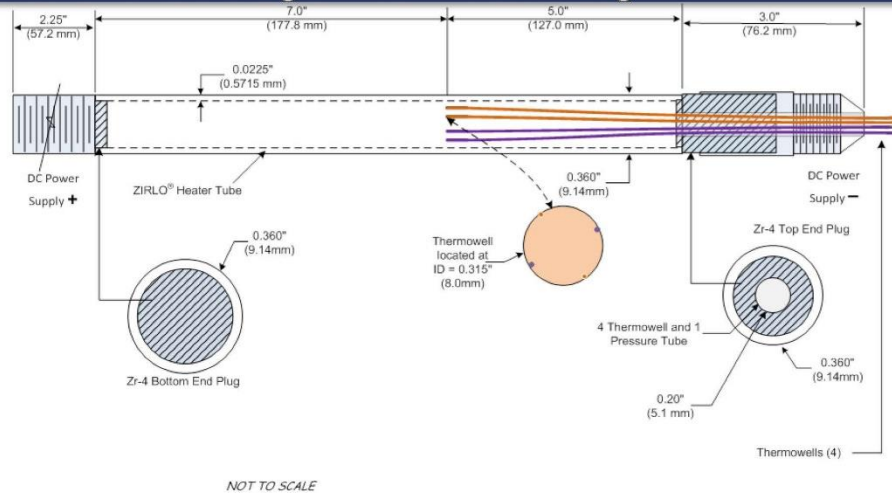
Thermocouples can be moved axially

7

128

Key Parameters of WALT Loop

PARAMETERS	UPPER LIMITS
System pressure, MPa	17.22
DC power supply, kW	90
DC power supply, Amps	1800
DC power supply, Volts	100
Heat exchanger, kW	31.8
Flow velocity, m/s	6.00
Inlet temperature, °C	<Tsat
Axial Power Shape	Uniform
Heater rod materials	Inconel, Zr-4, ZIRLO®
Heater rod length, m	<1.35 (0.33 heated typical)
Heater rod OD, mm	9.50
Heater rod ID, mm	8.35~9.2
Test section shroud ID, mm	20.96
Test section flow area, mm^2	274.0

Westinghouse

Coolant used in tests 1000 ppm Boric Acid, 2.2 ppm LiOH

8

WALT CHF Test Method and Procedure

DNB Test Procedures:

- Establish Initial DNB Test Conditions
  - ❑ Setup desired Flow, exit pressure, and inlet temperature
  - ❑ Setup 75~80% predicted CHF power
- Slowly increase power
  - ❑ About 5~6 amps per step (for the current WALT loop design)
- Monitor heater rod cladding temperatures
- Observe the temperature excursion
  - ❑ See the figures in the left column
- Record DNB conditions
  - ❑ Maximum power

Westinghouse

9
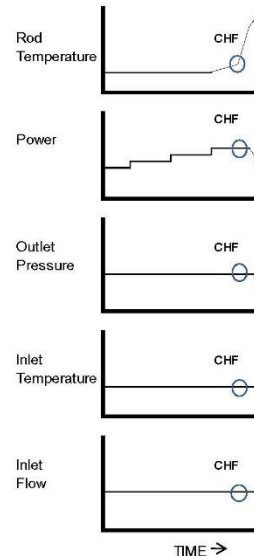
129

Electrical Resistance Measurement

Rod-198 Resistance (ohm/in) vs Cladding Temperature

$y = 9.617210E\text{-}07x + 1.164478E\text{-}03$
$R^2 = 9.949689E\text{-}01$

Rod-199 Resistance (ohm/in) vs Cladding Temperature

$y = 8.626462E\text{-}07x + 8.439864E\text{-}04$
$R^2 = 9.981742E\text{-}01$
where, y = Resistance (ohm/in)
x = average cladding temperature (°F)
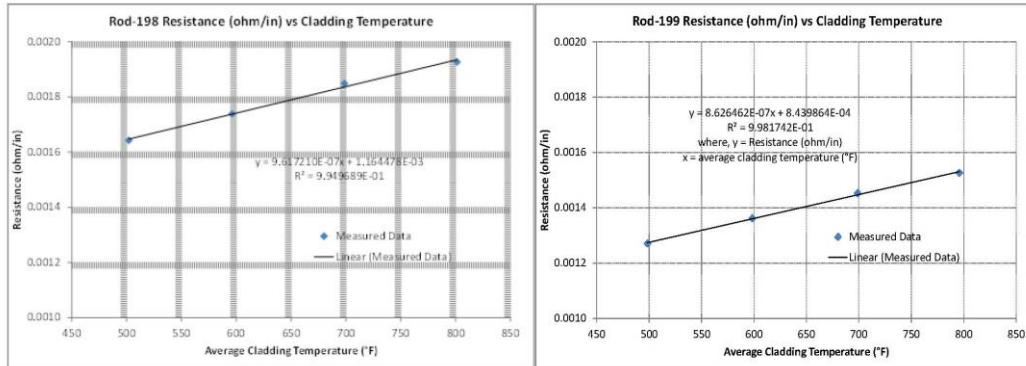
Uncoated Cladding   Coated Cladding

Chromium coating had a noticeable impact on measured resistance

Westinghouse

10

WALT Loop CHF Test Results

- CHF Tests performed with and without coating

- Test results grouped according to approximate constant TH conditions

- CRUD was deposited on some tests

- CHF variation in each region approximately +/- 6%

Westinghouse

Rod #	Run #	Cr-Coating	Average Crud Thickness	Inlet Temperature	Flow	Pressure	CHF	Relative Change in CHF compared to Average
			Microns	Deg-C	m³/hr	bars	W/cm²	%
198	1a	No	0	336.8	2.42	152.63	233.12	4.74
198	1b	No	0	339.5	2.37	154.05	208.94	-6.12
198	1c	No	0	338.7	2.42	156.58	221.22	-0.60
193	1a	Yes	0	338.1	2.38	148.78	231.16	3.86
193	1b	Yes	0	338.1	2.40	158.99	218.37	-1.88
Average				338.2	2.40	154.21	222.56	
198	2a	No	0	339.9	3.49	156.21	245.91	-1.37
198	2b	No	0	340.6	3.49	156.72	256.16	2.74
194	1a	Yes	0	339.9	3.39	153.88	241.95	-2.96
195	1a	Yes	0	339.6	3.37	151.78	249.99	0.26
200	1a	Yes	0	338.8	3.39	153.46	239.53	-3.93
200	1b	Yes	43	341.7	3.38	155.16	249.97	0.26
201	1a	Yes	0	339.2	3.38	156.94	247.82	-0.61
201	1b	Yes	40	339.4	3.41	156.86	263.32	5.61
Average				339.9	3.41	155.13	249.33	
198	3a	No	0	329.1	3.34	128.57	258.74	0.92
198	3b	No	0	328.3	3.41	125.08	257.88	0.58
199	1a	Yes	0	328.7	3.22	126.78	275.70	7.53
202	1a	Yes	0	330.6	3.00	127.90	238.65	-6.92
202	1b	Yes	21	331.1	3.25	130.52	250.97	-2.11
Average				329.5	3.24	127.77	256.39	

11

130

Typical CHF Test for Rod 198 2b Uncoated No Crud

Westinghouse
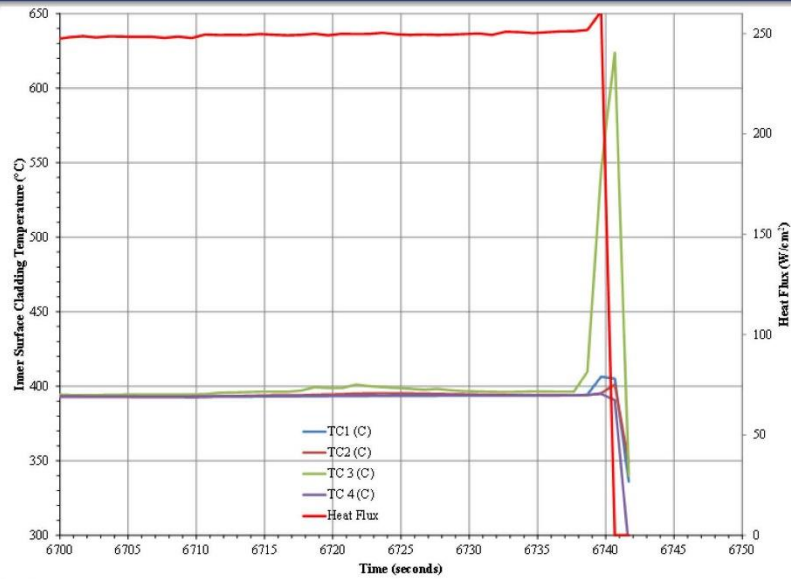
12

CHF measurements for approximate average T-H conditions (Tinlet 338.2°C, Flow 2.40 m3/hr, Pressure 154.21 bar)

Westinghouse

13

131
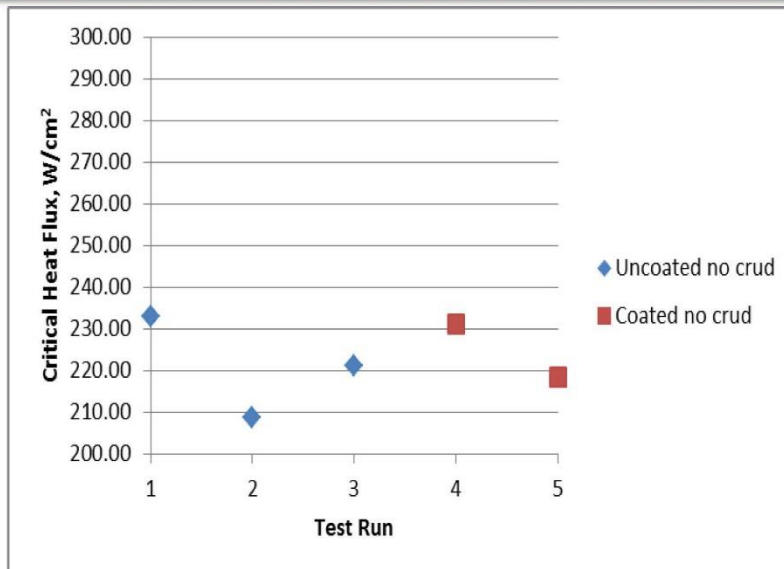
CHF measurements for approximate average T-H conditions (Tinlet 339.9°C, Flow 3.41 m3/hr, Pressure 155.13 bar)

Westinghouse

14

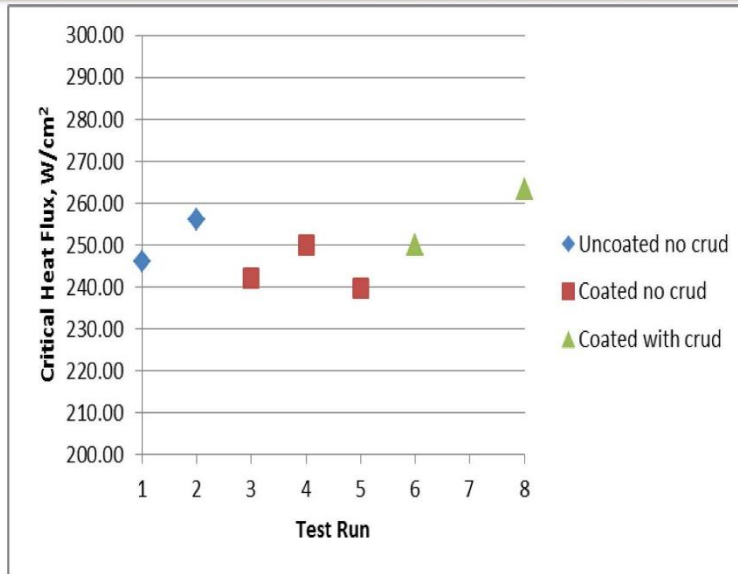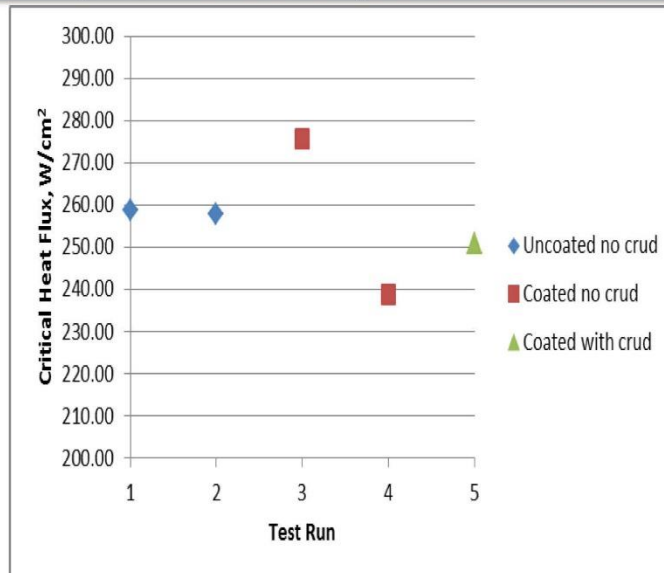## CHF measurements for approximate average T-H conditions (Tinlet 329.5°C, Flow 3.24 m3/hr, Pressure 127.77 bar)

Westinghouse

15

132

CRUD Testing

- CHF impact due to coating and/or CRUD deposit appeared to be within the normal variation observed for a clean surface without coating

- CRUD was deposited on coated rods 200, 201 and 202 where CRUD adhered on average of ~5.1 microns per injection, where CRUD adhered on an uncoated rod ~6.75 microns suggesting that the coated surface did not increase CRUD adherence
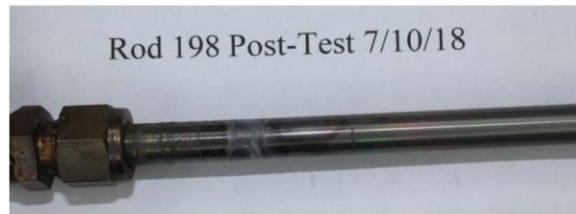
Post-test observation of Rod 198 uncoated surface no crud

Post-test observation of Rod 200 coated surface with crud

Some CRUD can come off during or after CHF testing

Westinghouse

16

Conclusions and Recommendations

- Current CHF test data for Cr-coated and crud surfaces using direct type heating suggest CHF performance is within CHF variation for clean uncoated cladding surfaces therefore no adverse CHF impact is expected due to the Westinghouse Cr coating application.

- The variation observed in WALT loop CHF tests for uncoated and Cr-coated surfaces appear to be somewhat large possibly due to use of direct type heating and not being able to keep T-H conditions close to target for making relative comparisons. It is recommended that future CHF tests be performed with indirect type heater or more accurate direct heating to possibly reduce scatter and modify loop instrumentation to better control T-H conditions.

- The application of Cr-coating significantly affects electrical resistance. This large change in electrical resistance can introduce more uncertainty in CHF measurements. The use of indirect type heating may help reduce this uncertainty. Some improvement in CHF maybe observed due to Cr-coated and crud surfaces as a result of using indirect heating.

Westinghouse

17

133

Conclusions and Recommendations (Cont.)

- Further testing is recommended on crud adherence for uncoated and coated surfaces using indirect heating on a single heater rod. The use of electrical current through cladding may have an impact on CRUD deposits and CHF measurements

- Future CHF testing is recommended to be performed to determine how long an ATF cladding surface can stay in DNB without damage to the cladding. These tests shall be performed for Cr coated and SiC cladding type surfaces.

Current CHF testing of ATF surfaces at reactor conditions and chemistry appear to show no adverse impact

Westinghouse

18

WALT DNB Tests for the NEUP Program

Westinghouse

19

Heater Rod Design – Direct Heating
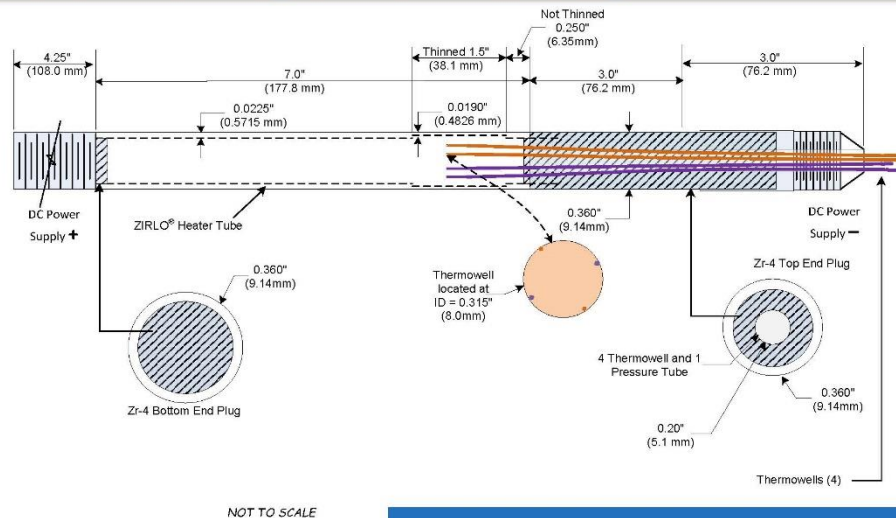
Thermocouples can be moved axially and current heater wall will be thinned down

20

WALT DNB Tests – High Level Planning

- WALT DNB/CHF Test Planning
  - ❑ **_Low Flow Cases_** To provide benefits for DNB limiting cases of a loss of flow or locked rotor event, with a transient time of a few seconds
  - ❑ **_Core Limit Cases_**: To cover a pressure range from 1800 psia to close to 2400 psia
  - ❑ **_Tinlet Cases_**: To cover a range of inlet temperatures
  - ❑ **_Crud Cases_**: Perform DNB tests before and after crud deposition
  - ❑ **_Selected Cases_**: Listed on next table

21

WALT DNB Test Matrix – Selected Cases

	Flow (gpm)		Pressure (psia)		Tinlet (°F)	
	60%	Normal	1800	2250	605	635
Tube-1	✓			✓		✓
Tube-2		✓		✓		✓
Tube-3		✓	✓		✓	
Crud		✓		✓		✓
Transient	✓			✓		✓

Westinghouse

22

DNB Test Results for Rod#239 – With Clean Optimized Zirlo Tube

Parameters	Rod239-Case1	Rod239-Case2	Rod239-Case3
System Pressure, MPa	15.5	15.5	15.5
Chimney Inlet Temperature, °F	636.0	635.0	635.0
Chimney Inlet Flow Velocity, m^3/h	3.27	3.29	3.21
Heat Flux (main center section), W/cm^2	399.3	367.3	374.3

Westinghouse

After the initial DNB run, the 2nd and 3rd repeated CHF results are within 2%

23

136

CHF Test Results for Rod 239 Uncoated No Crud

Westinghouse
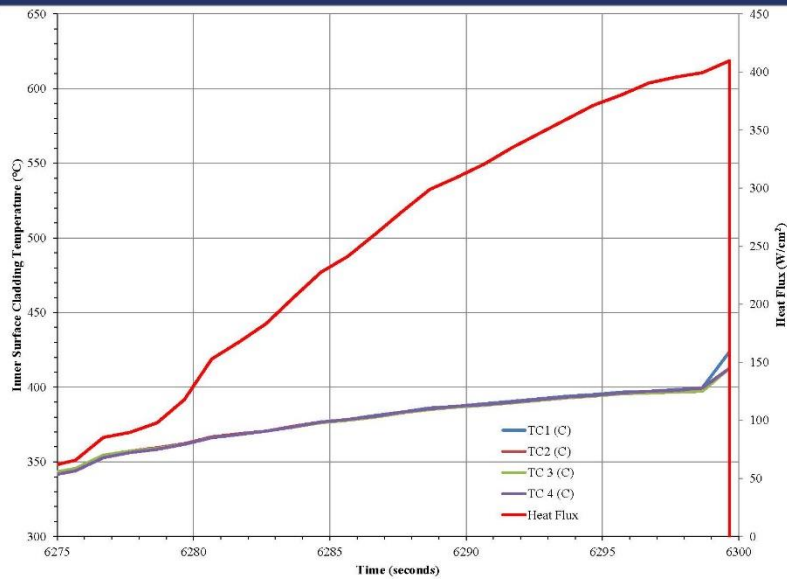
24

DNB Test Results for Rod#242 – With Cr-Coated Optimized Zirlo Tube (Flow was higher than the Ref.)

Parameters	Rod242
System Pressure, MPa	15.5
Chimney Inlet Temperature, °F	634.0
Chimney Inlet Flow Velocity, m^3/h	3.52
Heat Flux (main center section), W/cm^2	450.2

Comparing with the Optimized Zirlo Tube, the CHF results are increased by 12.7%

Westinghouse

25

137

CHF Test Results for Rod 242 Cr-coated
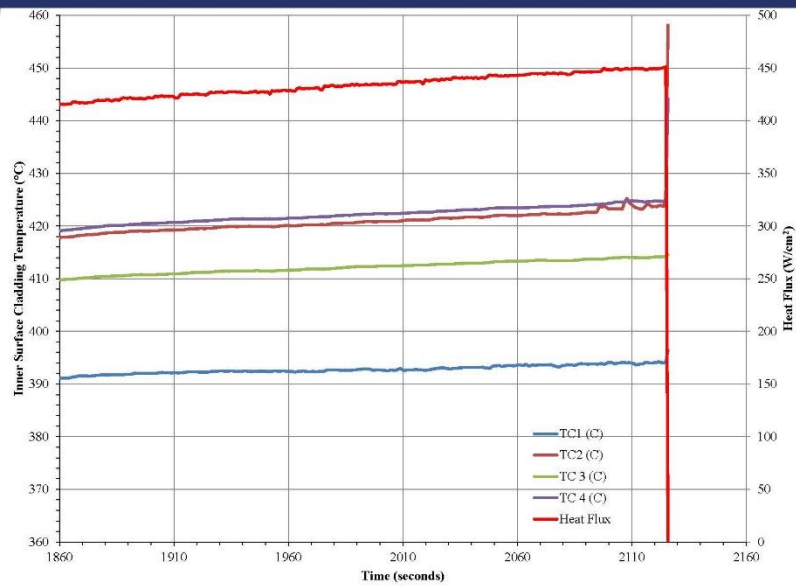
Appendix J

In-Pile CHF Experiments at TREAT
and Related CHF Activities

Appendix J

In-Pile CHF Experiments at TREAT
and Related CHF Activities
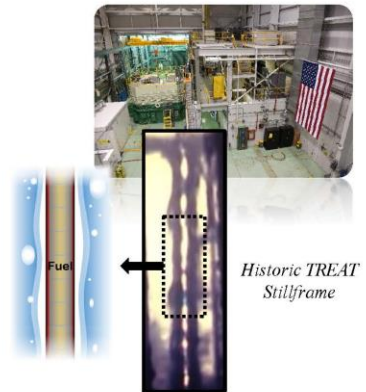
Introduction

- Cladding-to-coolant heat transfer during transient irradiation conditions remains a critical area of uncertainty in fuel performance predictive capability
- Key safety limits for LWRs are intended to avoid critical heat flux (CHF)
  - In the US a limiting DNBR is defined such that fuel rods will not experience CHF during normal or expected operation (Condition I and II events). This limit is also used to indicate fuel failures for some postulated accidents (Condition III and IV events) in evaluating off-site dose rates.
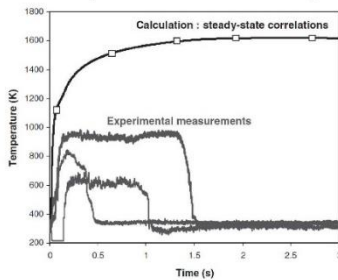
Experimental measured cladding surface temperature during RIA experiments in NSRR V. Bessiron, (2007) J. Nucl. Sci. Technol. 44 (5) 723-732
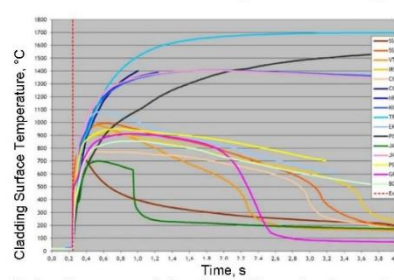
Fuel performance predictions for cladding surface temperature during RIA (NEA/CSNI/R(2013)7)
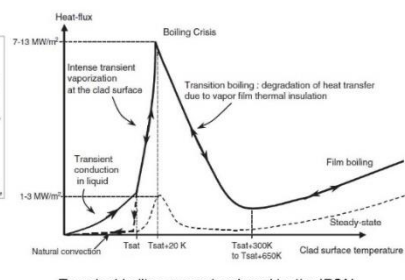
Transient boiling curve developed by the IRSN V. Bessiron, (2007) J. Nucl. Sci. Technol. 44 (5) 723-732

2

Experimental Background

- Few relevant out-of-pile experimental transient boiling studies (exponentially escalating heat input)
  - Primarily ribbons and wires over a very limited range of pressures[1]
- Noteworthy studies for relevant geometry and conditions:
  - NSRR in-pile tests
  - JMTR study on radiation induced surface activation (RISA)[2]
  - PATRICIA facility - out-of-pile with prototypic thermal-hydraulic capability (few data)[3]
- For RIA transients, data shows small dependence on mass flux and subcooling – important effect from irradiation

Pre-irradiation effect on transient boiling performance in NSRR experiments, Udagawa et al., Proc. of WRFPM 2014

[1] Su, G., et al., *Int. J. Heat Mass Transfer*, Vol. 96, 2016, pp.667-684
[2] Sibamoto, Y., et al., *J. Nucl. Sci. Technol.*, Vol. 44, No. 2, 2007, pp. 183-193.
[3] Bessiron, V., et al, *J. Nucl. Sci. Technol*, Vol. 44, No. 5, 2007, pp. 723-732

3

141

Impacts on Fuel Performance

- Bison uncertainty quantification and sensitivity analysis using 21 inputs on fuel rod geometry, thermal-hydraulic boundary conditions, core power conditions, and physical properties/models
  - ±25% factor on HTC
  - One sided factor on CHF varied from 1-2 (SD of 50%)

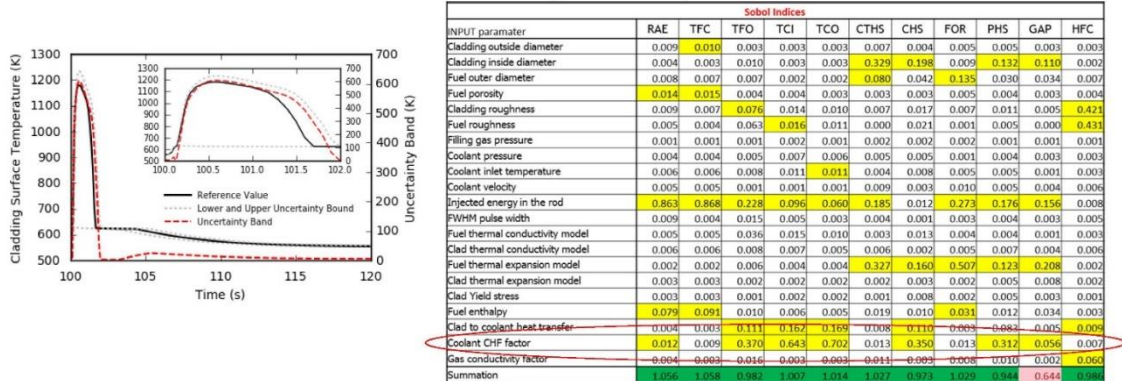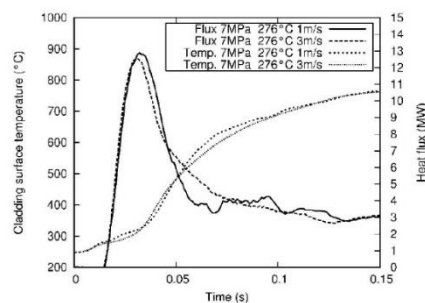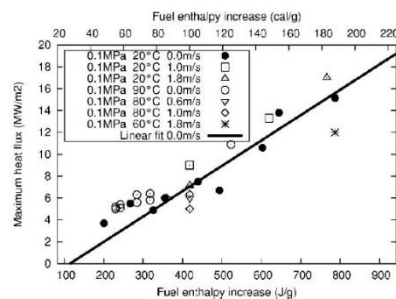| INPUT paramater	RAE	TFC	TFO	TCI	TCO	CTHS	CHS	FOR	PHS	GAP	HFC
Cladding outside diameter	0.009	0.010	0.003	0.003	0.003	0.007	0.004	0.005	0.005	0.003	0.003
Cladding inside diameter	0.004	0.003	0.010	0.003	0.003	0.329	0.198	0.009	0.132	0.110	0.002
Fuel outer diameter	0.008	0.007	0.007	0.002	0.002	0.080	0.042	0.135	0.030	0.034	0.007
Fuel porosity	0.014	0.015	0.004	0.004	0.003	0.003	0.003	0.005	0.004	0.003	0.004
Cladding roughness	0.009	0.007	0.076	0.014	0.010	0.007	0.017	0.007	0.011	0.005	0.421
Fuel roughness	0.005	0.004	0.063	0.016	0.011	0.000	0.021	0.001	0.005	0.000	0.431
Filling gas pressure	0.001	0.001	0.001	0.002	0.001	0.002	0.002	0.002	0.001	0.001	0.001
Coolant pressure	0.004	0.004	0.005	0.007	0.006	0.005	0.005	0.001	0.004	0.003	0.003
Coolant inlet temperature	0.006	0.006	0.008	0.011	0.011	0.004	0.008	0.005	0.005	0.001	0.003
Coolant velocity	0.005	0.005	0.001	0.001	0.001	0.009	0.003	0.010	0.005	0.004	0.006
Injected energy in the rod	0.863	0.868	0.228	0.096	0.060	0.185	0.012	0.273	0.176	0.156	0.008
FWHM pulse width	0.009	0.004	0.015	0.005	0.003	0.004	0.001	0.003	0.004	0.003	0.005
Fuel thermal conductivity model	0.005	0.005	0.036	0.015	0.010	0.003	0.013	0.004	0.004	0.001	0.003
Clad thermal conductivity model	0.006	0.006	0.008	0.007	0.005	0.006	0.002	0.005	0.007	0.004	0.006
Fuel thermal expansion model	0.002	0.002	0.006	0.004	0.004	0.327	0.160	0.507	0.123	0.208	0.002
Clad thermal expansion model	0.003	0.003	0.002	0.002	0.002	0.002	0.003	0.002	0.005	0.008	0.002
Clad Yield stress	0.003	0.003	0.001	0.002	0.002	0.001	0.008	0.002	0.005	0.003	0.001
Fuel enthalpy	0.079	0.091	0.005	0.005	0.005	0.019	0.010	0.031	0.012	0.034	0.003
Clad to coolant heat transfer	0.004	0.003	0.111	0.162	0.169	0.008	0.110	0.003	0.082	0.005	0.009
Coolant CHF factor	0.012	0.009	0.370	0.643	0.702	0.013	0.350	0.013	0.312	0.056	0.007
Gas conductivity factor	0.004	0.003	0.016	0.003	0.003	0.011	0.003	0.008	0.010	0.002	0.060
Summation	1.056	1.058	0.982	1.007	1.014	1.027	0.973	1.029	0.944	0.644	0.986

4

How to capture early phase RIA Thermal Hydraulics?

- Coolant flow-rate has no clear effect on the CHF from RIA experiments
- Pool conditions in autoclave and MARCH-SERTTA capsules will be adequate to assess early phase (pre-DNB) transient boiling behavior
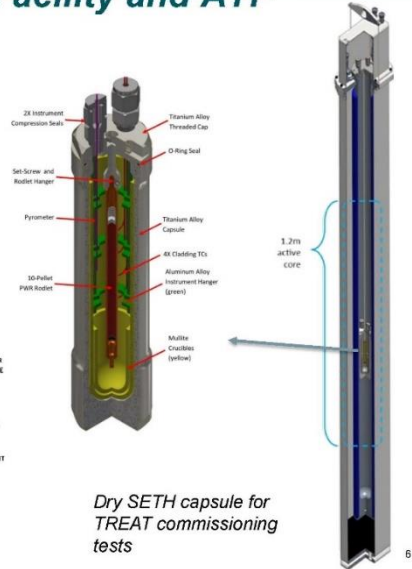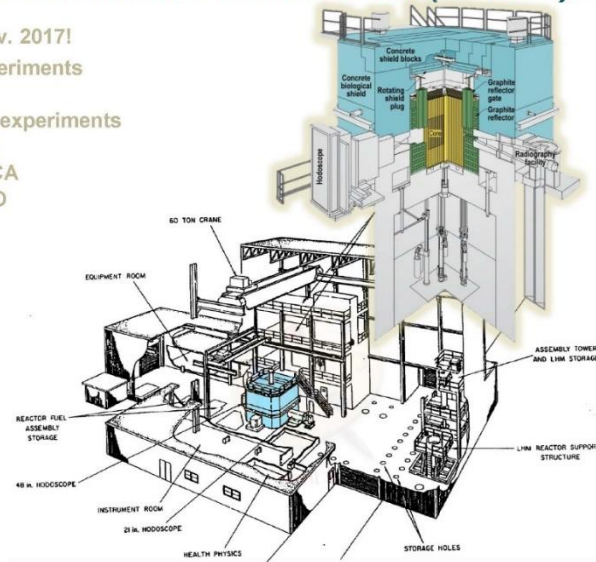

5

Restart of Transient Reactor Test (TREAT) Facility and ATF

- Restarted Nov. 2017!
- First fuel experiments Sept. 2018!
- Planned ATF experiments
  - RIA
  - LOCA
  - AOO

Historic TREAT Stillframe

Dry SETH capsule for TREAT commissioning tests
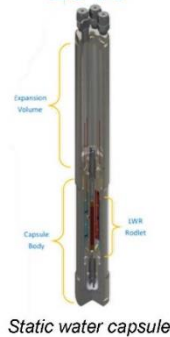

Crucial Experimental Infrastructure

- TREAT is open for business running experiments since 2018!

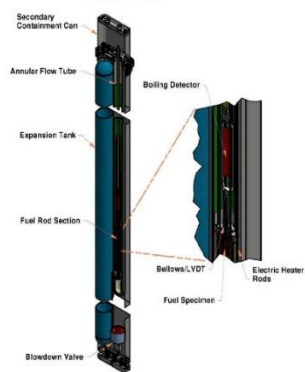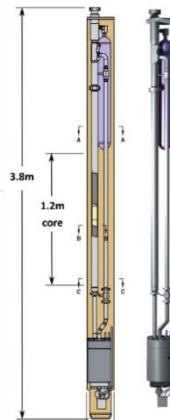**Integral testing of fuels under AOO, DBA, to BDBA conditions**
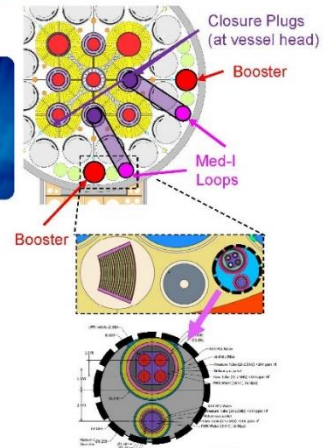
2019

Static water capsule

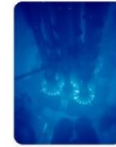**2020**

Natural circulation capsule with blowdown capability

Full flow recirculating loop

2023

Proposed i-loop in ATR – includes dryout studies

Full PWR/BWR pressures and temperatures – varying by flow

In-Pile CHF-SERTTA Experiment Design

- Planned to utilized MARCH-SERTTA module for water-submerged rodlet testing
- Conaxes for up to 12X 1mm leads
- Enables significant instrumentation opportunity
  - Boiling detector
  - Dual IR pyrometer (rod internal)
  - Surface TC's
  - Acoustic sensor
- Planned experiment in 1st half FY20

Optical fibers for Infrared Thermometry internal to heated rod

Hollow borated SS rod

Pyrometer and TCs for surface temperature

Novel boiling detector
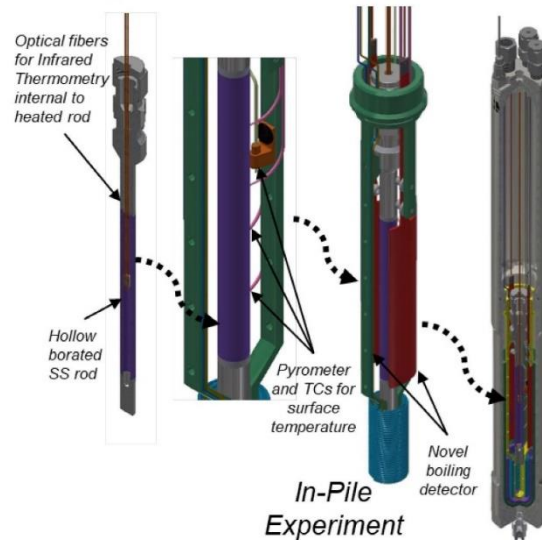
In-Pile Experiment

## In-Pile Experiment Design: Nuclear-Heated Simulator Rod

- N-alpha heater inside cladding
  - Hampers internal instrumentation options
  - Complicated by gap, but more prototypic
  - Offers the ability to test different cladding types
- Empty n-alpha-heated tube
  - More direct comparison to joule-heated out-of-pile tube tests
  - Much easier to instrument inside the tube
- Solid rod
  - Off-the-shelf rods, easier fabrication
  - Extra mass needed for gamma heat only option

	J/gMJ
NUO2 pellet	0.77
B4C pellet	0.65
BN pellet	0.56
Bor SST tube 0.45% B	0.16
Bor SST tube 0.97% B	0.26
Bor SST tube 1.48% B	0.32
Bor SST tube 2.03% B	0.37
Li-Cu	TBD
Tungsten	TBD

Radial Distribution of HGR and PCF Pellet Summation K=0.97325 0.00004
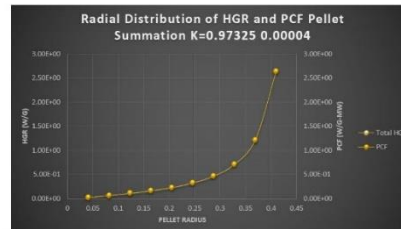
In-Pile Experiment Design: Nuclear-Heated Simulator Rod

• Nuclear-heated simulator rod has gone through some design iterations to provide the right axial energy deposition
  – Finalized on an hourglass shape
  – Works neutronically, thermal studies are underway

0.25 in. Axial Mesh, 2.25 wt.% B in SS304, Rodlet


0.25 in. Axial Mesh, 2.25 wt.% B in SS304, Hourglass
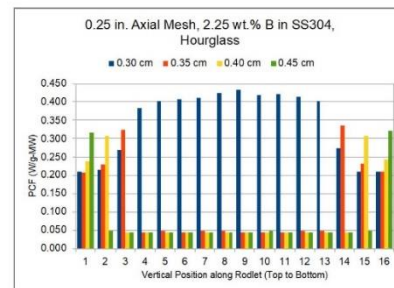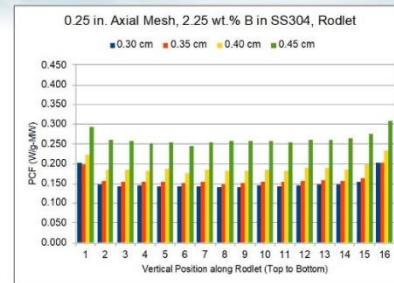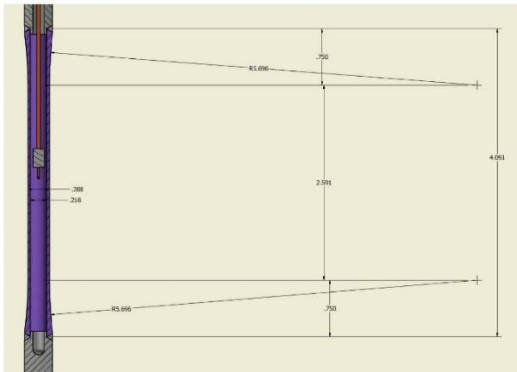
How to Validate System Performance outside of TREAT?

• In-pile experiment offers a lot of flexibility for a R&D sandbox with instrumentation and power control

1. Advanced instrumentation requires sufficient validation out-of-pile to maximize efficiency of in-pile testing with validated uncertainty

2. Even with great flexibility, out-of-pile facility offers opportunity to extend study parameter space to wider range of heating rates (overlap with NSRR/CABRI)

3. Advantage for separate effects evaluation excluding effects of irradiation with experiment as identical as possible

→ Need out-of-pile companion facility to support TH evaluations

Out-of-Pile Transient Boiling System Design

- Desire up to full PWR thermal hydraulic conditions (mass flux control is < priority objective), desire ability to simulate NSRR to TREAT heating rates (bounding commercial LWR RIA)
- Utilize existing water autoclaves
  - Stay within design specification
  - Support feedthroughs for gas lines, electrical feeds, instrumentation, imaging,…
- Build custom, controllable power delivery system to simulate reactor transients
  - Off the shelf components

Autoclave Area
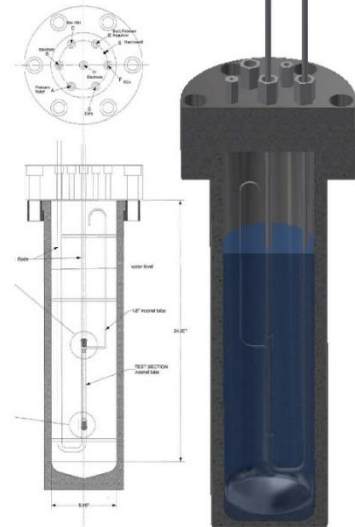
12

Capacitor Banks

- Electrical heating will be driven by 4 capacitor banks (>220 kW max power, 760 kJ total stored energy, < 20 kJ max experiment)
  - Each with an independent switch and current probe
  - Flexible system data acquisition and control
    - Switching system enables power shaping; e.g. ramps, pulses (10ms-200ms FWHM)
  - Full electrical model to predict electrical performance
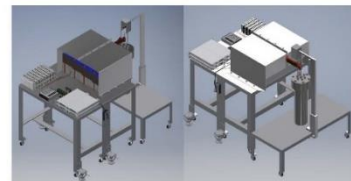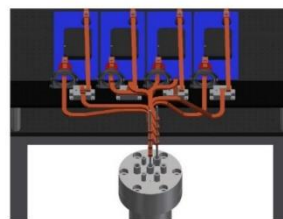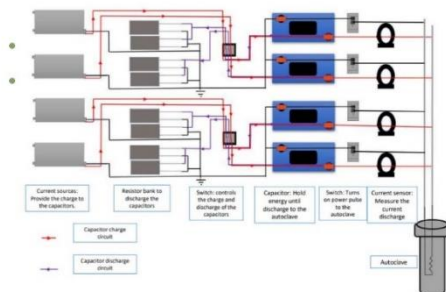
13

Instrumentation is the key!

- Incorporate the same instrumentation planned for in-pile testing and more...
  - Infrared pyrometers for inner and outer heater tube temperatures
  - Thermocouples on heater surface
  - Capacitive boiling detector
  - Fast response pressure transducer
  - High speed underwater imaging system

Targeted Power Cases

- RELAP5 model built from autoclave dimensions
- Power modeled as an RC decay circuit with power terminated at specified pulse width
- Initial conditions set at 300ºC and 15.5 MPa
- Modeled a range of pulse widths
  - 11 ms (narrowest – SPERT/NSRR/CABRI)
  - 90 ms (TREAT)
  - 40 ms (PWR)
  - 200 ms (36 V)

15

147

… Targeted Power Cases Cont.

- Narrowest pulse with current configuration is ~0.011 s
  - A factor of 5 on CHF increases the narrowest pulse to 0.025 s
- All cases reach CHF with default correlations in Relap5
- Pressure increases in water is negligible (~10 psi)

Additional Topics

- BWR AOO Event
 - Boiling transition effects on irradiated fuel from test or commercial reactor
  - Perform "integral" experiments on irradiated fuel rods that create appropriate temperature vs time history
  - MARCH-SERTTA capsule shows promising results

- Coated Cladding PIRT
  - Introduction of coated cladding might lead to additional questions that need to be answered
    - Changes to hydraulic diameter due to the coating thickness
    - Changes to boiling crisis behavior, including effects of surface roughness
    - For boiling water reactor applications, changes to rewet temperature following dryout (i.e. Tmin)
    - Potential for defects such as cracks and delamination

Conclusions

- In-pile transient boiling remains an area of uncertainty in fundamental understanding and predictive capability for RIA conditions

- Restart of TREAT provides ideal opportunity to investigate AOO and DBA transients

- Out-of-pile facility designed to complment in-pile experiments and extend experimental database for pre-DNB conditions
  - Simple design, based on capacitive discharge system
  - Facility can extend range of heating rates bridging integral test facilities and commercial LWR
  - System operational this month!

- Support in-pile testing - ATF, AOO studies, etc., with collaboration with universities, EPRI, GE, IRSN, JAEA
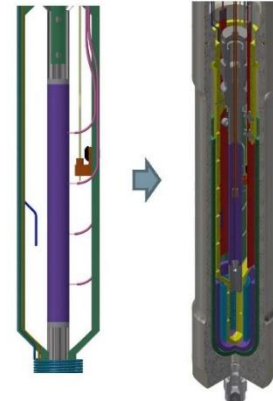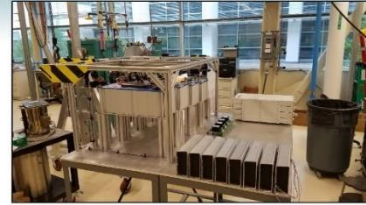
Thank you for your attention!

Appendix K

Thermal-Hydraulics of ATF Cladding Materials, NEUP-ATF Meeting

Appendix K

Thermal-Hydraulics of ATF Cladding Materials, NEUP-ATF Meeting

Thermal-Hydraulics of ATF Cladding Materials

NEUP – ATF Meeting

Organizers: Matteo Bucci (MIT) & Piyush Sabharwall (INL)

August 13th 2019

NEUP Project Number	Title	University	PI
17-12647	Determination of Critical Heat Flux and Leidenfrost Temperature on Candidate Accident Tolerant Fuel Materials	MIT	Matteo Bucci
17-12688	An Experimental and Analytical Investigation into Critical Heat Flux (CHF) Implications for Accident Tolerant Fuel (ATF) Concepts	UNM	Youho Lee
17-13019	Evaluation of Accident Tolerant Fuels Surface Characteristics in Critical Heat Flux Performance	VCU	Sama Bilbao y León
17-12549	Critical Heat Flux Studies for Innovative Accident Tolerant Fuel Cladding Surfaces	UW	Michael Corradini

	Project PIs			
	MIT	UWM	UNM	VCU
ZIRLO + Cr Spray Coating (WEC)	ZIRLO + Cr Spray Coating (WEC)	ZIRLO + Cr Spray (WEC)		
SiC Cladding (GA)	SiC Cladding (GA)	SiC (GA)		
ZIRLO + FeCrAl Coating (WEC)	ZIRLO + FeCrAl Coating (WEC)			
SiC/SiC (GA)		SiC/SiC (GA)		
ZIRLO + Cr PVD		ZIRLO + Cr PVD		
ZIRLO + FeCrAl Cold Spray		ZIRLO + FeCrAl Cold Spray		
CVD SiC Cladding		CVD SiC Cladding		
ZIRLO + ZrSi PVD		ZIRLO + ZrSi PVD		
FeCrAl Cladding		FeCrAl Cladding	FeCrAl Cladding	FeCrAl Cladding
Zirc-4 + Cr PVD (AREVA)			Zirc-4 + Cr PVD (AREVA)	Zirc-4 + Cr PVD (AREVA)
SiC (AREVA)				SiC (AREVA)

Project Overviews

VCU
- Perform separate-effects experiments to characterize surface properties
- System-wide tests
- Develop enhanced models & correlations to predict CHF, and implement in sub-channel codes

UWM
- Study surface coating methods
- Characterize surface properties
- Pool boiling experiments
- Flow boiling experiments

MIT
- Characterize CHF properties for 3 candidate ATF cladding materials
- Measure CHF under both steady-state and transient conditions
- Quantify the effects of CRUD deposition on CHF

UNM
- Determine change in CHF for candidate claddings
- Assess impact on reactor performance, design, and safety characteristics
- Conduct low & high pressure boiling experiments
- System simulations
- Boiling modeling

Integrating Efforts - CHF

- Completed a survey of the different cladding/coating systems to be analyzed. Several potential areas for collaboration were identified.
    - While multiple entities may be investigating the same or similar systems, they are often looking at different properties or using different methods.
    - MIT and UWM have areas of synergy for WEC systems.
    - UNM and VCU have areas of synergy with Framatome (AREVA) systems.
- PIs noted the relative priority of the various systems, based on their interactions with vendors.
- INL is working to facilitate collaborations among the researchers.
- **Importance of NQ-1 Data**

	Project PIs			
	MIT	UWM	UNM	VCU
ZIRLO + Cr Spray (WEC)	High Priority	High Priority		
Zirc-4 + Cr PVD (AREVA)			High Priority	High Priority
FeCrAl Cladding			No Priority Specified	No Priority Specified
ZIRLO + Cr PVD		No Priority Specified		
SiC/SiC (GA)		No Priority Specified		
SiC Cladding (GA)	Low Priority	Low Priority		
ZIRLO + FeCrAl (WEC)	Low Priority			
ZIRLO + FeCrAl Cold Spray		Low Priority		
SiC (AREVA)				Low Priority

Legend:
- Green = High Priority
- Yellow = No Priority Specified
- Red = Low Priority

Combined/ Integrated Report on Findings

Thermal-hydraulics of Accident Tolerant Fuel cladding materials

(Coordination of NEUP projects)

- Introduction and Significance of Work
- Overall Objective
- Methodology (details)
- Experiment and modeling
- Verification and validation
- Data (gathering, quality assurance)
- Overall Challenges
- Path Forward
    - Near term efforts
    - Long term efforts
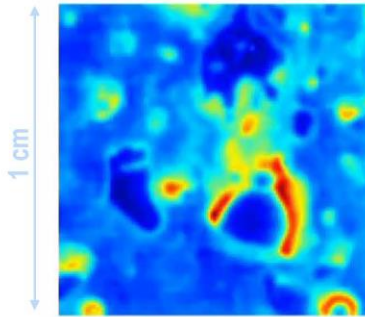- Publications (if any)
- Main Conclusions and Summary

Appendix L

The Red Lab and ATF Facilities in NSE, MIT

Appendix L

The Red Lab and ATF Facilities in NSE, MIT

Heat flux on a boiling surface
(approaching the boiling crisis)

The Red Lab and "ATF" Facilities in NSE, MIT

The study of thermal-hydraulics of accident tolerant fuel cladding materials

Matteo Bucci
Massachusetts Institute of Technology
Department of Nuclear Science and Engineering
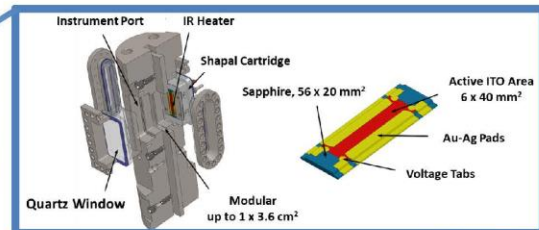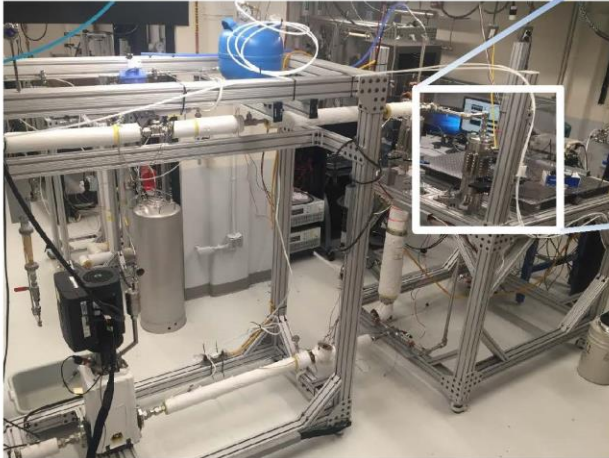
Flow loop #1 – Test section #1: Pressurized

PEThER

NSE
Nuclear Science
and Engineering

- DI water
- Up to **14 bars**
- Ambient temperature to saturation
- 400 to 2500 kg/m^2/s
- Dh ~1.5 cm (1 $\times$ 3 cm^2)
- Up to **CHF**
- **Diagnostics**

Flow loop #1 – Test section #2: Pressurized

Instrument Port   IR Heater

Shapal Cartridge

Sapphire, 56 x 20 mm^2

Active ITO Area
6 x 40 mm^2

Au-Ag Pads

Voltage Tabs

Quartz Window   Modular
up to 1 x 3.6 cm^2

- DI water
- Up to **14 bars**
- Ambient temperature to saturation
- Narrow channel
- Two side heating
- Side wall effects
- **Up to CHF**
- Diagnostics

Flow loop #2: Full PWR

LWR

NSE
Nuclear Science
and Engineering

- DI water
- Up to **PWR pressure**
- Ambient temperature to saturation
- Up to 3600 kg/m^2/s
- Up to **CHF**
- Dh ~ Dh PWR
- Mixing obstacles
- **Diagnostics**
- **Rod heaters / annular flow**

4

Flow loop #2 – Test section: Full PWR
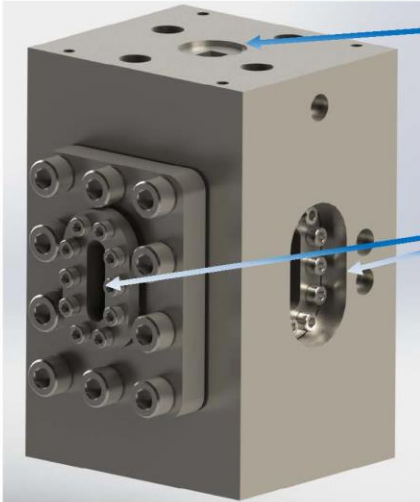
Square channel matches the hydraulic diameter of the inner PWR subchannel

Can accommodate upstream obstacles to mimic mixing grids

Multiple openings provide the view of the boiling process from all perspectives

The test section is designed to operate at full reactor pressure (155 bar) and up to the saturation temperature of water (345 °C)
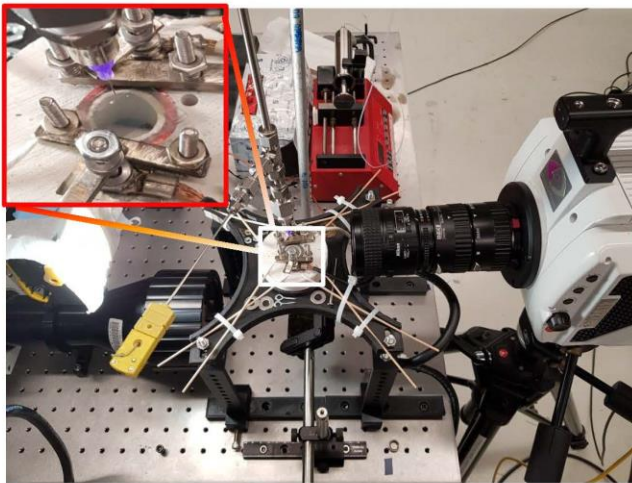
5

Autoclave contact angle measurement
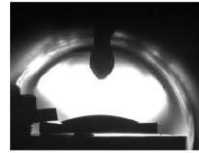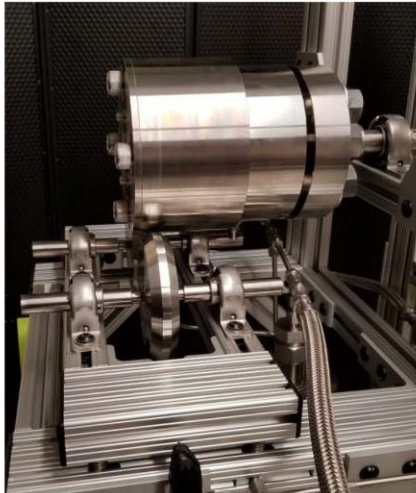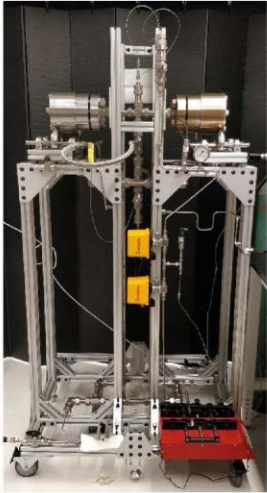
Autoclave

NSE
Nuclear Science
and Engineering

- Up to **221 bars** with water
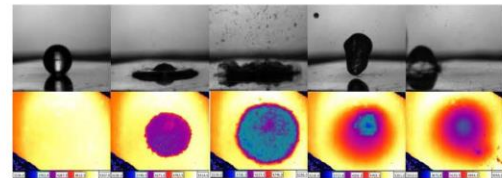- Steam saturated environment
- Contact angle (S,A,R)
- Wicking

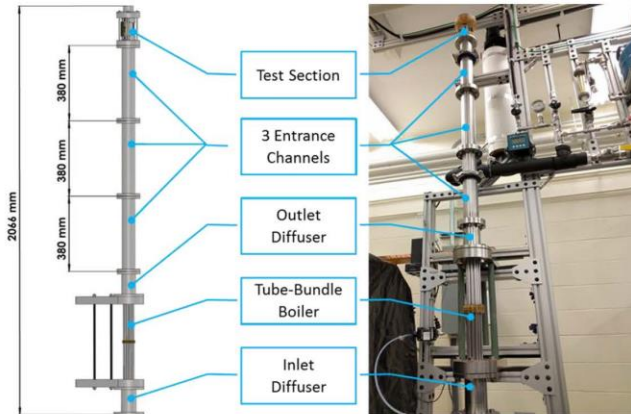## Droplet quenching on ATF material

Quenching

NSE
Nuclear Science
and Engineering

- ~ 2 mm droplet
- Up to **500 ˚C** (Film boiling)
- Heating area ~ 1 cm^2
- IR and HSV diagnostics
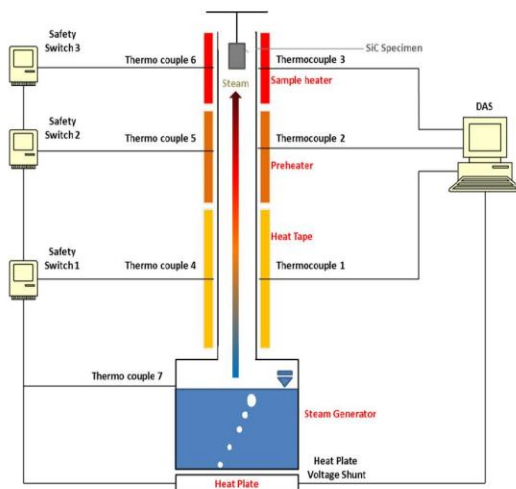
Flow loop #3: BWR or accident condition

KAPL

NSE
Nuclear Science
and Engineering

- DI water
- Ambient pressure
- Ambient temperature to saturation
- All flow regimes up to **annular flow**
- Below CHF
- Dh ~ 1 cm
- **Diagnostics**

Impact of superheated steam on ATF material

Oxidation Column

NSE
Nuclear Science
and Engineering

Duplicate post-LOCA conditions
- Steam T: 1140 °C~1500°C
- Re: 40~300
- V: 1~9m/sec
- Ambient pressure